Pandey, D.K., Clift, P.D., Kulhanek, D.K., and the Expedition 355 Scientists
*Proceedings of the International Ocean Discovery Program* Volume 355
publications.iodp.org

doi:10.14379/iodp.proc.355.101.2016

# Expedition 355 summary[1]

D.K. Pandey, P.D. Clift, D.K. Kulhanek, S. Andò, J.A.P. Bendle, S. Bratenkov, E.M.Griffith, G.P. Gurumurthy, A. Hahn, M. Iwai, B.-K. Khim, A. Kumar, A.G. Kumar, H.M. Liddy, H. Lu, M.W. Lyle, R. Mishra, T. Radhakrishna, C.M. Routledge, R. Saraswat, R. Saxena, G. Scardia, G.K. Sharma, A.D. Singh, S. Steinke, K. Suzuki, L. Tauxe, M. Tiwari, Z. Xu, and Z. Yu[2]

Keywords: International Ocean Discovery Program, IODP, *JOIDES Resolution*, Expedition 355, Site U1456, Site U1457, Arabian Sea monsoon, Arabian Sea, tectonics, Climate and Ocean Change, Earth Connections, Laxmi Ridge, Laxmi Basin

Contents

## Abstract

The Indian (southwest) summer monsoon is one of the most intense climatic phenomena on Earth, with its long-term development possibly linked to the growth of high topography in South and Central Asia. The Indian continental margin, adjoining the Arabian Sea, offers a unique opportunity to investigate tectonic–climatic interactions and the net impact of these processes on weathering and erosion of the western Himalaya. During International Ocean Discovery Program Expedition 355, two sites (U1456 and U1457) were drilled in Laxmi Basin in the eastern Arabian Sea to document the coevolution of mountain building, weathering, erosion, and climate over a range of timescales. In addition, recovering basement from the eastern Arabian Sea provides constraints on the early rifting history of the western continental margin of India with special emphasis on continental breakup between India and the Seychelles and its relationship to the plume-related volcanism of the Deccan Plateau.

Drilling and coring operations during Expedition 355 recovered sediment from Sites U1456 and U1457 in Laxmi Basin, penetrating 1109.4 and 1108.6 m below seafloor (mbsf), respectively. Drilling reached sediment dated to 13.5–17.7 Ma (late early to early middle Miocene) at Site U1456, although with a large hiatus between the lowermost sediment and overlying deposits dated at <10.9 Ma. At Site U1457, a much longer hiatus occurs near the base of the cored section, spanning from ~10.9 to ~62 Ma. At both sites, hiatuses span ~8.2–9.2 and ~3.6–5.6 Ma with a possible condensed section spanning ~2.0–2.6 Ma, although the total duration for each hiatus is slightly different between the two sites.

A major submarine fan probably draining the western Himalaya and Karakoram must have been supplying sediment to the eastern Arabian Sea since at least ~17 Ma. Sand mineral assemblages indicate that the Greater Himalayan Crystalline Sequence was fully exposed to the surface by this time. Most of the recovered sediment appears to be derived from the Indus River and includes minerals that are unique to the Indus Suture Zone, in particular glaucophane and hypersthene, most likely originating from the structural base of the Kohistan arc (i.e., within the Indus Suture Zone). Pliocene sandy intervals at Site U1456 were deposited in lower fan "sheet lobe" settings, with intervals of basin–plain turbidites separated by hemipelagic muddy sections deposited during the Miocene. Site U1457 is more distal in facies, reflecting its more marginal setting. No major active lobe appears to have affected Laxmi Basin since the late early Pleistocene (~1.2–1.5 Ma).

We succeeded in recovering sections spanning the 8 Ma climatic transition, when monsoon intensity is believed to have changed strongly, although the nature of this change awaits postcruise analysis. We also recovered sediment from large mass transport deposits measuring ~330 and ~190 m thick at Sites U1456 and U1457, respectively. These sections include an upper sequence of slump-folded muddy and silty rocks, as well as underlying calcarenites and limestone breccias, together with smaller amounts of volcanic clasts, all of which are likely derived from the western Indian continental shelf. Identification of similar facies on the regional seismic lines in Laxmi Basin suggests that these deposits form parts of one of the world's largest mass transport deposits.

Coring of igneous basement was achieved at Site U1457. Recovery of massive basalt and associated volcaniclastic sediment at this site should address the key questions related to rifting and volcanism associated with formation of Laxmi Basin. Geochemical analysis indicates that these are low-K, high-Mg subalkaline tholeiitic basalts and do not represent a typical mid-ocean-ridge basalt. Other observations made at the two sites during Expedition 355 provide vital constraints on the rift history of this margin. Heat flow measurements at the two drill sites were calculated to be ~57 and ~60 mW/m$^2$. Such heat flow values are compatible with those observed in average oceanic crust of 63–84 Ma age, as well as with the pres-

---

[1] Pandey, D.K., Clift, P.D., Kulhanek, D.K., Andò, S., Bendle, J.A.P., Bratenkov, S., Griffith, E.M., Gurumurthy, G.P., Hahn, A., Iwai, M., Khim, B.-K., Kumar, A., Kumar, A.G., Liddy, H.M., Lu, H., Lyle, M.W., Mishra, R., Radhakrishna, T., Routledge, C.M., Saraswat, R., Saxena, R., Scardia, G., Sharma, G.K., Singh, A.D., Steinke, S., Suzuki, K., Tauxe, L., Tiwari, M., Xu, Z., and Yu, Z., 2016. Expedition 355 summary. *In* Pandey, D.K., Clift, P.D., Kulhanek, D.K., and the Expedition 355 Scientists, *Arabian Sea Monsoon.* Proceedings of the International Ocean Discovery Program, 355: College Station, TX (International Ocean Discovery Program). http://dx.doi.org/10.14379/iodp.proc.355.101.2016

[2] **Expedition 355 Scientists' addresses.**

MS 355-101: Published 29 August 2016

ence of highly extended continental crust. Postcruise analyses of the more than ~1722 m of core will provide further information about the nature of tectonic–climatic interactions in this global type area for such studies.

# Introduction

The theory of plate tectonics established that the solid Earth's lithosphere interacts intimately with the underlying, circulating asthenosphere. However, more recently the geoscience community has started to recognize that the lithosphere also has significant interactions with the overlying atmosphere and oceans. Such interactions can influence atmospheric and oceanic circulation patterns and thereby control Earth's climate by changing the distribution of heat across the planet. Furthermore, feedback from the atmosphere to the lithosphere provides a new vision of how orogenic belts and even passive margins evolve under the stress of surface processes. Interactions between the solid Earth and the climate system can occur in at least two different ways. The opening and closure of deep-ocean gateways are believed to have caused large-scale climate changes by affecting heat transport between ocean basins or between polar and tropical regions (e.g., Haug and Tiedemann, 1998; Cane and Molnar, 2001; von der Heydt and Dijkstra, 2006). Alternatively, mountain building may perturb planetary-scale atmospheric circulation, influencing continental environments and oceanography of the surrounding basins as mountain barriers divert air streams and affect continental temperatures and humidity (e.g., Huber and Goldner, 2012). Furthermore, changes in continental erosion can profoundly impact Earth's carbon and biogeochemical cycles (e.g., Berner et al., 1983). These various pathways for interaction occurred throughout the Cenozoic with the closure of the Tethys Ocean by subduction under the southern edge of Eurasia during the northward motion of Africa, Arabia, India, and a host of smaller continental fragments whose accretion caused the uplift of the Alpine-Himalayan mountain belt.

The suggestion that mountain building in Asia has intensified monsoon strength in the Indian subcontinent is the most dramatic proposed example of lithospheric–atmospheric interactions (Prell and Kutzbach, 1992; Molnar et al., 1993; An et al., 2001; Molnar et al., 2010; Boos and Kuang, 2010). This is partly a reflection of the scale of the tectonism and the resultant mountains. Nonetheless, there is increasing recognition that other factors, such as the retreat of shallow seas in Central Asia, may have also played a role in controlling monsoon intensity (Ramstein et al., 1997). Asia is the only continent that experiences such a strong monsoon, which is partly a reflection of landmass size but is also linked to its tectonic history and anomalously high altitude across a broad region. Understanding what controls monsoon intensity is of great scientific interest and has substantive societal as well as economic importance, considering the large number of people whose livelihood depends on the monsoon and who would be affected if it varied significantly.

Quantifying the various processes that control monsoon intensity over geologic timescales will improve the context for shorter term modeling of how future climate change may affect the densely populated environments of Asia. Specifically, we aim to answer the question of what links exist between the Indian monsoon and the building of high topography in Asia, and whether climatic feedbacks have influenced the tectonic evolution of the western Himalaya and Karakoram.

The Arabian Sea in the northern Indian Ocean (Figure **F1**) preserves regional sedimentary records of rifting, tectonic subsidence, and paleoceanographic history and also provides archives of long-term erosion of the Himalaya since the start of continental collision between India and Eurasia. Although the timing is controversial (Aitchison et al., 2007; DeCelles et al., 2014; Wu et al., 2014), it is thought that collision probably began in the Eocene (Garzanti et al., 1987; Rowley, 1996; Najman et al., 2010). Scientific drilling in the Arabian Sea was designed to reconstruct the evolution of erosion and weathering in the western Himalaya and Karakoram, as well as the environmental conditions that existed in the flood plains of the Indus Basin through the Cenozoic. This was done in an area where Indian monsoon evolution is already partly reconstructed (Kroon et al., 1991; Prell et al., 1992). Thus erosion, tectonism, and climate can be directly compared to one another for the first time over long time spans and at high resolution.

In addition to being a repository of information about past climate and mountain building, the Arabian Sea also holds potentially illuminating records of continental rifting and breakup tectonics dating from the time of Gondwana fragmentation in the Cretaceous (Heine et al., 2004). Paleogeographic reconstructions based on seafloor magnetic anomalies, as well as similarities in structural/tectonic elements, suggest a conjugate relationship between the western continental margin of India and the eastern continental margin of Madagascar and the Seychelles (Storey et al., 1995; Collier et al., 2008). In-depth studies of the conjugate margins in this region offer new data to complement our knowledge from other well-studied conjugate margins, such as the Iberia-Newfoundland and Greenland-Norway pairs of the Atlantic Ocean (e.g., Whitmarsh et al., 2001; Hopper et al., 2003). The nature of the continent/ocean boundary is controversial in the Arabian Sea, especially with regard to Laxmi Ridge, an enigmatic block located offshore of the western Indian coast (Figure **F1**).

The widely held view among geoscientists is that Laxmi Ridge is a continental sliver rifted away from India (Naini and Talwani, 1983); however, contrary views have also emerged that suggest it could be stretched/oceanic crust (Bhattacharya et al., 1994; Miles et al., 1998; Talwani and Reif, 1998). The proximity of this margin to the volcanic Deccan Traps makes this potentially a classic margin for investigating plume-rift interactions. However, links are presently only conjectural because the nature of the breakup, including the style of strain accommodation, and the timing of the extension in relation to the Deccan volcanic event are unconstrained and require physical sampling of the basement on the continental margin.

An international workshop on scientific drilling in the Indian Ocean was organized in Goa, India, in October 2011 at which understanding the evolution of the Asian monsoon was highlighted as a crucial theme. Following this workshop, several proposals related to the evolution of the Asian monsoon were developed. International Ocean Discovery Program (IODP) Expedition 355 was based on drilling Proposal 793-CPP2. The primary objectives of this expedition can be summarized under two major themes, "Climate and Ocean Change" and "Earth Connections," which are described in the IODP Science Plan (**http://www.iodp.org/about-iodp/iodp-science-plan-2013-2023**). Specific goals of this proposal include

1. Testing whether the timing of the exhumation of the Greater Himalaya correlates with enhanced erosional flux and intense chemical weathering at ~23 Ma;

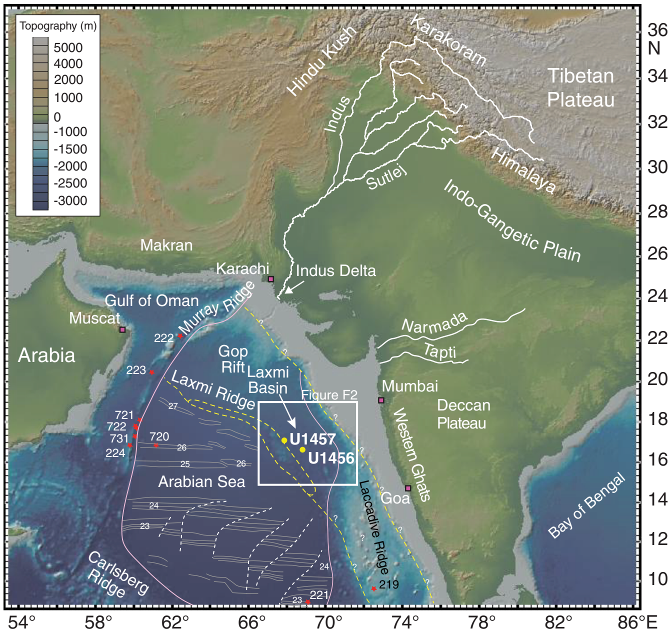

Figure F1. Bathymetric map of the Arabian Sea and surrounding landmasses from GeoMapApp (Ryan et al., 2009). Yellow circles = Expedition 355 sites, white lines = major rivers and tributaries, red stars = earlier scientific drilling sites that have sampled the Indus Fan, pink line = approximate extent of the fan after Kolla and Coumes (1987), yellow dashed lines = speculated location of the continent/ocean boundary, depending on whether Laxmi Basin is oceanic or continental, gray lines with numbers = magnetic anomalies from Royer et al. (2002), white box = location of detailed map in Figure **F2**.

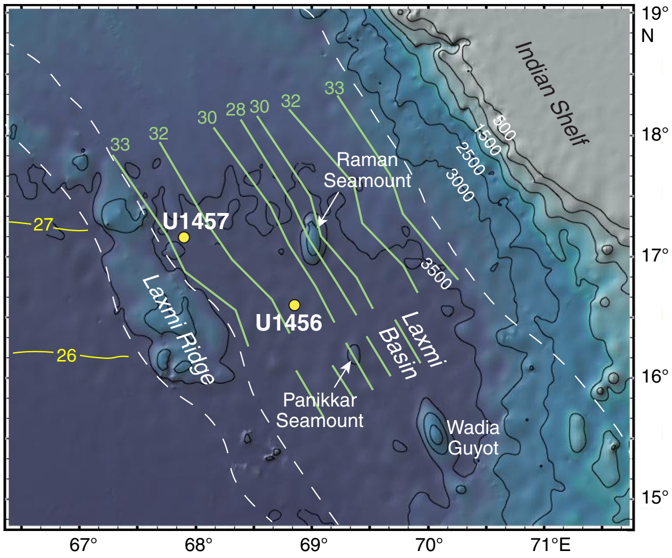

Figure F2. Bathymetric map of the region around Laxmi Basin showing the location of Expedition 355 sites in relation to other major bathymetric features, especially Laxmi Ridge. White dashed lines = possible locations of the continent/ocean boundary, depending upon whether the crust in Laxmi Basin has continental or oceanic affinity. Magnetic anomalies (yellow lines) from the Arabian Basin are from Miles et al. (1998), whereas those in Laxmi Basin (green lines) are from Bhattacharya et al. (1994). Contours (black lines) are in meters below sea level. Bathymetric data from GeoMapApp (Ryan et al., 2009).

2. Determining the amplitude and direction of environmental change at ~8 Ma and other times of major climatic variation during the Cenozoic;
3. Dating the age of the base of the fan to constrain the timing of India/Eurasia collision and subsequent uplift of the Himalaya and Tibetan Plateau; and
4. Deciphering the nature of the crust in Laxmi Basin (eastern Arabian Sea), which has a significant bearing on paleogeographic reconstructions along conjugate margins in the Arabian Sea and models of continental breakup and rifted volcanic margin formation.

# Background

## Geological setting

The eastern Arabian Sea presents an intriguing case for the study of continental breakup between India and Madagascar, differing in important ways from both the classic nonvolcanic Iberia-Newfoundland conjugate (Boillot et al., 1995; Whitmarsh et al., 2001) and the volcanic Norway-Greenland margin (Skogseid et al., 2000; Hopper et al., 2003). The northern Arabian Sea is characterized by the presence of large structural blocks located between the western continental shelf of India and the deep seafloor of the Arabian Basin. Laxmi Ridge is presumed by most geoscientists to be mostly continental (Talwani and Reif, 1998), and is separated from the western Indian margin by Laxmi Basin (Figure **F2**). There are isolated highs east of Laxmi Ridge, namely Wadia Guyot, together with Panikkar and Raman Seamounts, which are collectively referred to as Panikkar Ridge (Karlapati, 2004; Krishna et al., 2006; Bhattacharyya et al., 2009; Mishra et al., 2015). The oldest clear seafloor spreading–related magnetic anomalies identified in this region are Anomalies 27n (62.2–62.5 Ma) and 28n (63.5–64.7 Ma), located southwest of Laxmi Ridge in the Arabian Basin and north of the Seychelles, respectively (Chaubey et al., 2002; Royer et al., 2002) (Figures **F1**, **F2**). Magnetic anomalies in Laxmi Basin itself are rather erratic, and whereas some researchers have argued that these correspond to seafloor spreading (Bhattacharya et al., 1994; Mishra et al., 2012), it is possible that instead these could have been caused by dikes intruded within a hyperextended continental crust (e.g., Talwani and Reif, 1998; Krishna et al., 2006).

Previous studies using magnetic anomalies from the oceanic crust describe the juxtaposition of India and the Seychelles immediately before the onset of extensional tectonics (Chaubey et al., 1998; Royer et al., 2002). However, most plate tectonic reconstruction models for this region suggest a wide deepwater offshore region (Laxmi Basin, Gop Rift, and offshore Indus Basin) of ~300 km width between the Seychelles and the Indian subcontinent before the onset of seafloor spreading (Chaubey et al., 2002; Royer et al., 2002). The tectonic complexity in this region is further increased when considering the massive Deccan magmatic event at ~65 Ma. It is not yet convincingly known whether eruption of the Deccan flood basalt predates the rifting in Laxmi Basin or otherwise. Lack of geochronological data from Laxmi Basin makes it difficult to correlate the opening of the basin to the Deccan volcanism in the Late Cretaceous. Numerous geophysical studies to investigate the nature of crust in Laxmi Basin remain inconclusive, with some authors favoring the presence of rifted continental crust (Naini, 1980; Naini and Talwani, 1983; Kolla and Coumes, 1990; Miles and Roest, 1993; Miles et al., 1998; Radha Krishna et al., 2002; Krishna et al., 2006; Minshull et al., 2008), whereas others argue for oceanic crust (Biswas and Singh, 1988; Bhattacharya et al., 1994; Malod et al., 1997; Talwani and Reif, 1998; Singh, 1999; Bernard and Munschy, 2000). Testing of these competing models, largely based on indirect geophysical data, requires direct sampling of rocks from the basement of Laxmi Ridge and Laxmi Basin since existing data are not conclusive.

Significant sediment cover overlies the basement of Laxmi Basin, with the oldest parts representing a rifted passive margin sequence. Since the onset of the India/Eurasia collision, the Indus River and its associated tributaries have been the primary source of clastic sediment into the Arabian Sea (Clift et al., 2001), and this Indus-derived sediment likely accounts for most of the postrift sedimentary section targeted during Expedition 355. Far lesser amounts are discharged into the Arabian Sea from mostly small rivers on the steep western margin of India; however, these may have been important sediment sources prior to the India/Eurasia collision and during phases when Indus Fan sediment was being fed to lobes on the western side of the Arabian Basin. The substantial runoff from the Narmada River in central western India (Figure **F1**) is likely to have been buffered by the wide and gently sloping shelf near the margin. This is evident from the thick hydrocarbon-rich sedimentary sequences under the Indian shelf (Biswas, 1987; Gombos et al., 1995), but this river may have been an important supplier at certain times, such as during sea level lowstands.

Much of the present Indus River discharge represents runoff during the summer monsoon rains, enhanced with the seasonal melting of Karakoram and Himalayan glaciers (Garzanti et al., 2005). The Indus Fan covers more than one million square kilometers, stretching ~1500 km into the Arabian Sea from the present delta front. It is the second largest submarine fan in the world and is >10 km thick at the northernmost part (Clift et al., 2002). As the proto-Indus Fan prograded southward, characteristic sediment eroded from the Indus drainage began to accumulate on the distal parts, as observed at Deep Sea Drilling Project (DSDP) Site 221 (Shipboard Scientific Party, 1974; Kolla and Coumes, 1987). The Indus River may have experienced major drainage capture during the Miocene (Clift and Blusztajn, 2005) but has otherwise been stable within the Indus Suture Zone and western syntaxis of the Himalaya since the Eocene.

Drilling can provide erosion records through analyses of the sediment cores, as well as by providing age control for the regional seismic stratigraphy. It is only by quantifying the volume of sediment deposited in the fan that we will be able to mass balance the volume of bedrock eroded from the mountains, constrained by thermochronology, with the volume of eroded rock deposited in the offshore and in the foreland basin.

## Stratigraphic framework

The general stratigraphy of the Indus Fan has already been defined by seismic surveying of the drilling region and the more proximal part of the fan (Figures **F3**, **F4**, **F5**). The youngest unit is characterized by strongly reflective sequences that show small internal onlapping relationships in the vicinity of Laxmi Basin. Complex "cut-and-fill" channel bodies are also visible in this thick uppermost sequence. Closer to the Indus Delta, this sequence is dominated by channel-levee complexes that are typical of deep-water turbidite sequences (Kolla and Coumes, 1987; Clift et al., 2002). Sedimentation was active in such bodies during the Last Gla-

Figure F3. Uninterpreted seismic reflection profile Line W06 (top) and interpreted (bottom) seismic sections with location of Site U1456 (see Figure **F5** for seismic line locations). Orange bar = proposed penetration at Site U1456, white box = actual penetration.

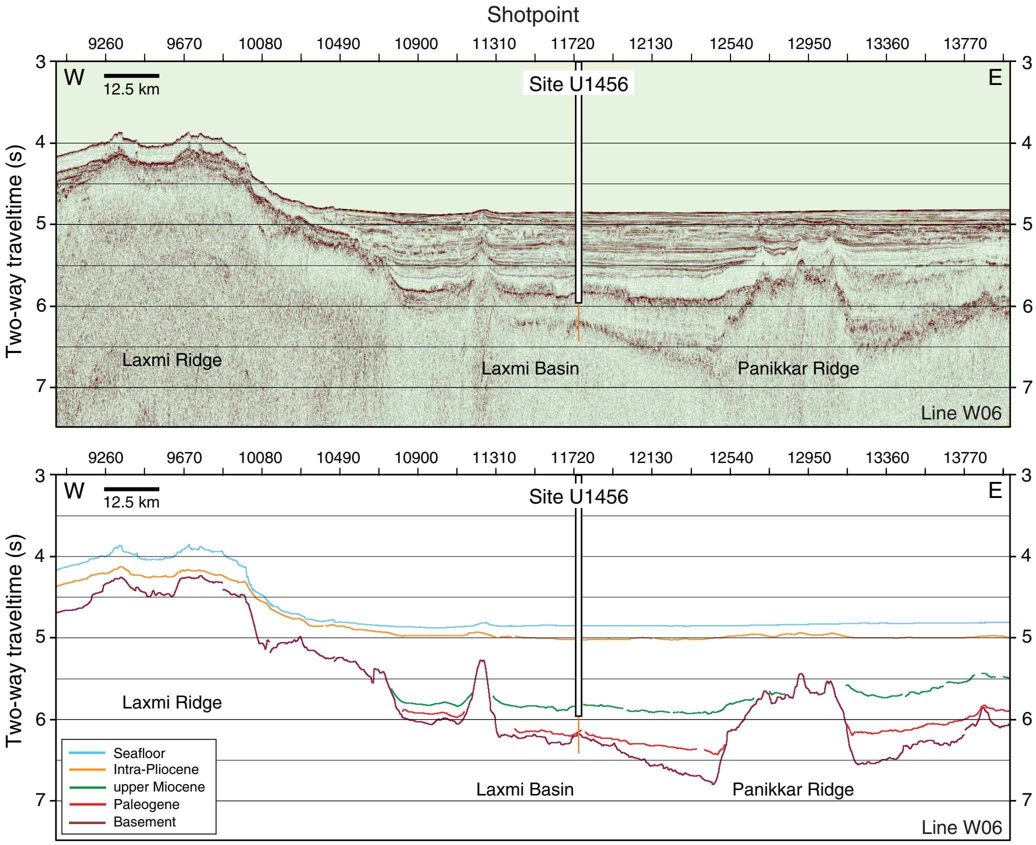

Figure F4. Uninterpreted (top) and interpreted (bottom) seismic reflection profile Line IODP-04 sections with location of Site U1457 (see Figure **F5** for seismic line locations).

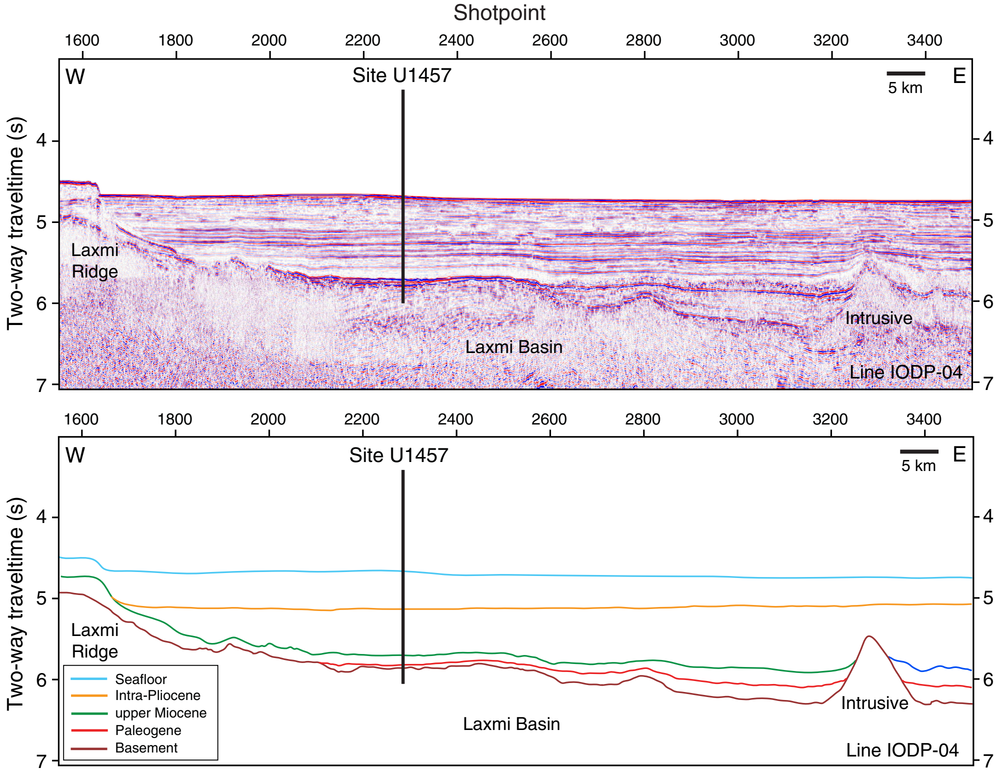

Figure F5. Multichannel seismic grid (orange and red lines) in the eastern Arabian Sea. Blue squares = industry wells, green stars = locations of existing shallow cores. Cores with published data include Core ABP-25 (Gupta et al., 2011); Cores 2491, J7, 2506, and 3268G5 (Bhushan et al., 2001); and Core SK17/MD76-131 (Singh et al., 2011). Red stars = Expedition 355 sites, blue shaded area = area surveyed by high-resolution multibeam bathymetry (see Figure **F7**). RS = Raman Seamount, PS = Panikkar Seamount, WG = Wadia Guyot.

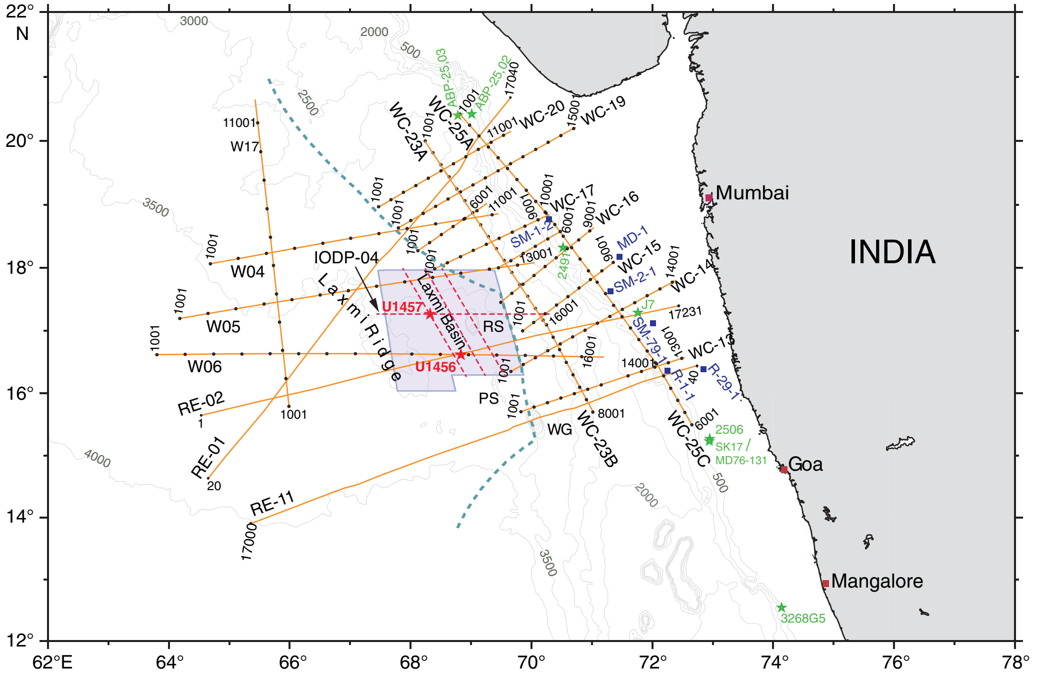

cial Maximum, but the fan has been largely dormant since the start of the Holocene (Kenyon et al., 1995; Prins et al., 2000). This uppermost unit is interpreted to be dominated by siliciclastic turbidites fed from the Indus Delta and interbedded with occasional pelagic carbonate deposits associated with sea level highstands when fluvial sediment was trapped on the shelf. This sequence was termed the

"Indus Fan Megasequence" by Droz and Bellaiche (1991). In the area targeted by Expedition 355, additional sediment may also be derived from the Narmada River and other smaller basins on the west coast of India, as well as even some wind-blown dust from the deserts of Arabia (Figure **F1**).

Toward the northeast, the Indus Fan Megasequence overlies a series of less reflective bedded units that are presumed to represent distal muddy fan deposits. However, in Laxmi Basin, strongly reflective sediment overlies an acoustically transparent unit that thins from north to south and from east to west across Laxmi Basin (Figure **F3**) and is inferred to have been derived from the Indian continental margin. This sequence is interpreted as a large mass transport deposit called the Nataraja Slide and was shed from the shelf edge around the middle/late Miocene boundary (Calvés et al., 2015). It is unclear if the unit significantly eroded the underlying deposits, but its top is rugged in places and inclined so that the Indus Fan Megasequence disconformably overlies it, progressively onlapping over the submarine topography generated by the mass transport deposit as the basin filled. The transparent unit itself has very little in the way of internal patterns or structure but is bounded by very prominent reflectors at the top and base.

The unit underlying the Nataraja Slide is not well bedded or clearly reflective but is also not transparent like the succeeding sequence. This unit, tentatively dated as Eocene–Oligocene in age before drilling, was interpreted as shales and siltstones forming the early, distal Indus Fan. Regional considerations argue that the base of the fan may lie close to the base of the Eocene, below which lies a highly variable, weakly bedded Paleocene unit that infills the rugged basement topography. The unit between the rift onset and breakup unconformities can be clearly identified on the seismic images. This basal unit represents sedimentation during and after rifting along the western continental margin of India. The Paleogene unit thins from east to west and reaches a maximum of ~0.4 s two-way traveltime (TWT) in the central Laxmi Basin just to the east of Site U1456 (Figure **F3**), although it is thinner further north and west near Site U1457 (Figure **F4**). Further west, between Site U1456 and Laxmi Ridge this unit is disrupted by a late-stage igneous intrusion that penetrates well up into the Neogene and Quaternary section. The Paleogene, and indeed much of the younger cover, onlaps against and is cut out entirely against the side of Laxmi Ridge (Figures **F3**, **F4**). The Paleocene is thought to predate fan sedimentation and probably the onset of India/Eurasia collision. However, there is no seismic evidence indicating the base of the fan, implying that the lithologic change may be quite subtle. The source of sediment in the Paleocene is inferred to be dominantly either rift related or from peninsular India to the east.

The lowermost Paleocene section thickens toward the east to a maximum thickness of ~0.4 s TWT near parts of the Panikkar Ridge (Figure **F3**), especially where the ridge is very large. This Paleocene section is ponded away from the basement high underlying the drilled section at Site U1456 and onlaps the basement to the west. The seismic signatures exhibited by this lower Paleocene unit are slightly more reflective than the upper Paleocene section and are associated with early rifting in Laxmi Basin. Although it is difficult to infer its composition, the reflective character compared to the overlying distal Indus Fan sediment and hemipelagic units suggests that it may be composed of coarser grained clastic sedimentary rocks, and possibly volcaniclastic sedimentary rocks, linked to Laxmi Ridge and neighboring seamounts along Panikkar Ridge.

## Seismic studies/site survey data

Extensive 2-D multichannel seismic data from the eastern Arabian Sea (Figures **F5**, **F6**) were utilized to develop a seismic stratigraphic framework. The regional seismic lines run in east–west (coast perpendicular) and northwest–southeast (coast parallel) directions (Figure **F6**). The seismic images exhibit major reflective surfaces from the shelf through the deep Arabian Basin. We identified seismic units through correlation to available lithologic data from industrial boreholes in the vicinity, located on the Indian continental shelf. A high-resolution multibeam bathymetric survey was carried out to map seafloor morphology before selection of the proposed drill sites (Figure **F7**), all of which were located on relatively smooth, muddy seafloor. Three primary and three alternate sites were chosen to meet planned scientific objectives of this expedition, and we ultimately cored at two of these sites, U1456 and U1457 (Figures **F1**, **F2**). A broad seismic network provides good general control on the sediment thickness in the area.

Figure F6. Locations of all seismic profiles (white lines acquired by the Ministry of Earth Sciences, Government of India; black lines acquired by Directorate General of Hydrocarbons, India) in the Arabian Sea. Site U1456 is located on Line W06 and Site U1457 is located on Line IODP-04 (not shown).

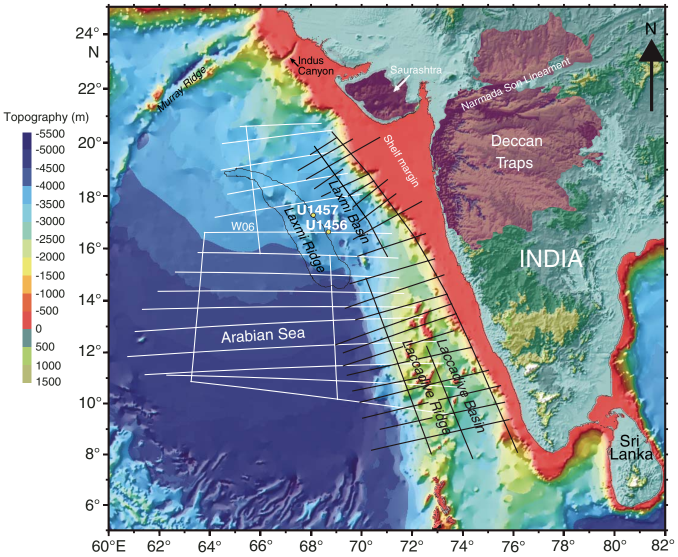

Figure F7. High-resolution multibeam bathymetry data acquired around the Expedition 355 drill sites. Contours (white lines) are in meters below sea level. Black lines are seismic lines with shotpoint numbers around site locations shown in white.

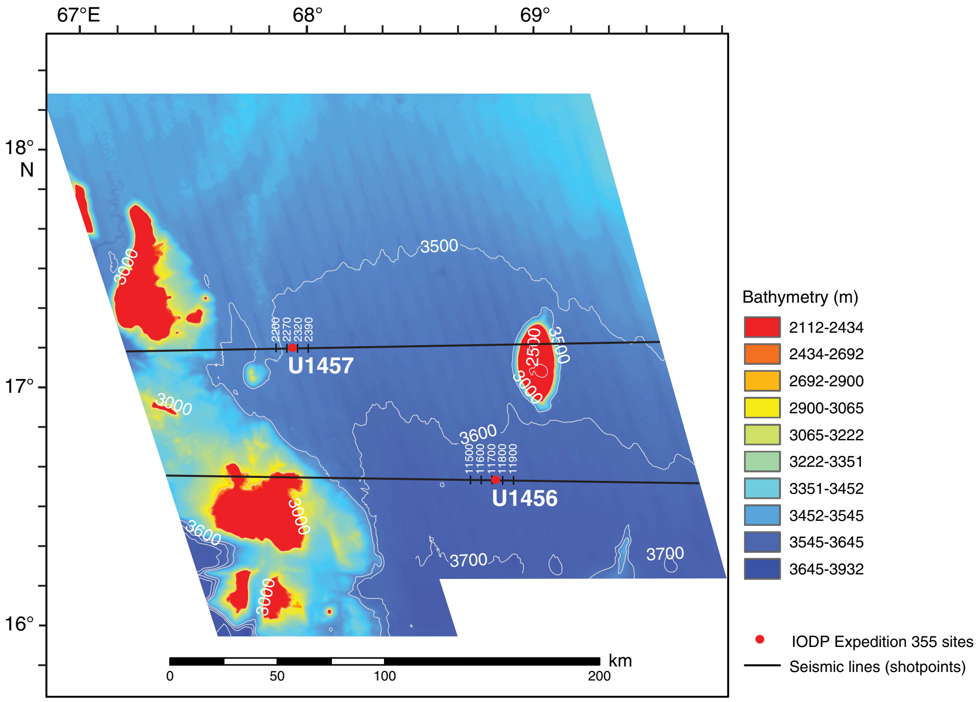

# Scientific objectives

Expedition 355 was designed to drill deep into the Indus submarine fan and sample the underlying basement at two of the sites. The primary objective was to better understand the erosional and weathering response of the western Himalaya, Karakoram, and Hindu Kush to the changing intensity of the southwest Asian monsoon since the onset of the India/Eurasia collision in the early Paleogene. Such interactions lie at the heart of many popular models for Himalayan tectonic evolution, such as the "channel flow" model in which focused erosion, driven by climate (i.e., monsoon), controls the exhumation of deeply buried igneous and metamorphic rocks (Figure **F8**) (Beaumont et al., 2001; Hodges, 2006; Whipple, 2009). If such models are correct, then there should be close coupling among structural evolution of the mountains, climate change, and sedimentation in the Arabian Sea (Clift et al., 2008; Whipple, 2009); however, testing this onshore is impossible because of the large Oligocene unconformity in the foreland that removed most of that record (Najman, 2006). Only in the offshore can continuous, readily dateable erosion records be found. One goal of this expedition was to understand what feedbacks exist among climatic evolution, mountain building, and surface processes in the global-type area for these processes.

In addition, coring the basement of Laxmi Basin should allow dating of the age of continental breakup and so constrain the style of strain accommodation between Laxmi Ridge and the western margin of India. Proximity to the Deccan Traps suggests that this margin could be a volcanic passive margin; however, this depends on the relative timing of rifting and magmatism (Minshull et al., 2008). The role that mantle thermal anomalies, most notably the Réunion Plume, have played in the breakup and subsequent formation of the Indian Ocean and emplacement of the Deccan Traps is crucial. This particular event has implications for biotic mass extinction events, as well as for continental margin tectonics (Courtillot et al., 1988, 1999). Specifically, our objectives were

Figure F8. Depiction of the channel flow model, as described by Beaumont et al. (2001), in which surface processes in the form of erosion driven by focused precipitation along the mountain front allows deep-buried rocks from within the partial melt zone under southern Tibet to be brought to the surface in the Greater Himalaya. Uplift of the Indian foreland is expected to accompany enhanced erosion of the Himalaya, resulting in inversion of the foreland basin and loss of the erosion record onshore during this critical time (Clift and VanLaningham, 2010). STD = South Tibet Detachment, MCT = Main Central Thrust, MBT = Main Boundary Thrust.

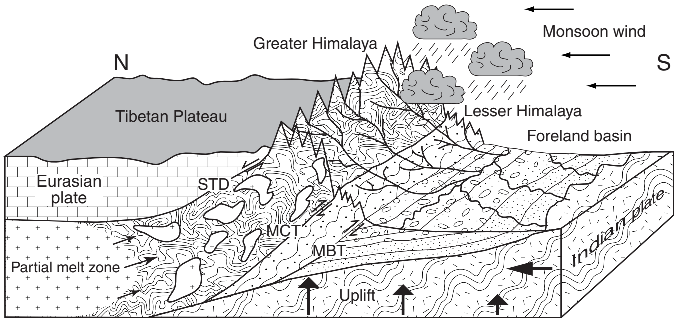

1. *To reconstruct long-term changes in erosion and weathering rates at submillennial to millennial timescales in order to compare with existing records of high-frequency climatic variability.*

Neogene sedimentary sections from the Indus Fan are expected to record the erosional and weathering responses of the Indus drainage basin to changing climate, which has been reconstructed using speleothem (Fleitmann et al., 2003), eolian dust (deMenocal et al., 1991; Clemens and Prell, 2003), and upwelling/productivity records (Kroon et al., 1991; Prell et al., 1992), largely from the Oman margin on the western side of the Arabian Sea. However, these records mostly do not extend back in time before 18 Ma.

Links between climate and erosion on short timescales would be expected if those proposed on longer timescales are correct. Attempts to understand the erosional response of landscape to climate change in southwest Asia have largely been limited to the last glacial cycle (Bookhagen et al., 2005; Dortch et al., 2009; Giosan et al., 2012; Blöthe et al., 2014); however, our sediment cores may permit us to examine the changes spanning many such cycles. Specific questions include whether monsoon intensification causes less or more erosion, and whether this erosion occurs in the Himalaya or other mountainous regions, such as the Karakoram or western Tibet. Does a strengthening monsoon result in more grassland (C4) or woodland (C3) flora? Are phases of increased productivity in the Arabian Sea paralleled by changes in the continental environments onshore, both driven by change in monsoon wind intensity? What role does the westerly jet play in controlling continental environments within the Indus Basin? Could the intensity of chemical weathering linked to monsoon intensity have a role in controlling glacial cycles in the Northern Hemisphere through its role in controlling atmospheric $CO_2$?

Weathering intensity will be reconstructed using bulk sediment geochemical analysis, selected isotope systems (such as Sr), and clay mineralogy. These measurements must be performed in concert with provenance work to establish whether any of the chemical changes could be driven by changes in source composition or drainage capture rather than weathering intensity. Bulk sediment and single-grain provenance methods, including heavy mineral studies, U-Pb dating of detrital zircons, Ar-Ar dating of detrital mica grains, Nd isotopes, and apatite fission tracks represent some of the methods known to be effective in this drainage system that will allow tracking of changing patterns of erosion caused by waxing and waning of the monsoon (Clift et al., 2004; Garzanti et al., 2005; Alizai et al., 2011).

Age control is central to the success of this objective, especially if we are to estimate the lag times between climate change and the sediment record of the deep basin. This is achieved using a combination of biostratigraphy and magnetostratigraphy. Oxygen isotope stratigraphy is also intended to build a high-resolution age model that contributes toward the proposed objectives. Palynology, carbon isotopes, and leaf-wax organic geochemical studies will provide further information on the evolving onshore landscape, as they are known to be effective at making such reconstructions in this region (Budziak et al., 2000; Ponton et al., 2012). The data from our expedition can then be correlated with existing climate records to determine links between erosion and climate on shorter timescales.

2. *To reconstruct changes in erosion and weathering intensity over tectonic timescales and assess whether any changes occurred at ~23, 15, and 10–8 Ma to test earlier hypotheses that invoke changes in monsoon intensity at those times.*

Competing hypotheses exist for the timing of initial monsoon intensification based on a variety of proxies from across Asia, with some invoking the growth of the Tibetan Plateau (Molnar et al., 2010), the rise of the Greater Himalaya (Boos and Kuang, 2010), or the retreat of shallow seas from Central Asia (Ramstein et al., 1997). Unfortunately, most of the existing climate reconstructions do not span tectonic timescales, especially the critical start of Greater Himalayan exhumation and movement along the Main Central Thrust at ~23 Ma (Catlos et al., 2001; Godin et al., 2006; Tobgay et al., 2012). Without a long-term reconstruction of the erosion history, it is impossible to judge which surface processes might control tectonic processes. At the same time, erosion of older sediment from the flood plain, as opposed to directly from the Himalaya, implies that the deep-sea fan sediment can be used to constrain environmental conditions in the drainage basin. These in turn can be used to infer the age of monsoon intensification and test the assumption that stronger monsoon rains change the flora and likely increase rates of chemical weathering, due to higher heat and humidity, which in turn should result in delivery of more altered sediment to the ocean.

Improved understanding of how the monsoon and erosion/weathering interact on short timescales (Objective 1) will allow us to better use the long-term erosion and weathering record to reconstruct monsoon intensity through the Cenozoic. Upper Miocene to recent proxy records of monsoon intensity can be compared to weathering and environmental proxies so that the relationship between the monsoon and weathering can be established. For the period before ~18 Ma we have no independent climate record, and the monsoon intensity for that time will likely be constrained from weathering and erosion records whose interpretation will be ground-truthed in the younger section where both types of reconstruction exist. Many tectonic models for the Himalaya link intensified erosion, driven by stronger summer monsoon rains, to the start of Greater Himalaya exhumation (Hodges, 2006; Harris, 2007; Clift et al., 2008); however, currently no well-dated, high-resolution erosion record spans this critical interval. Available records provide only subepoch resolution (Rea, 1992; Métivier et al., 1999; Clift, 2006), so these models remain untested. Correlating changes in Himalayan-Tibetan tectonics with the marine record of erosion and weathering is the key test for these mechanisms.

Changes in sediment provenance tracked by a variety of bulk and single-grain proxies are needed to identify the focused erosion that is predicted during Greater Himalayan exhumation. The timing of the final unroofing of the Greater Himalaya is also poorly defined (White et al., 2002; Bernet et al., 2006; Najman, 2006; Szulc et al., 2006) and should be indicated by influxes of high-grade metamorphic minerals into the Indus Fan. Seeing whether the arrival of material from the Greater Himalaya coincides with, or likely follows, intensification of the summer monsoon rains would be a critical test of the channel flow and competing orogenic wedge models. Comparison of detrital mineral cooling ages with depositional ages will allow us to assess changing rates of exhumation in Himalaya source regions in order to see how these are linked to climate change. Combining biostratigraphic and magnetostratigraphic studies to generate an integrated high-resolution chronostratigraphy will allow the age of these provenance and thermochronologic changes to be fixed.

Determining the age of the base of the Indus Fan is a key objective, as this is only known in distal (and therefore young) locations at present (e.g., DSDP Site 221; Shipboard Scientific Party, 1974). Provenance methods and mass accumulation rates are expected to show when the first detritus sourced from the northern side of the Indus Suture Zone arrived in the Arabian Sea, beyond the tentative finding of before 45 Ma inferred from sediment cored on the Owen Ridge at DSDP Site 224 (Clift et al., 2001). This age would provide an important constraint on the much debated timing of initial India/Eurasia collision (Aitchison et al., 2007; Najman et al., 2010; Wu et al., 2014). This age is of broader significance to Himalayan tectonics than simple local paleogeographic reconstruction because it constrains how much Indian continental crust has been underthrust into the collision zone, since the rate of convergence is well known. Simple comparison of that volume with the size of the Tibetan Plateau will allow us to assess whether horizontal compression can explain all of the strain accommodation since the onset of collision (England and Houseman, 1986; Dewey et al., 1989), or if major “extrusion” of crust as rigid blocks along major strike-slip faults is needed to accommodate the impact of Greater India (Molnar and Tapponnier, 1975; Replumaz and Tapponnier, 2003).

3. *To decipher the nature of basement rocks in Laxmi Basin and constrain the timing of early seafloor spreading and its relationship to the emplacement of Deccan Flood Basalts. Does mantle plume initiation predate or postdate rifting and early spreading?*

We planned penetration of 50–100 m of basement at two sites in order to determine the nature of basement rocks and the age of their formation. Although biostratigraphic and magnetostratigraphic analyses conducted during the expedition will provide an age for the oldest sediment overlying the basement, postcruise radiometric dating, using methods such as $^{40}Ar/^{39}Ar$, will be employed to constrain the age of formation. Because the Deccan Traps have been very precisely dated onshore (Baksi, 1994; Courtillot et al., 2000; Chenet et al., 2008), the relationship between opening of Laxmi Basin and emplacement of the Deccan Traps will be revealed if the basin crust can be dated. This would further improve our knowledge of whether or not, and how far, Deccan Flood Basalts extend offshore (Pandey et al., 2010, 2011). The potential cause behind the failure of rifting in Laxmi Basin to progress to seafloor spreading shortly after the opening in the more clearly oceanic Gop Basin (Yatheesh et al., 2009; Chatterjee et al., 2013) is also not yet fully understood.

Because the precise timing of rifting in Laxmi Basin is unknown (Minshull et al., 2008), the indistinct nature of the magnetic anomalies in the basin leaves open the possibility that it is floored by either slow-spreading oceanic crust (Bhattacharya et al., 1994; Misra et al., 2015) or hyperextended continental crust (Krishna et al., 2006). Geochemical analyses allow the composition of the volcanic rocks to be compared with Deccan Flood Basalts, rift volcanic rocks, and mid-ocean-ridge basalts (MORB) that would have no linkage to a deep-seated mantle plume or other mantle compositional anomalies. Sediment overlying the basement may potentially allow reconstruction of the margin subsidence, which can further be used to look at the thermal state of the mantle under Laxmi Basin during its rifting because positive thermal anomalies drive surface uplift (Sleep, 1990). Many rifted volcanic margins, including those in the Arabian Sea, are characterized by subaerial eruption and rapid subsidence (Calvés et al., 2008). The petrography and geochemistry of overlying sediments, as well as igneous basement rocks, and the seismic stratigraphic information should enable us to build the syn- and postrift history of the Laxmi Basin. If the volcanic sequences of Laxmi Basin are linked to the Deccan Traps, then this would add significantly to their volume and thus to their potential environmental impact and role in the biotic mass extinctions at the Cretaceous/Paleogene boundary (Courtillot et al., 1988; Self et al., 2008). The timing of rifting and bathymetric evolution of Laxmi Basin also has significant implications for precise paleogeographic reconstructions of the Arabian Sea during the Paleogene (Chaubey et al., 2002; Royer et al., 2002), as well as for the lithospheric processes involved in the rift basin formation.

# Principal results

## Site U1456

### Background and objectives

Site U1456 (proposed Site IND-03C), the first site drilled during Expedition 355, lies within Laxmi Basin in the eastern Arabian Sea (16°37.28′N, 68°50.33′E) in 3640 m of water (Figure **F2**). The site is situated ~475 km west of the Indian coast and ~820 km south from the modern mouth of the Indus River, which is presumed to be the primary source of sediment to the area, at least since the Neogene and likely since the Eocene (Clift et al., 2001).

Laxmi Basin is flanked to the west by Laxmi Ridge and to the east by the Indian continental shelf (Figures **F1**, **F2**). The nature of the crust in Laxmi Basin has been the subject of vigorous debate. Some workers have proposed that it is stretched continental crust (Miles et al., 1998; Todal and Edholm, 1998; Krishna et al., 2006) based on the reduced crustal thickness in Laxmi Basin (~6–7 km) compared to the neighboring thicker crust on either side (as thick as 17 km under Laxmi Ridge [Misra et al., 2015] and ~40 km under peninsular India [Singh et al., 2015]). In this view, Laxmi Ridge would be a continental fragment rifted from peninsular India (Naini and Talwani, 1983; Talwani and Reif, 1998; Minshull et al., 2008). In contrast, some workers interpret Laxmi Basin to be of oceanic affinity based on asymmetrical magnetic anomalies within the basin (Figure **F2**). Such a model relates these magnetic anomalies to the early phases of seafloor spreading in the Arabian Sea (Bhattacharya et al., 1994; Pandey et al., 1995), which removed a microcontinental Laxmi Ridge block from mainland peninsular India. In this case, Laxmi Basin would be more similar to its along-strike equivalent in the Gop Rift to the northwest.

Since the time of continental breakup in the Late Cretaceous–early Paleocene, Laxmi Basin has been largely tectonically inactive because seafloor spreading migrated away toward the southwest of Laxmi Ridge (Royer et al., 2002). The seismic data from this region suggest that the process of gradual postrift thermal subsidence may have been interrupted by the emplacement of localized magmatic intrusions. Nevertheless there has been no strong deformation of the basin since the end of extension, estimated to be prior to ~65 Ma based on magnetic anomalies within the basin (Bhattacharya et al., 1994), or before 63 Ma based on the timing of onset of seafloor spreading west of Laxmi Basin (Chaubey et al., 2002). Laxmi Basin, separated from the main Arabian Sea by the high topography of Laxmi Ridge, has nevertheless been supplied by sediment from the Indus River and forms the easternmost part of the Indus submarine fan, the second largest such sediment body in the modern oceans. Proximity to peninsular India means that the basin has been the recipient of some sediment discharged from rivers flowing to the west coast of the subcontinent, most notably the Narmada and Tapti Rivers (Figure **F1**), although their discharge is much less than that of the Indus River. Milliman and Syvitski (1992) estimated 125 × $10^6$ ton/y for the modern Narmada River versus 250 × $10^6$ ton/y for the Indus River, although some studies estimate premodern Indus discharge as high as 675 × $10^6$ ton/y (Ali and de Boer, 2008)

Site U1456 is the focus of several scientific objectives central to Expedition 355. Sampling and dating the base of the Indus Fan is a primary objective of this expedition. The proposed deep penetration at Site U1456 was aimed at revealing the Cenozoic evolution of the Indus Fan with the intention of reconstructing the weathering and erosion history of the western Himalaya. Sediment recovered at this site should allow us to reconstruct patterns and rates of erosion, as well as to constrain how and when continental environmental conditions changed (e.g., humidity and vegetation patterns) in the Indus drainage since the onset of the India/Eurasia collision. In particular, we aimed to test the hypothesis that the exhumation of the Himalaya was driven by the changing strength of summer monsoon precipitation. For instance, increased erosion along the southern flank of the Tibetan Plateau in response to a stronger monsoon rainfall allowed the Greater Himalaya to be exhumed (Clift et al., 2008). Direct coupling of erosion rates and exhumation is a prediction of the popular channel flow model for Himalaya evolution (Beaumont et al., 2001; Hodges, 2006). Such coupling would also be applicable to some tectonic wedge models for structural evolution (Robinson et al., 2006) and is not unique to the Himalaya (Willett, 1999). Because Site U1456 is located in the distal fan and we estimated reasonably high sedimentation rates based on seismic ties to industrial wells with age control on the outer western continental shelf of India, the site was also designed to document high-resolution changes in weathering, erosion, and paleoenvironment during the Quaternary that can be related to millennial-scale monsoonal changes linked to insolation and ice sheet–related forcing.

In addition to the objectives related to Cenozoic evolution of the Indus Fan, drilling Site U1456 was also planned to address questions pertaining to the nature of the basement of Laxmi Basin. In order to test the hypotheses of whether Laxmi Basin is oceanic or continental, we need to directly sample the basement underlying the basin. The type of basement has significant implications for the breakup history of India and the Seychelles. In addition, analyses of sediment retrieved from Laxmi Basin will allow us to constrain depositional conditions in a rifted basin. Such sediment may be used to reconstruct vertical tectonic motions and so determine the response of the lithosphere to the syn- and postrift tectonic stresses associated with continental breakup.

At Site U1456, we planned to core to ~100 m into basement through the base of the Indus Fan to address the primary expedition objectives. However, we were forced to terminate coring in the deepest hole of this site at ~1109 mbsf (Figure **F9**), well above the target depth of ~1590 mbsf because of technical difficulties encountered when drilling through complex lithologies within a Miocene mass transport deposit. The cored interval at Site U1456 includes an expanded section of upper Miocene to recent strata punctuated by several hiatuses (Figure **F10**). Nonetheless, using the sediment samples and data generated at this site, we should be able to address the questions related to changes in the monsoon at ~8 Ma, as well as how monsoon intensity varied after the onset of Northern Hemisphere glaciation. In addition, we cored through ~350 m of a mass transport deposit that likely represents the second largest known deposit of this type in the geological record on a passive margin (Calvès et al., 2015). Studies focused on this interval will help to identify the source of these deposits, as well as examine how such large deposits are emplaced, and may help us to understand the mechanism through which they are formed.

## Operations

After a 941 nmi transit from Colombo, Sri Lanka, the vessel stabilized over Site U1456 at 1054 h (UTC + 5.5 h) on 9 April 2015. We cored five holes at Site U1456. The original operations plan called for three holes: the first to advanced piston corer (APC) refusal, followed by a second APC hole with extended core barrel (XCB) coring to ~650 mbsf. The third hole was a planned reentry of the hole including 650 m of casing, followed by coring to a total depth of ~1590 mbsf, which included 100 m of basement. The plan was modified to include a short APC hole for high-resolution microbiological and geochemical sampling of the upper ~30 m of section (Table **T1**).

When APC refusal was reached at a much shallower depth than anticipated (~140 mbsf), we opted to deepen Hole U1456A using the half-length APC (HLAPC). Because of good hole conditions, we continued coring in Hole U1456A with the XCB to 426.6 mbsf when the XCB cutting shoe detached and was left in the hole, forcing us to abandon the hole. Hole U1456B was cored with the APC to 29.1 mbsf. We then cored Hole U1456C with the APC and HLAPC to 221.6 mbsf, drilled ahead without coring to 408.0 mbsf, and then continued coring with the XCB to 465.2 mbsf. We terminated coring operations in Hole U1456C when we determined that the lithology at 465.2 mbsf would be ideal for the base of the casing for our deep hole. After conditioning the hole for logging, we conducted three logging runs in Hole U1456C. The triple combo tool string was run first without the radioactive source to 465 m wireline depth below seafloor (WSF), and then the Formation MicroScanner (FMS)-sonic tool string was run to 465 m WSF with two upward passes. The last logging run was made with the triple combo tool string with the radioactive source after the hole was determined to be in good condition.

In Hole U1456D, we drilled-in a 10¾ inch casing string to 458.8 mbsf and then began coring with the rotary core barrel (RCB) coring assembly. When we reached 1024.2 mbsf, we pulled out of the hole for a bit change; however, we encountered difficulties reentering the hole. The drill string became stuck in the open hole below the casing and ultimately had to be severed, effectively terminating the hole. We then decided to install a longer 10¾ inch casing string to 748.2 mbsf in Hole U1456E, drill without coring to 970 mbsf, and then continue to RCB core to 1109.4 mbsf. We pulled out of the hole for a bit change and again encountered difficulties trying to trip the drill string back to the bottom of the hole. After little progress was made to advance the bit over a 12 h period and several instances of the drill string getting temporarily stuck, we decided to terminate the hole and end operations at Site U1456. The total time spent on Site U1456 was 885 h (36.9 days).

A total of 197 cores were collected at this site. The APC coring system was deployed 35 times, recovering 276.91 m of core over 301.9 m of penetration (92% recovery). The HLAPC was deployed 72 times, recovering 287.55 m of core over 334.8 m of penetration (86% recovery). The XCB coring system was deployed 13 times, recovering 44.58 m of core over 94.3 m of penetration (47% recovery). The RCB coring system was deployed 77 times, recovering 401.63 m of core over 705.0 m of penetration (57% recovery).

## Principal results

The cored section at Site U1456 is divided into four lithologic units based on a compilation of Holes U1456A through U1456E (Figure **F9**). Lithologic Unit I consists of an ~121 m thick sequence of Pleistocene light brown to light greenish nannofossil ooze and foraminifer-rich nannofossil ooze interbedded with clay, silt, and sand. The sand layers show normal grading and sharp erosive bases and are interpreted as distal basin plain turbidites. The hemipelagic nannofossil ooze and nannofossil-rich clay show intense bioturbation and also include common pyrite concretions. Quartz, feldspar, and mica grains are common in Unit I. Heavy minerals are rare in abundance but include hornblende, kyanite, tourmaline, augitic clinopyroxene, apatite, and glauconite.

Figure F9. Lithostratigraphic and physical properties (Holes U1456A and U1456C–U1456E) summary for cored section, Site U1456. Downhole measurements are from Hole U1456C. WRMSL core data (dots): green = GRA bulk density, blue = magnetic susceptibility, purple = *P*-wave velocity. Red dots = core logger NGR. Black dots = discrete MAD bulk density and *P*-wave caliper (*x*-axis) data. Gray lines = downhole measurements from end of pipe at ~81 mbsf. Natural gamma ray (in gAPI) plotted from downhole measurements continuously from open hole, through pipe to seafloor.

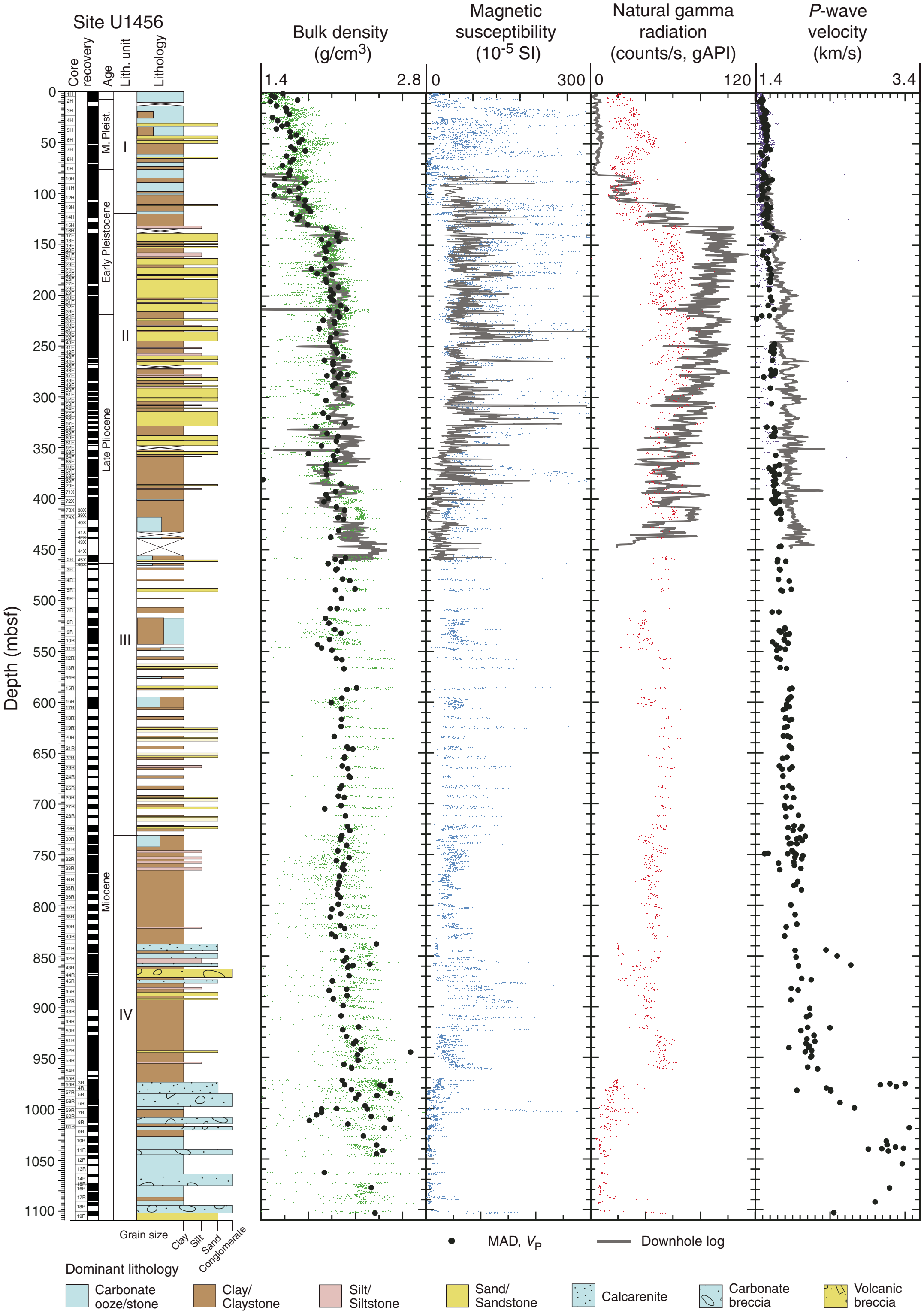

Lithologic Unit II is ~240 m thick and is dated to the late Pliocene to early Pleistocene using biostratigraphy and magnetostratigraphy. The unit consists mainly of massive dark grayish to blackish sand and silt interbedded with thinly bedded nannofossil-rich clay. This sediment also shows normal grading and common sharp erosive bases, which are interpreted as a series of turbidites, likely deposited in a sheet lobe setting. Unit II contains similar sets of light and heavy minerals as Unit I, although the heavy minerals are more

Figure F10. Age-depth model for Site U1456 created by synthesizing nannofossil and foraminifer bioevents with magnetic chron assignments. Top = last occurrence, base = first occurrence.

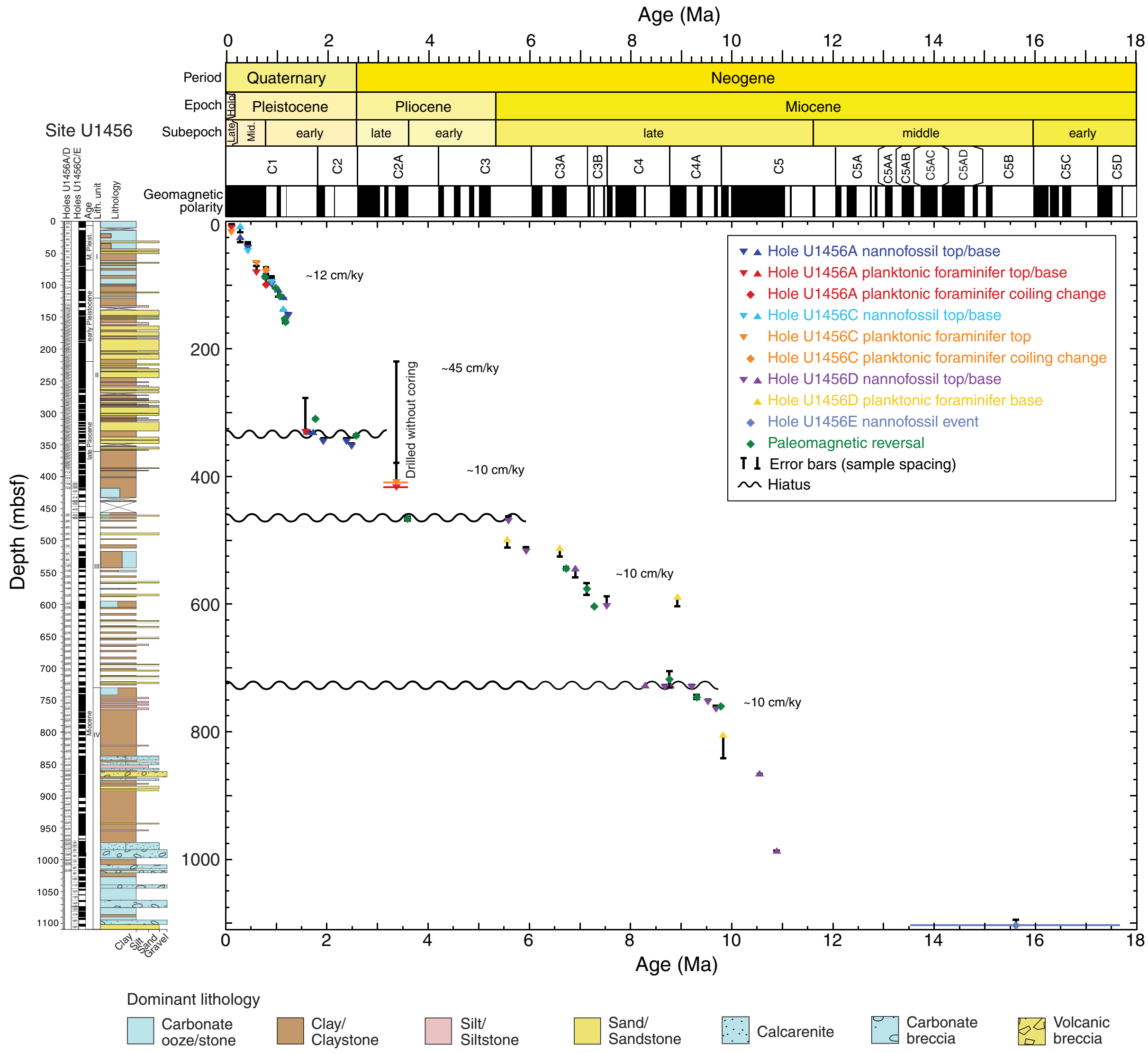

abundant in this unit. The presence of diagnostic high-pressure sodic amphiboles (glaucophane) and pink-green hypersthene is distinctive of Unit II and indicative of erosion from the Indus Suture Zone. The most likely source of glaucophane is blueschists exposed along the Main Mantle Thrust in the suture zone in Kohistan (Anczkiewicz et al., 2000) and these would have to be delivered to the main stream by the Swat and Kabul Rivers from the west.

Upper Miocene to upper Pliocene lithologic Unit III is ~370 m thick and mainly consists of semi-indurated to indurated light brown to dark green clay/claystone, light brown to dark gray sand/sandstone, light greenish nannofossil chalk, and light to dark greenish gray nannofossil-rich claystone. Clay/claystone and sand/sandstone cycles of sedimentation are separated by intervals dominated by nannofossil chalk and nannofossil-rich claystone. Sand layers typically have sharp erosive bases and normal grading into the clay-rich intervals. Low recovery in this unit makes it harder to assign a depositional setting, but the turbidites may have been deposited in a sheet lobe. The lower part of Unit III contains common wood-rich layers (as thick as ~1 cm). Bioturbation is mostly limited to intervals of nannofossil chalk and nannofossil-rich claystone. The mineral assemblage of the silt fraction observed under the microscope is similar to that of Unit II, but heavy mineral abundances are different in the clay fraction. The assemblage is typical of erosion from the Greater Himalaya (Garzanti et al., 2005), although glaucophane is not observed.

Miocene lithologic Unit IV is ~380 m thick and consists of a mixture of interbedded lithologies dominated by dark gray massive claystone, light greenish massive calcarenite and calcilutite, and conglomerate/breccia, with minor amounts of limestone, especially toward the base of the unit (Figure **F9**). A variety of deformation structures indicative of mass transport deposits, including microfaults, soft-sediment folds, slickensides, and tilted to vertical bedding, are observed in this unit. The most common minerals in Unit IV are quartz and micas, with trace to very rare occurrences of heavy minerals. Clasts of vesicular volcanic rock and shallow-water limestone in the breccia point to a source on the Indian continental shelf (Biswas, 1987; Whiting et al., 1994), with probable erosion from the Deccan Plateau province. No significant sediment supply

Table T1. Expedition 355 hole summary. DSF = drilled depth below seafloor. APC = advanced piston corer, HLAPC = half-length advanced piston corer, XCB = extended core barrel, RCB = rotary core barrel. **Download table in .csv format.**

| Hole | Latitude | Longitude | Water depth (m) | Penetration (m DSF) | Cored interval (m) | Recovered length (m) | Recovery (%) | Drilled interval (m) | Drilled interval (*N*) | Total cores (*N*) | APC cores (*N*) | HLAPC cores (*N*) | XCB cores (*N*) | RCB cores (*N*) |
|---|---|---|---|---|---|---|---|---|---|---|---|---|---|---|
| 355- | | | | | | | | | | | | | | |
| U1456A | 16°37.2855′N | 68°50.3272′E | 3639.2 | 426.6 | 426.6 | 365.25 | 86 | 0.0 | 0 | 74 | 16 | 54 | 4 | 0 |
| U1456B | 16°37.2851′N | 68°50.3454′E | 3645.0 | 29.1 | 29.1 | 28.79 | 99 | 0.0 | 0 | 4 | 4 | 0 | 0 | 0 |
| U1456C | 16°37.2940′N | 68°50.3366′E | 3638.4 | 465.2 | 275.3 | 215.00 | 78 | 189.9 | 4 | 42 | 15 | 18 | 9 | 0 |
| U1456D | 16°37.2766′N | 68°50.3365′E | 3637.1 | 1024.4 | 565.6 | 319.18 | 56 | 458.8 | 1 | 60 | 0 | 0 | 0 | 60 |
| U1456E | 16°37.2857′N | 68°50.3541′E | 3636.9 | 1109.4 | 139.4 | 82.45 | 59 | 970.0 | 2 | 17 | 0 | 0 | 0 | 17 |
| U1457A | 17°90.9487′N | 67°55.8037′E | 3523.1 | 144.8 | 130.4 | 122.76 | 94 | 14.4 | 3 | 16 | 12 | 4 | 0 | 0 |
| U1457B | 17°90.9485′N | 67°55.7955′E | 3523.5 | 204.7 | 159.4 | 151.19 | 95 | 45.3 | 10 | 23 | 12 | 11 | 0 | 0 |
| U1457C | 17°90.9486′N | 67°55.8121′E | 3522.7 | 1108.6 | 917.0 | 436.96 | 48 | 191.6 | 1 | 97 | 0 | 0 | 0 | 97 |
| | | | Expedition 355 totals: | | 2642.8 | 1721.58 | | 1870.0 | 21 | 333 | 59 | 87 | 13 | 174 |

| Hole | Start | | End | | Time on hole (days) |
|---|---|---|---|---|---|
| | Date (2015) | Time UTC (h) | Date (2015) | Time UTC (h) | |
| 355- | | | | | |
| U1456A | 9 April | 0525 | 13 April | 1235 | 4.30 |
| U1456B | 13 April | 1235 | 13 April | 1825 | 0.24 |
| U1456C | 13 April | 1825 | 18 April | 2050 | 5.10 |
| U1456D | 18 April | 2050 | 3 May | 1630 | 14.82 |
| U1456E | 3 May | 1630 | 16 May | 0230 | 12.42 |
| U1457A | 16 May | 800 | 17 May | 1445 | 1.28 |
| U1457B | 17 May | 1445 | 19 May | 0240 | 1.50 |
| U1457C | 19 May | 0240 | 29 May | 1730 | 10.62 |

from the Indus River is found in this unit, except for a 2 m thick sandstone and claystone bed below the base of the mass transport deposit. This lowermost sequence suggests that an early to middle Miocene Indus submarine fan was active in the area at that time.

Calcareous and siliceous microfossils recovered at Site U1456 are typical of subtropical to tropical assemblages. Diatoms and radiolarians are only found in the mudline and uppermost cores from this site, whereas calcareous nannofossils and planktonic foraminifers occur in varying numbers throughout the succession. Diatoms in the mudline samples are well preserved and consist mainly of coastal species, but these taxa are absent in the cored sediment. Diatoms are sparse and moderately preserved in the uppermost 10 mbsf, and the assemblage includes benthic and freshwater taxa that indicate transport to the site. Radiolarians are very rare but well preserved in the upper 120 mbsf and absent below this depth. Abundance and preservation of calcareous nannofossils and planktonic foraminifers depends on lithology. In general, calcareous nannofossils are moderately to well preserved throughout Site U1456, whereas planktonic foraminifer preservation varies from poor to good. Both groups are common to abundant in Unit I. Nannofossils are sparse and foraminifers are usually absent in the coarse-grained intervals of Units II and III. Reworked Cretaceous and Paleogene nannofossils are common through Units I–III. In lithologic Unit IV, nannofossil and foraminifer abundance varies significantly, from absent to abundant, and the assemblage is characterized by a mixture of Paleogene to early Neogene taxa that hamper age interpretation.

The age model for Site U1456 is based on calcareous nannofossil and planktonic foraminifer biostratigraphy, together with magnetostratigraphy (Figure **F10**). The succession of bioevents indicates that Site U1456 spans the lower to middle Miocene to recent but is punctuated by several hiatuses of varying duration. The Indus submarine fan sediment at the base of the succession below the mass transport deposit contains a nannofossil assemblage characteristic of the early to middle Miocene. The mass transport deposit of Unit IV appears to have been rapidly emplaced in the late Miocene based on the presence of late Miocene nannofossils within two short hemipelagic intervals within the transported unit. After deposition of the mass transport deposit, the sedimentation rate appears to have been relatively consistent in the late Miocene at ~10 cm/ky, although deposition was interrupted for ~0.5 million years between ~8 and 9 Ma. Another hiatus spanning ~2 million years encompasses the Miocene/Pliocene boundary. The sedimentation rate in the late Pliocene to early Pleistocene was again ~10 cm/ky. After a 0.45 million year hiatus, sedimentation rates in the early Pleistocene were much higher (~45 cm/ky) during deposition of Unit II. The sedimentation rate decreased in the late early Pleistocene to recent, averaging ~12 cm/ky.

Geochemical measurements at Site U1456 were designed to characterize the distribution of hydrocarbon gases, sediment geochemistry (including carbon, nitrogen, sulfur, and carbonate contents), and interstitial water compositions. Sulfate concentration in the interstitial water decreases sharply in the uppermost 60 mbsf, indicating anaerobic sulfate reduction. Below the sulfate reduction zone, methanogenesis becomes an important process, which is reflected by an increase in methane concentrations between 60 and 120 mbsf. Methane concentrations decrease to ~2000 ppmv near the boundary between Units I and II (~120 mbsf) and then reach maximum values within Unit II at ~360 mbsf. This pattern could be partly controlled by lithology, with higher gas accumulating in the relatively porous silty sand and silt with sand layers.

Alkalinity and ammonia in interstitial water are produced as byproducts of organic matter degradation in the upper 60 mbsf within the sulfate reduction zone. Increased alkalinity in this interval causes calcium and magnesium to precipitate as carbonate, resulting in decreases in calcium and magnesium concentrations. Manganese concentrations in the interstitial water also decline sharply in the uppermost 70 mbsf within the sulfate reduction zone, where hydrogen sulfide is produced. Total dissolved iron is consistently low over this interval and may be removed, together with manganese, by metal sulfide formation under anaerobic conditions. Silicon concentrations are higher (300–520 μM) in the uppermost 120 mbsf, which may be caused by its release during the dissolution of biogenic silica, consistent with the near-absence of siliceous microfossils over this interval. Barium concentrations in the interstitial water increase from 250 to 450 mbsf, which could suggest high organic matter diagenesis through this interval. Alternatively, barium could also be released through dissolution of barite under low sulfate conditions or through mineral leaching.

Total carbon and $CaCO_3$ contents are variable at this site and vary in concert with each other, indicating that most of the carbon is present as $CaCO_3$. Carbonate content is generally higher in Unit I, particularly in the nannofossil ooze and nannofossil-rich clay (60–80 wt%). Carbonate content is lower (10–30 wt%) in the silt and sand-rich intervals of Unit I and throughout most of Units II and III, which are dominantly siliciclastic. Very high carbonate content (70–90 wt%) below 975 mbsf in Unit IV corresponds to the presence of calcarenite, calcilutite, and limestone. Total organic carbon (TOC) values at Site U1456 mostly vary between 0 and 2 wt%, with a few higher values in Unit IV. We report TOC/total nitrogen (TN) as a preliminary estimate for the source of organic material. In general, the TOC/TN separates predominantly marine (TOC/TN < 8) from predominantly terrestrial (TOC/TN > 12) organic input according to Müller and Mathesius (1999); however, a simple model of the factors influencing TOC/TN ratios is not always applicable. High TOC/TN ratios atypical for algal source organic matter have been measured in organic-rich Mediterranean sapropel layers, upper Neogene sediment from the Benguela upwelling region, Eocene horizons from the Arctic Ocean, and Cenomanian–Turonian black shales (Meyers, 1990; Stein and MacDonald, 2004; Stein et al., 2006; Twichell et al., 2002). In Unit I, three distinct intervals with high TOC/TN (>20), suggestive of predominantly terrestrial sources, correspond to beds of silty sand with nannofossils and silt with sand. In Units II and III, low TOC/TN values suggest predominantly marine to mixed sources of organic matter. Unit IV is characterized by high variability, with very high values within the 930–1018 mbsf interval suggesting predominantly terrestrial input of organic matter. Correlation between TOC and total sulfur provides a further general estimation of the source of organic matter in marine sediment (Berner and Raiswell, 1983) and is consistent with the interpretations based on TOC/TN.

A total of 72 whole-round samples (5–10 cm long) were collected at Site U1456 for microbiological studies. These samples were taken adjacent to interstitial water whole-round samples for comparison with interstitial water chemistry. Samples were mostly preserved for postcruise characterization of the microbial population using DNA/RNA, as well as lipid and cultivation-based studies. Fluorescent microspheres were added to the core catcher sub before the core barrel was deployed during APC coring to use as a contamination tracer. Samples were collected from the exterior, interior, and an intermediate position from each of the whole-round samples to determine the potential extent of contamination. Examination of the microsphere content of these samples was carried out on board and indicates that samples from the exterior contain higher concentrations of microspheres than those from the intermediate position. Microspheres were completely absent in samples from the interior of the cores, indicating no apparent contamination. Some samples were also analyzed for presence of a new microbial community. Sediment from 0–27 mbsf in Hole U1456B contains many specimens of eukaryotic species (fungi) and deep-marine invertebrates (meiofauna). Additional analyses are required to pinpoint the phylogenetic positions of these new taxa, which will be addressed after the cruise.

Paleomagnetic analyses of Site U1456 cores produced a magnetic polarity stratigraphy defined on the basis of inclination data because attempts to orient cores met with mixed success. A composite polarity log was constructed from detailed demagnetization experiments on discrete samples from Holes U1456A, U1456C, and U1456D (Figure **F10**). The polarity log was correlated with some confidence to the geomagnetic polarity timescale with a total of 12 tie points ranging from the Brunhes (Chron C1n; beginning at 0.781 Ma) to the top of Chron C5n (9.786 Ma). In collaboration with biostratigraphic results, we identified three substantial hiatuses. The youngest spanned from within Chron C2n to the top of Chron C2An.1n. The second spanned all of Chron C3n to the top of Chron C3An, and the third eliminated Chron C4n through part of Chron C4r.

Rock magnetic studies were carried out on samples from Holes U1456A and U1456D and point to a complex array of magnetic minerals including iron sulfides (greigite) and iron oxides (magnetite, maghemite, and hematite). No magnetic behavior indicative of goethite was observed. Further study is necessary to determine which minerals are likely detrital (with the potential of constraining weathering on the continent) and which formed during diagenesis.

The physical property data collected for Site U1456 includes *P*-wave velocity, bulk density, magnetic susceptibility, and natural gamma radiation (NGR) on whole-round cores from Holes U1456A–U1456E and additional measurements on split cores and discrete samples including thermal conductivity; shear strength; *P*-wave velocity; porosity; and bulk, dry, and grain densities (Figure **F9**). Acquired data correlate with lithology, composition, and induration of the recovered section. Bulk density, *P*-wave velocity, shear strength, and thermal conductivity generally increase with depth from 0.8 to 2.4 g/cm$^3$, 1500 to 3400 m/s, 10 to 220 kPa (at ~360 mbsf), and 0.8 to 2.0 W/(m·K), respectively, whereas porosity decreases from nearly 80% to 50% at 150 mbsf, and then to ~20% at the base of the recovered section. This indicates that sediment compaction plays a significant role in physical property variations.

Lithologic changes correlate with variations in NGR and magnetic susceptibility, which range from 10 to 80 counts/s and 0 to 400 $\times 10^{-5}$ SI, respectively. Carbonate sediment has low NGR activity (10–35 counts/s average) and low magnetic susceptibility (0 to 20 $\times 10^{-5}$ SI) and is dominant in Unit I and the lower part of Unit IV (deeper than ~975 mbsf) (Figure **F9**). Detrital sediment (such as sand, silt, and clay, or their lithified equivalents) that are abundant in Unit II have much higher average NGR activity (50–80 counts/s), magnetic susceptibility (50 $\times 10^{-5}$ to 150 $\times 10^{-5}$ SI), and bulk density (1.8–2.0 g/cm$^3$) than the sediment of Unit IV. Unit III and the upper part of Unit IV show variable NGR but generally lower and less variable magnetic susceptibility than the other units (Figure **F9**). Grain density varies between 2.75 and 3.0 g/cm$^3$ with no visible downcore trend except for characteristically low and consistent values of 2.7 g/cm$^3$ in the lower part of Unit IV. Shear strength indicates that sediment ranges from soft (0–50 kPa) above 200 mbsf to stiff (150–220 kPa) from 200 to 360 mbsf, below which core material has a shear strength >220 kPa.

Two downhole logging tool strings were run in Hole U1456C, the triple combo (NGR, porosity, density, electrical resistivity, and magnetic susceptibility) and the FMS-sonic (NGR, sonic velocity, and electrical resistivity images) (Figure **F9**). All runs reached the total depth of the hole at 465 m WSF. Borehole log quality was affected by an enlarged borehole above 200 m wireline matched depth below seafloor (WMSF) and large and rapid variations in borehole size were found between 200 and 370 m WMSF. Below 370 m WMSF, the hole diameter was mostly in gauge, with few washed-out zones. Lithologic variations are apparent in the NGR, bulk density, porosity, and magnetic susceptibility logs, and these correlate well with measurements made on the recovered cores from Holes U1456A and U1456C. Density and sonic velocity increases from the top of the logs at ~80 m WMSF to the bottom of the hole are due largely to compaction and cementation with depth (Figure **F9**). Large increases in NGR and bulk density occur between logging Units 2 and 3, which correlates to an increase in grain size from clay to silt and sand. Formation temperature measurements made with the advanced piston corer temperature tool (APCT-3) on Cores 355-U1456A-7H, 10H, and 13H indicate a geothermal gradient of ~57°C/km for the upper ~120 mbsf.

Distinctive changes in color, magnetic susceptibility, NGR, and gamma ray attenuation (GRA) bulk density were used to make hole-to-hole correlations among the sediment from Holes U1456A–U1456C. We constructed a spliced section for Site U1456 from the seafloor to ~142 m core composite depth below seafloor (CCSF). This spliced interval includes the lower Pleistocene (~1.3 Ma) to recent.

We were also able to correlate core data from Holes U1456A and U1456C to wireline logging data collected in Hole U1456C. The NGR signal was sufficiently high that we could make unambiguous correlations between the core data and logs in the interval logged through pipe (0–81 mbsf). Distinctive magnetic susceptibility signals were very useful for correlating cores to the logs between 150 and 450 mbsf.

## Site U1457

### Background and objectives

Site U1457 (proposed Site IND-06B), the second drill site of Expedition 355, lies within Laxmi Basin in the eastern Arabian Sea (17°9.95′N, 67°55.80′E) in 3534 m water depth (Figures **F1**, **F2**). The site is ~490 km west of the Indian coast and ~760 km south from the present-day mouth of the Indus River, which is presumed to be the primary source of sediment to the area, at least since the Neogene and likely since the Eocene (Clift et al., 2001).

Laxmi Basin is flanked to the west by Laxmi Ridge and to the east by the Indian continental shelf (Figures **F1**, **F2**). Site U1457 lies on the western side of the basin at the foot of the slope leading to Laxmi Ridge. The seafloor appears to be relatively flat in the vicinity of Site U1457 (Figure **F2**); however, seismic reflection data show that the basement depth gradually increases to the east away from the site (Figure **F4**). The nature of the crust in Laxmi Basin is an enigma. Some workers have proposed that it is stretched continental crust (Miles et al., 1998; Todal and Edholm, 1998; Krishna et al., 2006) based on the reduced crustal thickness in Laxmi Basin (~6–7 km) compared to the neighboring thicker crust on either side (as thick as 17 km under Laxmi Ridge [Misra et al., 2015] and ~40 km under peninsular India [Singh et al., 2015]). In this view, Laxmi Ridge would be a continental fragment rifted from peninsular India (Naini and Talwani, 1983; Talwani and Reif, 1998; Minshull et al., 2008). In contrast, some workers interpret Laxmi Basin to be of oceanic affinity based on magnetic anomalies reported within the basin. This latter model relates these magnetic anomalies to the early phases of seafloor spreading in the Arabian Sea (Bhattacharya et al., 1994; Pandey et al., 1995), which removed a microcontinental Laxmi Ridge block from mainland peninsular India. In this scenario, Laxmi Basin would be analogous to its along-strike equivalent in Gop Rift to the northwest and Site U1457 would lie seaward of the oldest magnetic anomaly, requiring Laxmi Basin to be floored by oceanic crust.

Since the time of continental breakup at the end of the Cretaceous, Laxmi Basin has for the most part been tectonically inactive as seafloor spreading jumped to the west of Laxmi Ridge after ~62 Ma (Royer et al., 2002) so that the active extension is now far to the southwest along the Carlsberg Ridge. Seismic data from this region suggest that the process of postrift thermal subsidence has been interrupted by localized magmatic intrusions, but there has been no strong deformation of the basin since the end of extension, estimated to be prior to ~65 Ma based on magnetic anomalies within the basin (Bhattacharya et al., 1994) or before 63 Ma based on the timing of the onset of seafloor spreading west of Laxmi Basin (Chaubey et al., 2002).

Although Laxmi Basin is separated from the main basin of the Arabian Sea by the high topography of Laxmi Ridge, it has nevertheless been supplied by sediment from the Indus River and forms the easternmost part of the Indus Fan, the second largest such sediment body in the modern oceans. Proximity to peninsular India means that the basin must have been the recipient of some sediment discharge from rivers flowing to the west coast of the subcontinent, most notably the Narmada and Tapti Rivers (Figure **F1**), although their discharge is much less than that seen from the Indus River. Much of the flux from the Narmada and Tapti Rivers would tend to be ponded on the eastern side or in the central part of the basin rather than at or around Site U1457.

Site U1457 was originally proposed as an alternate site for meeting our basement objectives. The proposed deep penetration at Site U1457 aimed to reveal the Cenozoic evolution of the Indus Fan with the intention of reconstructing the weathering and erosion history of the western Himalaya. However, predrilling seismic interpretation suggested that this record would be truncated compared to that found at Site U1456. Nonetheless, sediment recovered at this site should allow reconstruction of patterns and rates of erosion, as well as constrain how and when continental environmental conditions changed (e.g., humidity and vegetation patterns) in the Indus drainage since the late Miocene. In particular, we aim to test the hypothesis that major changes in the structural evolution of the Himalaya were driven by the changing strength of summer monsoon precipitation. For instance, the southward migration of the main thrust detachment fault to the location of the Main Boundary Thrust after 10 Ma (Meigs et al., 1995) may have accelerated the unroofing of the Lesser Himalayan Duplex (Huyghe et al., 2001; Bollinger et al., 2004) and may be linked to the change in monsoon strength at ~8 Ma. Because Site U1457 is located in the distal fan and we estimated reasonably high sedimentation rates based on seismic ties to industrial wells with age control on the outer western continental shelf of India, the site was also designed to document high-resolution changes in weathering, erosion, and paleoenvironment during the Quaternary that can be related to millennial-scale monsoonal changes linked to solar and ice sheet–related forcing.

Because we were unable to sample the older sediment section and basement at Site U1456, Site U1457 was specifically planned to address questions pertaining to the nature of the basement in Laxmi

Basin. In order to test the hypotheses of whether Laxmi Basin is oceanic or continental, we needed to directly sample the basement underlying the basin, which has potentially significant implications for the breakup history of India and the Seychelles. In addition, analyses of sediment retrieved from Laxmi Basin will allow us to constrain depositional conditions in the basin, which may be used to reconstruct vertical tectonic motions and so determine the response of the lithosphere to the syn- and postrift tectonic stresses associated with continental breakup.

At Site U1457, we planned to core ~50 m into basement after penetrating a series of submarine fan sediments, as well as the large mass transport deposit encountered at Site U1456. Drilling was successful in reaching the basement, although we had time to penetrate only 16.27 m of basement below the sedimentary cover, recovering 8.72 m of basalt (Figure **F11**). The cored section at Site U1457 includes expanded upper Miocene to recent strata punctuated by some hiatuses or condensed sections (Figure **F12**), as well as lower Paleocene sediment directly above basement. A long hiatus separates the Paleocene sediment below from the Miocene sediment above. Nonetheless, using the samples and data generated at this site, we should be able to address questions related to changes in the monsoon at ~8 Ma, as well as how monsoon intensity varied after the onset of Northern Hemisphere glaciation in response to this forcing. This is despite the moderate hiatus that occurs close to this time. In addition, we cored through ~190 m of mass transport deposit that likely represents the second largest known deposit of this type in the geological record (Calvès et al., 2015). Studies focused on this interval and comparisons with the thicker section sampled at Site U1456 will help to identify the source of these deposits, as well as to examine how such large deposits are emplaced, and may help us to understand the causes of this major event.

## Operations

After a 62 nmi transit from Site U1456, the vessel stabilized over Site U1457 at 1330 h (UTC + 5.5 h) on 16 May 2015. The original operations plan called for three holes: the first to APC refusal, followed by a second APC hole with XCB coring to ~500 mbsf. The third hole was planned as a single-bit RCB hole to 50 m into basement, which was estimated at ~970 mbsf. We ultimately cored three holes at Site U1457, although the second hole was cored to a shallower depth than originally planned (Table **T1**).

We reached APC refusal at ~110 mbsf. In order to deepen the hole more quickly, we opted to core a 4.7 m interval with the HLAPC, followed by a 4.7 m advance without coring. In the interest of time, we terminated the hole after reaching 144.8 mbsf. We then cored Hole U1457B for stratigraphic correlation purposes in the upper ~110 mbsf. After reaching APC refusal, we continued with the HLAPC using the coring by advance method to 204.7 mbsf, where we terminated the hole to preserve enough time to reach our objective in the deep hole. Hole U1457C was drilled without coring to 191.6 mbsf and then cored using the RCB to 1108.6 mbsf, which included ~16 m of basement penetration. Hole U1457C was terminated when time allotted for the expedition expired.

A total of 136 cores were collected at this site. The APC coring system was deployed 24 times, recovering 202.73 m of core over 218.9 m of penetration (93% recovery). The HLAPC system was deployed 15 times, recovering 71.22 m of core over 70.9 m of penetration (101% recovery). The RCB coring system was deployed 97 times, recovering 436.96 m of core over 917.0 m of penetration (48% recovery).

## Principal results

The cored section at Site U1457 is divided into five lithologic units based on Holes U1457A–U1457C (Figure **F11**). Lithologic Unit I consists of a ~74 m sequence of Pleistocene light brown to light greenish nannofossil ooze including foraminifer-rich nannofossil ooze and nannofossil-rich clay, interbedded with silty clay and silty sand. Unit I here is similar to Unit I at Site U1456 in being mostly muddy and carbonate-rich. The silty sand layers show normal grading and sharp erosive bases and are interpreted as turbidities. The hemipelagic nannofossil ooze and nannofossil-rich clay show intense burrowing and also include common pyrite nodules and veins. Quartz, feldspar, and mica grains are common in Unit I, whereas heavy minerals (hornblende, clinopyroxene, epidote, garnet, and augite) are rare.

Lithologic Unit II is ~311 m thick and is dated to the early Pleistocene. The unit consists mainly of light brownish gray to dark gray silty clay and dark gray sandy silt. Silty clay layers are typically massive and interbedded with very thin gray sandy silt layers, which are interpreted as turbidites. Unit II at Site U1457 is similar in age to Unit II at Site U1456, but the sediment is much finer grained. Light and heavy silt- to sand-sized mineral grains are more abundant in Unit II compared to Unit I.

Unit III is ~450 m thick and consists of upper Pliocene to upper Miocene semi-indurated to indurated light brown to dark green silty claystone, light brown to dark gray silty sandstone, light greenish nannofossil chalk, and light to dark greenish gray nannofossil-rich claystone. Nannofossil chalk and nannofossil-rich claystone cycles of sedimentation are separated by intervals dominated by clay/claystone and sand/sandstone deposition. Strong bioturbation is mostly observed in the nannofossil chalk and nannofossil-rich claystone. Silty sandstone layers are characterized by sharp erosive bases and grade upward into silty claystone intervals. The silty sandstone and silty claystone of Unit III occasionally have very thin (<1 cm) wood-rich layers, as well as large numbers of tiny wood particles. Unit III contains abundant light minerals with variable amounts of heavy minerals.

Miocene Unit IV is ~225 m thick and consists of a mixture of interbedded lithologies dominated by dark gray to greenish gray massive claystone, light greenish massive calcarenite and calcilutite, breccia, and limestone, particularly toward the base of the unit. Deformation structures are widespread throughout this unit, including microfaults, soft-sediment folds, slickensides, and gently to vertically tilted bedding, which are indicative of a mass transport deposit. Light minerals are abundant in Unit IV, whereas heavy minerals are only present in trace amounts. Clasts of vesicular volcanic rock and shallow-water limestone in the breccia point to a source from the Indian continental shelf, with probable erosion from the Deccan Plateau province.

The ~30 m thick Paleocene Unit V consists mostly of dark brown to dark greenish gray claystone and dark gray to black volcaniclastic sediment that overlies the basaltic basement. There is a major hiatus between Units IV and V determined from biostratigraphy, as well as the change in facies between debris-flow breccia above and mudstone underneath. The dark brown massive claystone shows very small amounts of interbedded dark greenish gray silty claystone. The thick-bedded dark greenish gray claystone contains black, discontinuous manganese layers and nodules, as well as small (1–3 cm) gray inclusions and rare parallel bands that are identified as carbonate-cemented nodules. Unit V contains abundant glass particles, trace amounts of light minerals, and no heavy minerals.

Figure F11. Lithostratigraphic and physical properties (Holes U1457A–U1457C) summary for the cored section at Site U1457. WRMSL core data (dots): green = GRA bulk density, blue = magnetic susceptibility. Red dots = core logger NGR. Black dots = discrete MAD bulk density and *P*-wave caliper (*x*-axis) data. Note log scale for magnetic susceptibility.

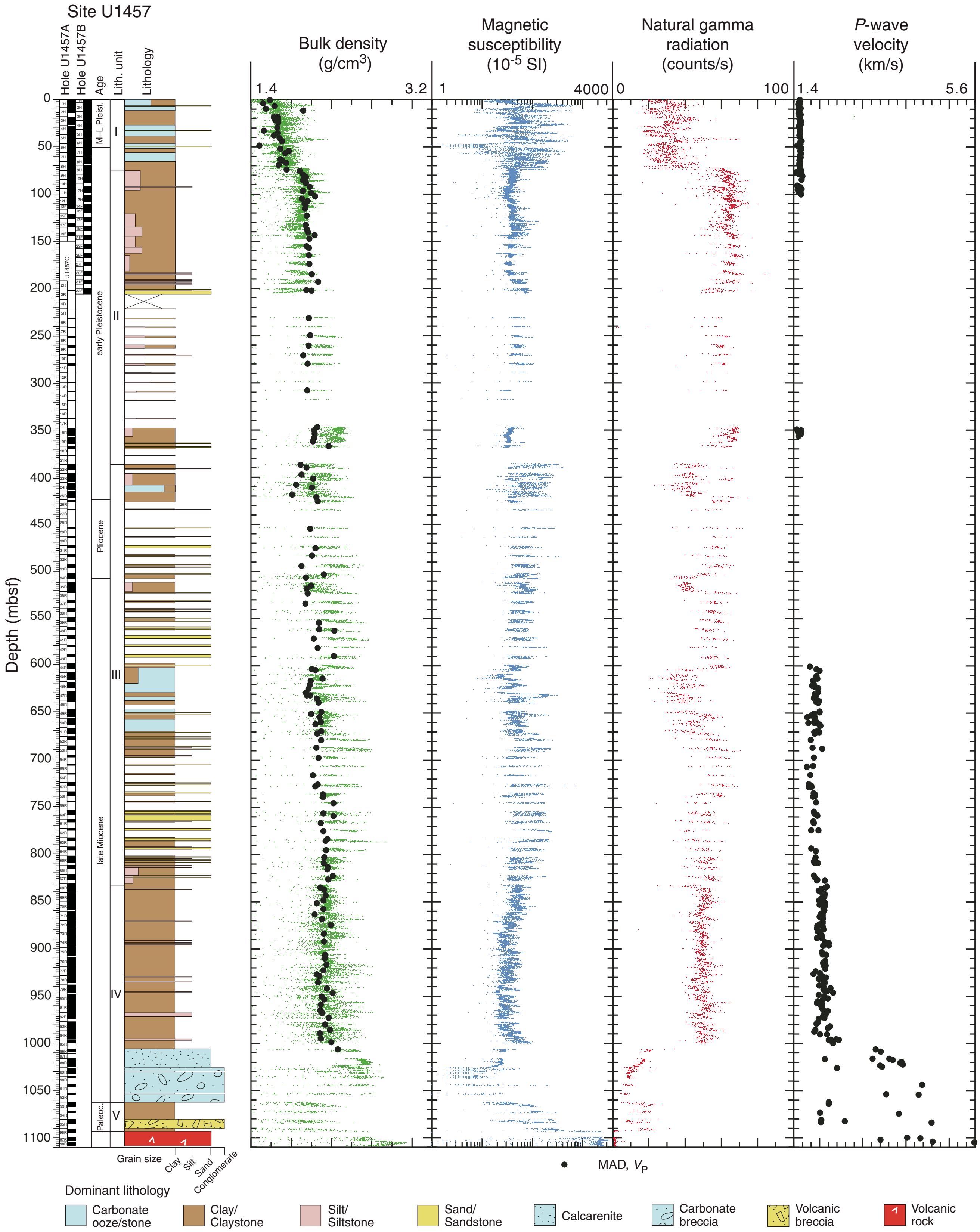

Figure F12. Age-depth model for Site U1457 created by synthesizing nannofossil and foraminifer bioevents with magnetic chron assignments. Note that the age depth model only extends to 1000 mbsf due to a long hiatus near the base of the cored section, with the top of lithologic Unit V at ~1062 mbsf dated to the early Paleocene. Top = last occurrence, base = first occurrence.

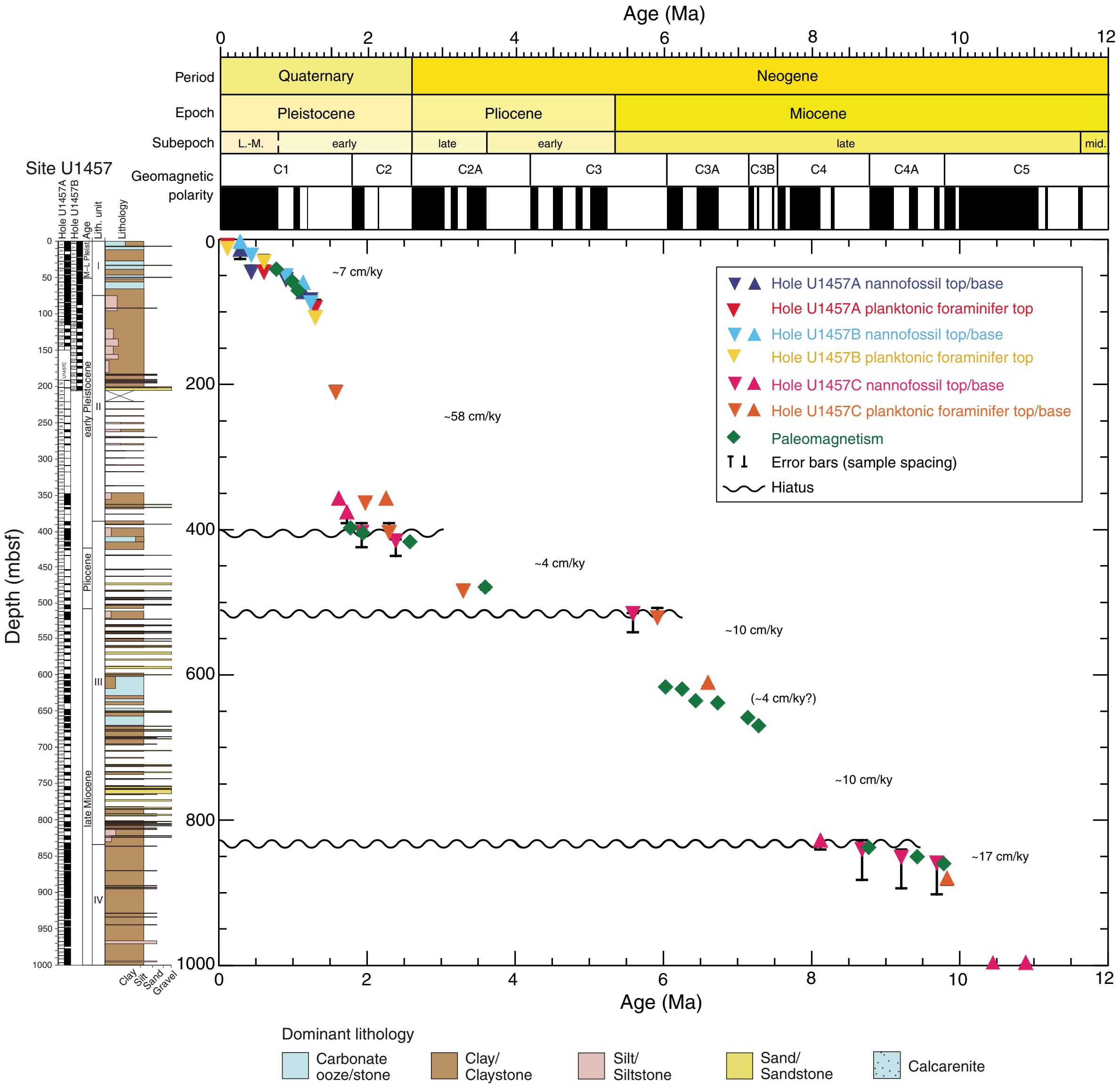

Core catcher samples and additional samples from split core sections at Site U1457 were analyzed for calcareous nannofossils, planktonic foraminifers, diatoms, and radiolarians. Microfossil assemblages are typical of subtropical to tropical water masses. Diatoms and radiolarians are found in the mudline sample in Hole U1457B, where they are well preserved. Diatoms in the mudline sample mainly consist of coastal species that have been transported to the site location. Diatom abundance decreases rapidly downcore, with specimens mostly restricted to the uppermost ~50 cm at Site U1457. Radiolarians are very rare and poorly preserved in the uppermost cores and only occur sporadically below.

Preservation of calcareous nannofossils and planktonic foraminifers varies from poor to good throughout Site U1457. Both groups are abundant in Unit I. Nannofossils are sparse and planktonic foraminifers usually absent in the clay/claystone that dominates Unit II. In Unit III, nannofossils are common in abundance, whereas planktonic foraminifers are less abundant and vary from rare to common. Reworked Cretaceous and Paleogene nannofossils are common through Units I–III. Within Units IV and V, both nannofossils and foraminifers are moderately to poorly preserved and present in varying abundances. There is also an interval characterized by mixed Paleogene to early Neogene taxa that hampers age interpretation within the lower part of Unit IV. Calcareous nannofossils and planktonic foraminifers are common in the uppermost part of Unit V but rapidly decrease in abundance downcore through this unit, which overlies the basement.

The chronostratigraphic framework for Site U1457 is based on calcareous nannofossil and planktonic foraminifer biostratigraphy, together with magnetostratigraphy (Figure **F12**). The succession of calcareous nannofossil and planktonic foraminifer events indicates that Site U1457 spans the early Paleocene through recent, albeit with a very long hiatus (~50 million years) between lower Paleocene and upper Miocene sediment. The biostratigraphic framework established at Site U1457 enables identification of three unconformities and an interval of mass transport in the recovered Neogene section. Calculated sedimentation rates at Site U1457 suggest that the sedimentation rate appears to have been relatively consistent in the late Miocene at ~17 cm/ky, although deposition was interrupted for ~0.50 million years around 8 Ma. Sedimentation rates were somewhat lower after sedimentation resumed following this hiatus, averaging ~10 cm/ky during the remainder of the late Miocene. There is some evidence for a short interval dominated by slower hemipelagic sedimentation between ~6 and 7.4 Ma. There is an ~2 million years hiatus that spans the Miocene/Pliocene boundary and early Pliocene. The sedimentation rate in the late Pliocene to early Pleistocene was ~4 cm/ky. After another ~0.45 million year hiatus in the early Pleistocene, sedimentation rates for the remainder of the early Pleistocene were much higher (~58 cm/ky) during deposition of Unit II. The sedimentation rate slowed down from the late early Pleistocene to present, averaging ~7 cm/ky.

We cored ~16.27 m into igneous basement at Site U1457, recovering 8.72 m of basalt. Texture ranges from aphyric to phyric. The aphyric material occurs in three intervals and consists mostly of altered glass. Phenocrysts vary from being absent to making up as much as 10% of the rock and are composed of clinopyroxene, plagioclase, and olivine. Phenocryst grain size ranges from 1 to 5 mm, with a mode of ~3 mm. The groundmass is mostly aphyric and may contain mesostasis. The basalt is nonvesicular and massive with calcite-filled veins up to 3 mm in width and of variable lengths. These rocks are classified as clinopyroxene-plagioclase-phyric basalt and plagioclase-clinopyroxene-phyric basalt, with the former the more dominant lithology. The basalt is only slightly altered. Geochemical analyses performed after the expedition demonstrate that these rocks are Mg-rich, low-K subalkalic tholeiitic basalts that are similar to melts of primary mantle source.

Geochemistry measurements at Site U1457 aimed at characterizing the distribution of hydrocarbon gases, sediment geochemistry (including carbon, nitrogen, sulfur, and carbonate contents), and interstitial water composition. Sulfate concentration in the interstitial water decreases sharply in the upper 60 mbsf, indicating anaerobic sulfate reduction. Below the sulfate reduction zone, methanogenesis is likely active, reflected by a peak in methane concentrations between 65 and 200 mbsf. A second interval of methane increase is observed between 400 and 550 mbsf, which correlates with Unit III. Higher TOC values through this interval are indicative of lithologic control on the methane concentrations. Below 590 mbsf, methane levels do not exceed 10,000 ppmv and progressively decrease with depth.

Alkalinity and ammonia in interstitial water are produced as byproducts of organic matter degradation in the upper 60 mbsf, within the sulfate reduction zone. Increased alkalinity in this interval helps to precipitate calcium and magnesium in carbonate minerals, resulting in a decrease in calcium and magnesium concentrations. Manganese concentrations in the interstitial water also decline sharply in the uppermost 60 mbsf within the sulfate reduction zone, where hydrogen sulfide is being produced as a result of anaerobic organic oxidation reactions. Dissolved iron concentrations are low and decrease downhole, suggesting its removal from the interstitial water through metal sulfide formation under anaerobic conditions. Silicon concentrations are high in the uppermost 110 mbsf, which may be caused by its release during the dissolution of biogenic silica, which is consistent with the near-absence of siliceous microfossils in this interval. Barium concentrations in the interstitial water increase somewhat between 600 and 850 mbsf, which could be a result of its release through barite dissolution under low-sulfate fluid conditions or through the leaching of aluminosilicate minerals.

Total carbon and $CaCO_3$ contents are highly variable at Site U1457 and are tightly coupled, indicating that most of the carbon is present as $CaCO_3$. Carbonate content is generally higher in Unit I, particularly in the nannofossil ooze and nannofossil-rich clay (20–75 wt%) intervals. A decrease in carbonate content downcore from Unit I and Unit II reflects a transition to lithologies that are dominantly siliciclastic. Carbonate-rich intervals (33–47 wt%) in Unit III correspond to intervals of nannofossil ooze. TOC values at Site U1457 vary between 0.02 and 2.58 wt%. As with Site U1456, we report TOC/TN as a preliminary estimate for the source of organic material. Typically high values (TOC/TN > 12) in marginal basins are interpreted as an indicator of terrestrial organic input (Müller and Mathesius, 1999). However, an alternative model to explain high TOC/TN ratios, such as those observed in some organic carbon-rich marine sediments (e.g., sapropels and black shales), invokes marine algae synthesizing lipid-rich organic carbon during times of abundant nutrient supply and/or diagenetic factors (Meyers, 1997). In Unit I, three distinct intervals with high TOC/TN (>12) correspond to beds of carbonate ooze. The dominantly hemipelagic nature of this lithology precludes confident assignment of the high TOC/TN values to terrestrial input and awaits further shore-based analysis. Intermediate TOC/TN values (4.5–11.4) suggest mixed marine-terrestrial organic input in Unit II and the upper part of Unit III. Low TOC/TN values (0.3–8.7) in Unit IV suggest predominantly marine organic matter input. Due to time constraints, shipboard analysis of samples from Unit V and the igneous basement were not conducted.

A total of 12 whole-round samples (5 cm long) were collected for microbiological studies at Site U1457. All samples were collected adjacent to interstitial water whole-round samples for comparison with geochemical analyses. After collection, samples were immediately flushed with $N_2$ and processed for shipboard analysis or preserved for shore-based analyses. Fluorescent microspheres were used as tracers during APC operations to help determine contamination in microbiology samples. Microsphere samples were collected from the exterior and interior of each core, as well as a location in between. Microspheres were completely absent in samples from the interior of the cores, indicating no apparent contamination. Samples from intermediate positions contained a low concentration of microspheres, and the presence of significant numbers of microspheres in exterior samples is a strong indication of surface contamination to the outside of the core during the coring process.

We analyzed some samples on board for microbial community structure. The direct microscopic observation of the core samples found different kinds of meiobenthos in sediment from Site U1457. Preliminary results of microbial community structure and enumeration show that fungal communities are present at very low concentrations in samples from 0 to 100 mbsf. Those fungi living in the subsurface form diverse communities and interactions with other living organisms. While surveying for possible symbioses between fungi and meiobenthos, we found abundant assemblages in certain zones showing that these may follow trends related to the carbon, nitrogen, and sulfur cycles. Shore-based molecular studies are required to support the evidence of their relationship and to pinpoint exactly the phylogenetic positions of these potentially new extremophiles.

At Site U1457 we performed paleomagnetic analyses on archive-half sections from Holes U1457A and U1457B and on discrete samples from all holes. Archive-half section measurements produced reliable results for the upper ~60 mbsf; results were more ambiguous in the deeper sections. Discrete samples were fully demagnetized by alternating field treatment, and the inclination of the magnetization's stable component was used to define the magnetostratigraphy. A composite polarity log was constructed from the three holes and correlated with some confidence to the geomagnetic polarity timescale with at least 16 tie points, which range from the Brunhes (Chron C1n; beginning at 0.781 Ma) to the top of Chron C5n (9.786 Ma).

Using the combination of magnetostratigraphy and biostratigraphic data, we identified three substantial hiatuses or condensed sections. The early Matuyama (much of Chron C2r) and the top of the Gauss (Chron C2An) may be missing or are condensed. Chrons C3n and C4n are completely missing. Similar to Site U1456, there is an "extra" subchron that is not in the official timescale, which is located between the Cobb Mountain (Chron C1r.2n) and the Olduvai (Chron C2n). The identity of this subchron (which could be the Garder [1.472–1.48 Ma] or the Gilsa [1.567–1.575 Ma] according to Channell et al. [2002]) could help constrain the age model during this interval of very rapid sedimentation.

Paleomagnetic data from the lowermost sediment cores are well behaved, with an average inclination of 39°. If these are indeed Paleocene in age, they are reversely magnetized and translate to a paleolatitude for the site of ~22°S, which is in reasonable agreement with a paleolatitude between 16°S and 25°S for 60–65 Ma (Besse and Courtillot, 2002).

The physical property data collected for Site U1457 includes bulk density, *P*-wave velocity, magnetic susceptibility, and NGR on whole-round cores from Holes U1457A–U1457C and additional measurements on split cores and discrete samples including thermal conductivity; shear strength; *P*-wave velocity; porosity; and bulk, dry, and grain densities (Figure **F11**). Acquired data correlate with lithology, composition, and induration of the recovered section. Bulk density, *P*-wave velocity, and thermal conductivity generally increase with depth from 1.4 to 3.0 g/cm$^3$, 1500 to 5600 m/s, and 1 to 2.6 W/(m·K), respectively, whereas porosity decreases from ~80% to 50% in the upper 100 mbsf, and then to ~20% at the base of Unit IV. Shear strength varies between 10 and 70 kPa in the upper 150 mbsf, indicating that the sediment is soft and uncompacted.

Generally, the changes in physical properties are gradual, indicating that sediment compaction plays a significant role in physical property variations (Figure **F11**). However, shifts in porosity, bulk density, and thermal conductivity are seen between lithologic units, demonstrating the influence lithology has on physical properties. For example, between Units I and II, lithology changes from soft carbonate ooze and clay to detrital silt, clay, and sand, resulting in increases in bulk density and thermal conductivity and a decrease in porosity. NGR also increases across this boundary (from ~30 to ~60 counts/s), whereas magnetic susceptibility becomes less variable and is generally lower in Unit II compared with Unit I. At the base of Unit IV below 1000 mbsf, *P*-wave velocity abruptly increases to values up to 4300 m/s, reflecting the occurrence of high-density calcarenite and breccia, which contrasts with lower values for the overlying claystone (2000 m/s). NGR and magnetic susceptibility dramatically decrease over this same interval. A return to lower bulk density (~2.0 g/cm$^3$) and *P*-wave velocity (~2000 m/s) occurs within Unit V above the igneous rock at the base of Core 355-U1457A-96R. The recovered basalt has characteristically high bulk densities (~2.6 g/cm$^3$), magnetic susceptibility (~3000 instrument units), and *P*-wave velocities (4500–5500 m/s) but low NGR (~1 count/s). A geothermal gradient of 53°C k/m for the upper ~100 m was estimated from the APCT-3 measurements taken on Cores 355-U1457A-4H, 7H, and 10H.

Distinctive changes in color, magnetic susceptibility, NGR, and GRA bulk density were used to make hole-to-hole correlations between the sediment in Holes U1457A and U1457B. Correlations were limited to these two holes because there was minimal overlap with the cored section of Hole U1457C, and there was no opportunity for wireline logging. We constructed a spliced sediment section for Site U1457 from cores recovered from Holes U1457A and U1457B. The splice is good down to ~88 m CCSF or ~1.2 Ma. With appended cores, the Site U1457 splice was extended to 123.55 m CCSF. Profiles in the spliced section of Site U1457 of magnetic susceptibility change (clay content) and color change ($CaCO_3$ variations) are similar to those at Site U1456. Initial age correlations support the hypothesis that lithostratigraphic correlations between the two sites may also be chronostratigraphic.

# Expedition synthesis

Two sites were drilled during Expedition 355 (31 March–31 May 2015) in the central and western parts of Laxmi Basin in the eastern Arabian Sea, Indian Ocean. Laxmi Basin separates the Indian continental shelf in the east from Laxmi Ridge in the west. Site U1456 lies within Laxmi Basin and was cored into the lower–middle Miocene. The second site, U1457, penetrated through the sediment column into igneous basement in the transition zone between Laxmi Basin and Laxmi Ridge. In total, we recovered 1712 m of sediment and sedimentary rock, as well as 8.72 m of igneous basement. We further collected downhole wireline logs at Site U1456 using the triple combo and FMS-sonic tool strings. We present here the initial findings of our analyses of these materials and data, which provide (1) an improved understanding of how the Indian Ocean first began to drift as India separated from the Seychelles and (2) partial constraints on erosion in the source regions that have supplied sediment into the Arabian Sea since that time. Much of the recovered sediment was derived from the Indus River, and this provides us with an opportunity to document the weathering and erosional responses of the western Himalaya to changes in monsoon strength during the time periods represented by the recovered intervals, largely during the latter parts of the Neogene. We also collected sediment that provides information about erosion and mass transport from the western continental margin of India.

## Rift tectonics in the eastern Arabian Sea

The eastern Arabian Sea formed as a result of the breakup of Madagascar and India in the mid-Cretaceous and subsequently between India and the Seychelles during the Late Cretaceous (Norton and Sclater, 1979; Courtillot et al., 1988). The rifting between India and the Seychelles is thought to have initiated in the Gop Rift, leading to final continental breakup. Rapid rifting (Royer et al., 2002) propagated southward into Laxmi Basin before aborting after a ridge jump at the time of Anomaly 28 to the west of Laxmi Ridge (Collier et al., 2008). The nature of crust in Laxmi Basin has been the subject of vigorous debate. Sampling the igneous basement to obtain a field-based constraint on the history of the rift tectonics was one of the primary scientific objectives of Expedition 355. In order to achieve this objective, we originally planned to core ~100 m into the basement at Site U1456 in Laxmi Basin. The sediment cover at this site was estimated at ~1470 m thick, so we planned a reentry system to improve our chances of success. We initially installed a casing string with reentry cone to ~455 mbsf in Hole U1456D and then continued to core to 1024.4 mbsf. After pulling out of the hole for a bit change, the drill string became stuck while trying to run back to the bottom of the hole. We ultimately had to sever the pipe and abandon Hole U1456D. Because we assumed that unconsolidated sands between ~500 and 720 mbsf had collapsed around the drill string while trying to reenter the hole, we decided to install a reentry system in a new hole (U1456E) to 750 mbsf, below the base of the sand. Coring continued to 1109.4 mbsf in Hole U1456E. After once again pulling out of the hole for a bit change, we encountered similar problems trying to work the bit back to the bottom of the hole. At this time it became apparent that swelling clays were binding the drill string and the drill bit and we decided to abandon the site and attempt to achieve our deeper objectives (Paleogene and basement) at an alternate site (see **Operations** in the Site U1456 chapter [Pandey et al., 2016]).

Although we were unable to core into basement at Site U1456, we did core through most of the postrift strata in the Laxmi Basin at this site, which can be used to reconstruct evolving erosion and environmental conditions in the Indus Basin. Furthermore, considering that surface processes (e.g., erosion) significantly control the dynamics of a rift basin by redefining the surface load distribution through infilling accommodation space, information collected at Sites U1456 and U1457 will be important for examining the postrift development of this basin and thus its origin. Physical and lithologic knowledge gathered from Site U1456 is equally important in determining the geometry and volumes of the sedimentary load. Wireline log data collected at Site U1456 should allow for better regional stratigraphic correlation and precise determination of postrift sediment budget.

Because coring through the base of the fan into the basement was one of the primary objectives of this expedition, we opted to core at Site U1457, which was originally an alternate site for the basement objective. Site U1457 is located in the western Laxmi Basin, with a similar, somewhat reduced (~1100 m), stratigraphy overlying the basement. We ultimately recovered 8.72 m of basalt, as well as associated volcaniclastic sediment above it, using a single RCB bit in an uncased hole. Because the igneous basement at Site U1457 was recovered at the end of the expedition, we only described the cores visually while at sea. Shore-based geochemical analysis carried out after the end of the expedition shows that the basalt are Mg-rich, low-K subalkalic tholeiites. Trace element discrimination plots indicate a petrogenesis similar to those of island arc basalts; however, Laxmi Basin is not known to have been in a subduction setting. We infer that this signature may have resulted from involvement of mantle sources developed by contribution of an old subduction slab. However, further postcruise geochemical and isotopic observations on the collected cores will establish their precise origin, affinity, and age.

Heat flow data measured at each site provide additional constraints to infer the rift history in Laxmi Basin. Average heat flow measured at Site U1456 is 57 mW/m², whereas heat flow at Site U1457 is 60 mW/m². Comparison with other data from the Arabian Sea (Figure **F13**) shows that Laxmi Basin is warmer than many parts of the Arabian Sea, in particular those regions close to the Indus Delta and the Murray Ridge (Calvés et al., 2011). Sites U1456 and U1457 also have higher heat flow than those in the eastern and northern sides of Laxmi Ridge. This could be attributed to the late-stage intrusion of volcanic features into the basin, west of Panikkar Ridge, as seen in Figure **F3**. Stein and Stein's (1992) compilation of oceanic crustal heat flow data indicates that the observed heat flow values at our sites are equivalent to oceanic crust of 76 and 84 Ma age. If the magnetic anomalies interpreted by Bhattacharya et al. (1994) are considered to be a reliable estimate of the timing of extension, then rifting in Laxmi Basin would have occurred between 63 and 84 Ma (Anomalies 28–33). This age would be consistent with the measured heat flow values but requires that no later thermal rejuvenation occurred. However, late-stage intrusions are seen in the seismic profiles, making this assumption somewhat problematic. This is because if the heat flow at our drill sites is normal and oceanic then the lower values in the eastern and northern Laxmi Basin would be anomalous in that they are colder than oceanic crust of corresponding age. This in turn would imply either that the crust in those areas is not oceanic or that the measured locations are positioned in cooler than average regions related to local heat flow patterns. Heat flow tends to be normal or higher than average where oceanic basement is flat but depressed in the vicinity of seamounts, which themselves are elevated due to discharge of warm fluids where the sediment cover is thin or nonexistent (Villinger et al., 2002).

Figure F13. Heat flow map of the Arabian Sea from the compilation of GeoMapApp, together with the two new measurements derived from Expedition 355.

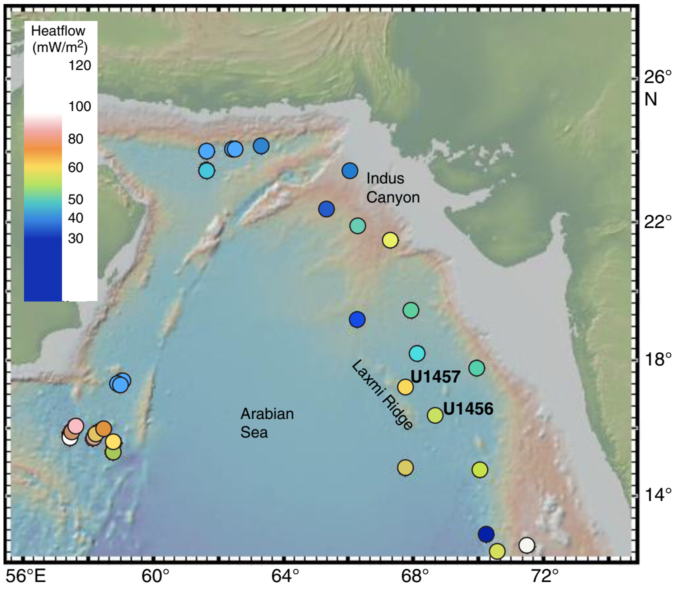

The measured heat flow values are also compatible with models that consider Laxmi Basin to be extended continental crust. The basin has significant water depths that imply large degrees of extension. This combined with the clear presence of volcanic seamounts in the basin, especially along Panikkar Ridge, implies at least 200% extension ($\beta > 3$) in order to explain melting in the ambient upper mantle (McKenzie and Bickle, 1988). Comparison with a pure shear rifting model (McKenzie, 1978) indicates that if $\beta > 3$, then heat flow should be >54 mW/m² (rifting finished at 63 Ma) or >48 mW/m² (rifting finished at 84 Ma). Because the younger age is more likely and extension should be somewhat more than $\beta = 3$ (200%), we conclude that our measured heat flow is also consistent with an extended continental origin for Laxmi Basin.

Therefore, in order to distinguish between the two plausible models as described above, geochemical analyses and radiometric age dating of basement rocks obtained at Site U1457 are essential. The precise radiometric dating of the recovered samples will establish the rifting age. Geochemical data suggest that the basement in the Laxmi Basin is high-Mg, low-K subalkalic tholeiitic basalt.

## Fan sedimentation

Drilling in Laxmi Basin at Site U1456 confirmed the presence of thick upper Miocene and younger strata (~700 m), as observed on the seismic profiles (Figures **F3**, **F14**). The presence of sandy channels within lithologic Units I–III shows that the fan is built up by a series of overlapping lobes. Units I–III at Site U1456 and Unit III at Site U1457 form parts of the Indus submarine fan. Although the locations of both sites are ~800 km from the modern river mouth, the reflective character of the seismic image covering these units marks them as being part of the Indus Fan Megasequence of Droz and Belaiche (1991). This means that they are lateral equivalents of sequences with clear channel-levee complexes in the proximal upper fan. In those more proximal areas the channels are accretionary, not erosive, features. Smaller channel-levee complexes are better developed around Site U1457 (Figure **F15**), but in both locations the reflectors tend to be mostly parallel and with only modest onlapping relations between successive depositional packages. In contrast, the seismic images show that the strata are incised by channels that have cut and fill geometries, and at Site U1457 drilling passed through the side of one of these channels (Figure **F15**). Taken in this context, the units drilled at Site U1456 can be understood as representing not only records of weathering and erosion but also different parts of the fan architecture. Presently both sites lie within an area that would be considered "lower fan" under the simple classification scheme of Walker (1978).

Unit II at Site U1456 is by far the coarsest grained of the sequences recovered, although the low recovery in Unit III, which was only sampled by RCB coring through all but the top of this unit, may also be more sandy than is apparent from the recovery (Figure **F9**). RCB coring is inefficient at recovering unconsolidated sand, and this may lead to a bias in our documentation of the unit if the coring preferentially recovered clay and claystone. The sand of Unit II may represent a depositional lobe on the fan where turbidity currents dropped their suspended load as they decelerated after exiting an incised or leveed channel. Seismic evidence rules out this sequence being a channel complex, and there is also little seismic evidence for leveed channels in this area. Channel deposits are often stacked massive sandstone (Hartog Jager et al., 1993; McCaffrey et al., 2002), but Unit II does not show this type of sequence. Instead, it is characterized by common muddy interbeds between the sand beds that suggest the depositional character is more distal. The cores, in conjunction with seismic data, indicate that Unit II is a "sheet lobe" complex as defined by Mutti (1992), contrasting with the coarser grained "mounded lobes" of Normark et al. (1979). Sheet lobes tend to be more subdued in their bathymetry and are associated with muddier depositional systems, much like the Indus Fan. They are also associated with moderate to strong incised channeling, which is a feature of the sequence in the area of operations (Figure **F14**).

If Unit III at Site U1456 is really sand rich below ~450 mbsf, then this sediment could also be a sheet lobe complex separated from Unit II by a ~75 m thick interval of more muddy sediment mixed with carbonate deposits that would correspond to overbank or distal hemipelagic sediments (Figure **F9**). However, if the bulk of Unit III is basically similar to the material that was actually recovered, then this unit would be more like a sequence of basin plain sheet turbidites that represent the distal equivalent of the coarser, thicker bedded sheet lobes (Mutti, 1977; Reading and Richards, 1994). In this context we can imagine Laxmi Basin being the recipient of sediment as sheet-like turbidites during deposition of Unit III, and then being abandoned as the active lobe avulsed to other parts of the Arabian Sea, followed by another pulse of coarse sand sedimenta-

Figure F14. Close-up (left) and interpretation (right) of seismic Profile W06 showing the location of Site U1456 and the major seismic units identified. Note in particular the major cut-and-fill channels and the body of strong chaotic reflectors in the mass transport deposit (MTD) that the drill site intersects.

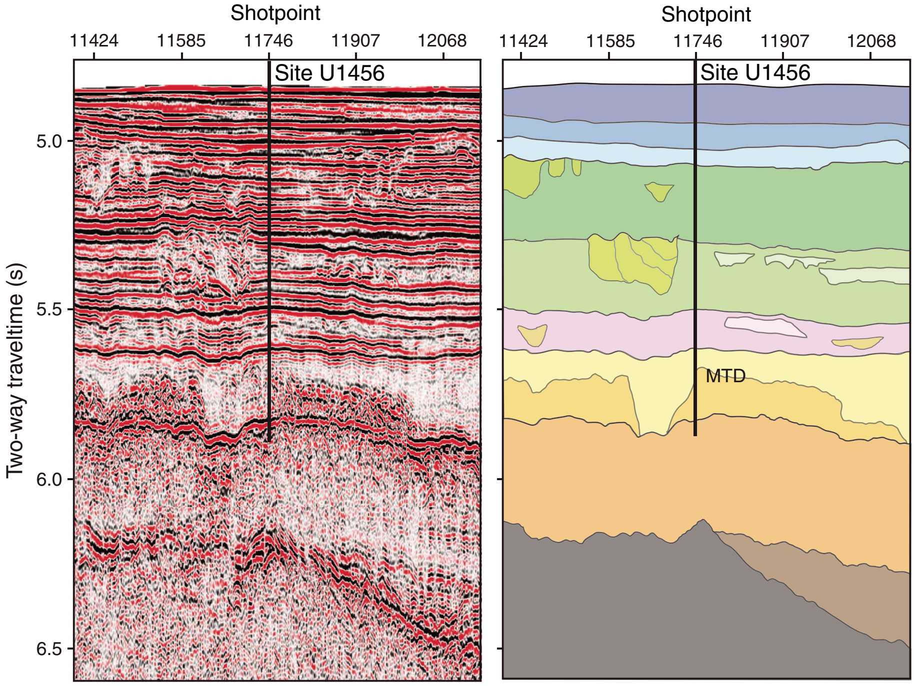

Figure F15. Close-up (left) and interpretation (right) of seismic Profile IODP-04 showing the location of Site U1457 and the major seismic units identified. Note that the mass transport deposit (MTD) is much thinner at this location compared to Site U1456. The drill site appears to cut the edge of one of the large channels in the Pleistocene section.

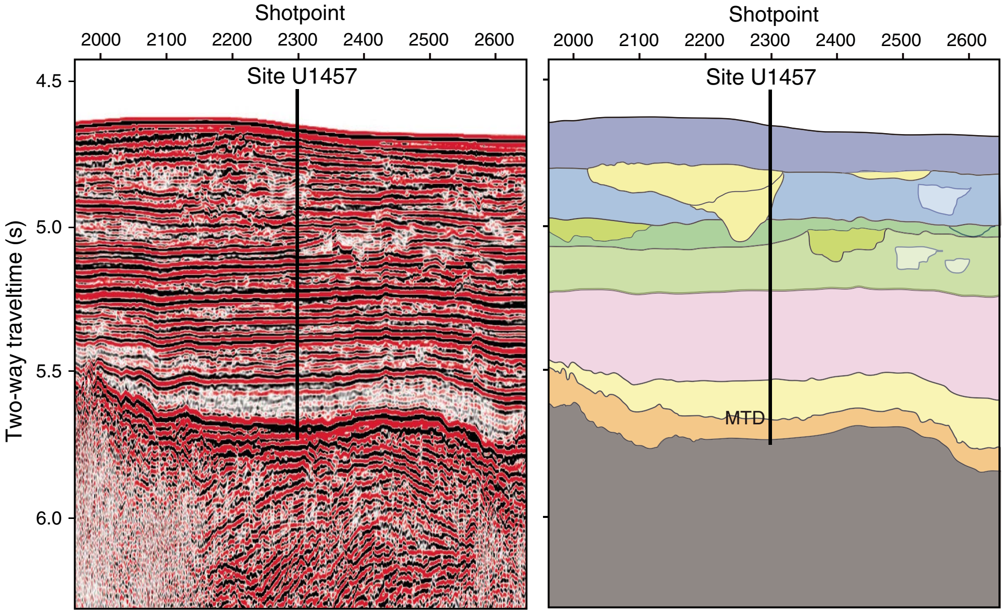

tion as an active lobe was reestablished east of Laxmi Ridge during deposition of Unit II. We emphasize that changes in grain size probably represent autocyclic processes of avulsion within a fan complex and probably do not represent changes in erosion rates onshore. Thus linear sedimentation rates at Sites U1456 and U1457 are not proxies for rates of sediment supply to the fan on a regional scale.

Why is Unit I so muddy and carbonate rich when global estimates of terrestrial erosion and deltaic/fan sedimentation point to this being a time of very high erosion and sediment transport (Métivier et al., 1999; Zhang et al., 2001)? The Holocene of the Indus Fan is characterized as mostly being a carbonate drape (Kolla and Coumes, 1984), which is interpreted to reflect cessation of deep-water sedimentation as a result of postglacial sea level rise (Prins et al., 2000) and subsequent sediment sequestration on the shelf and in the upper canyon (Clift et al., 2014). Such an explanation cannot answer the relative lack of clastic sedimentation through the entire lithologic Unit I because this covers the last ~1.2 million years, spanning much of the Pleistocene, during which time there have been many sea level cycles and plenty of opportunities for the accumulation of "lowstand" fan deposits. We speculate that since 1.2 Ma the active lobes of the Indus Fan have been located west of Laxmi Ridge, allowing a dominantly muddy and hemipelagic sequence to accumulate at our drill sites. It is possible that the higher carbonate content of Unit I could also reflect greater biogenic productivity and a deeper carbonate compensation depth (CCD) at that time. Unit I is a sequence in which there is also some influence related to discharge from peninsular India (see below).

## Sediment provenance

Reconstructing the erosion of the western Himalaya is a key goal of Expedition 355, and consequently we need to distinguish sediment delivered from the delta of the Indus River from that which might be a product of erosion in peninsular India. Some of this work requires shore-based geochemical work, but initial studies on board are able to pinpoint the influence of the Indus River using traditional microscopy applied to heavy minerals. Sand and silt in Unit I at Site U1456 show the presence of abundant muscovite, a mineral that is particularly common in the modern Indus River (Garzanti et al., 2005) and in the Indus Delta since the Last Glacial Maximum (Clift et al., 2010), as well as quartz and feldspars. Furthermore, a strong link to the Indus River is demonstrated by the presence of tourmaline, epidote, and especially high-grade metamorphic minerals such as kyanite and sillimanite (Figure **F16**). Augite was also observed (Figure **F16A**). Although this phase is indicative of a volcanic source, this mineral could either point to erosion from the Deccan Flood Basalts exposed on the peninsula or the Kohistan arc within the Indus Suture Zone, making this a nonunique proxy. Evidence from combined Sr and Nd isotopes close to the Laccadive Ridge indicates variable sediment supply from the Indus River and peninsular India to sedimentary basins at the foot of the continental slope and even perhaps from the Bay of Bengal driven by monsoon-controlled currents (Goswami et al., 2012). We do not rule out sediment supply from peninsular India to Laxmi Basin; we only argue that the provenance indicates that this source appears to be a minor portion of the flux for most time periods, at least at these drill sites.

Unit II at Site U1456 shows a similar heavy mineral assemblage to Site U1457, but the minerals are present in much greater abundance and with additional minerals including garnet, blue-green calcic amphibole, and clinopyroxene. Most significantly, microscopic analysis identified rare sodic amphiboles, such as glaucophane (Figure **F16D**) and hypersthene (Figure **F16F**), which require erosion from a source that experienced high-pressure, low-temperature metamorphism (blueschist facies) of a type normally associated with subduction complexes (Miyashiro, 1994). Few such sources are known in peninsular India. Proterozoic blueschists are known from the Delhi fold belt in Rajasthan (Sinha-Roy and Mohanty, 1988), but even those parts of this terrane that do drain into the Arabian Sea are not currently rapidly eroding and would not be expected to have undergone much exhumation during the Cenozoic. Instead, the presence of glaucophane and hypersthene strongly

Figure F16. Heavy minerals from Site U1456. A. Augite (U1456A-11H-7A, 20 cm). B. Tourmaline (U1456A-8H-4A, 35 cm). C. Epidote (U1456A-51F-3A, 60 cm). D. Glaucophane (U1456A-50F-1A, 70 cm). E. Kyanite (U1456A-56F-1A, 30 cm). F. Hypersthene (U1456A-60F-1A, 40 cm). G. Spinel (U1456D-30R-1A, 16 cm). H. Hornblende (U1456E-19R-3A, 70 cm). Scale bars = 100 µm.

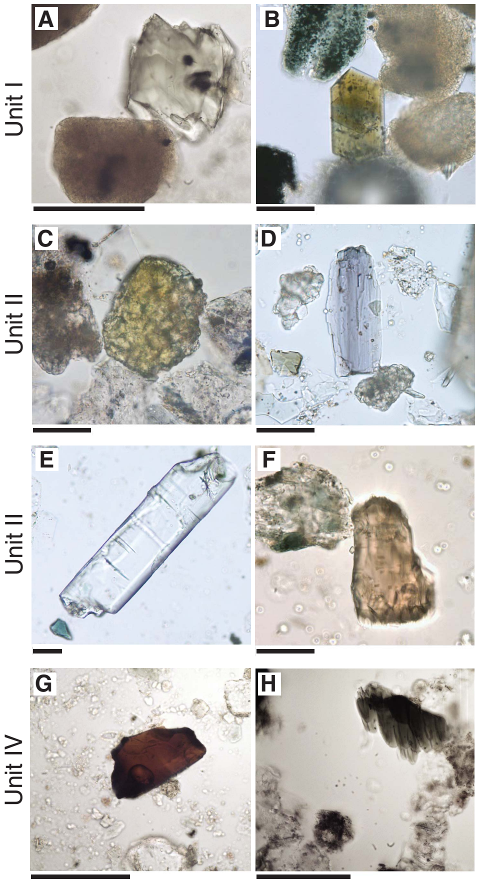

suggest erosion from the Indus Suture Zone where a series of subduction-related rocks are exposed. The best documented blueschist exposures within the Indus catchment lie along the Main Mantle Thrust in Kohistan in the Shangla area of that magmatic arc complex (Anczkiewicz et al., 2000). Other areas are known to have eclogites associated with continental subduction, such as the Tso Morari Complex in Ladakh, India (Donaldson et al., 2013), and Kagan in Pakistan (Tonarini et al., 1993), but these do not yield large volumes of glaucophane, and in the case of Tso Morari, were not likely areas of rapid erosion since the late Miocene. Other suture zone blueschists are eroded into the Brahmaputra and are not relevant here (Chatterjee and Ghose, 2010). This provenance demonstrates a direct link between the main stream of the Indus River and the fan at Sites U1456 and U1457.

Unit III at Site U1456 also shows a dominant Indus-derived mineralogy, including blue-green hornblende, clinopyroxene, epidote, rare garnets, and trace amounts of kyanite, chloritoid, apatite, zircon, tourmaline, and rutile, but no glaucophane. This does not necessarily mean that the river was not draining the Shangla blueschists at the time of sedimentation but rather that erosion from that area was heavily diluted by flux from other areas of the hinterland, much as it is today (Garzanti et al., 2005). Additional dilution from peninsular sources is possible, but with current information there is no suggestion that this was volumetrically significant.

Much of Unit IV, which is interpreted largely as a mass transport deposit, has a different provenance from the overlying units. Heavy minerals found in this unit include hornblende, actinolite, epidote, and garnet, with traces of zircon, tourmaline, spinel, and rutile, but not the typical high-grade assemblage with abundant mica seen in the three shallower units (Figure **F16**). For example, tourmaline can be found in granitic or metamorphic rocks but is not unique to the Greater Himalaya. Breccia interbedded with the siltstone (discussed below) is dominated by large fragments of shallow-water limestone, as well as much lower volumes of pebbles of vesicular basaltic rock. Unit IV provenance points to derivation from the western coast and continental margin of India, where similar sediment is found, such as Eocene–Miocene carbonates in the western parts of the Bombay offshore (Whiting et al., 1994; Rao and Wagle, 1997).

The only exception to this otherwise uniform pattern for Unit IV is the final lower–middle Miocene sandstone-dominated core at the base of the unit in Hole U1456E. This shows a return to a different, Indus-like provenance with a heavy mineral assemblage consisting of hornblende with common epidote and garnet and rare tourmaline, apatite, titanite, and chloritoid. These sediments represent the oldest evidence at Site U1456 for an active Indus River draining a Greater Himalayan source in the late early or early middle Miocene. With only 2.82 m of sediment recovered, it is not possible to define the depositional setting beyond this being a sandy fan turbidite, which is most similar to the sheet lobe deposits in the Pliocene–Pleistocene. There is a thin sequence of Paleocene brown and dark gray claystone at Site U1457 that underlies the mass transport deposit, but its origin and nature are even more obscured, beyond being a hemipelagic distal clastic deposit. Calcareous nannofossil and planktonic foraminifer assemblages date these deposits to ~62–63 Ma, which is a little older than most estimates of India/Eurasia collision (Najman et al., 2010; DeCelles et al., 2014). However, some reconstructions do predict collision even as early as 65 Ma (Jaeger et al., 1989; Beck et al., 1995), and a minimum age from the fan would be useful in assessing such end-members, if the Paleocene did prove to be derived from within or north of the Indus Suture Zone. The sediment itself is massive and muddy with modest amounts of silt. This could be a distal hemipelagic deposit to an early Indus Fan or base of slope deposits of the western Indian continental margin, two alternatives that can be tested by postcruise isotopic-based provenance analysis. The claystone becomes darker and interbedded with volcaniclastic sediment and shows more manganese mineralization downcore. The volcaniclastic sediment includes coarse breccia of basaltic character, similar to the underlying basalt interpreted as proximal hyaloclastite deposited synchronous with the volcanism during extension of Laxmi Basin. The flows are massive and not vesicular, which implies that they were erupted in significant water depths, likely >2000 m (Moore, 1970), as deepwater vesicular flows are mostly limited to subduction settings where volatile content is high. Although these depths imply normal depths for a seafloor-spreading center, they also indicate that there was no significant mantle thermal anomaly under the basin at the time of emplacement. This in turn indicates that Laxmi Basin may have opened before the start of Deccan Plateau magmatism at 65 Ma (Courtillot et al., 1988).

### Mass sediment transport

Drilling at both sites resulted in sampling of a large complex of mass transported sediment, which volumetrically is estimated to be ~19,000 km$^3$, making it the second largest such deposit known from any passive margin worldwide (Calvès et al., 2015). This deposit is substantially larger even than the Storegga Slide from the Norwegian margin that redeposited 3500 km$^3$ around 6200 years ago (Bünz et al., 2003). Prior to our operations, the age of this mass transport deposit was poorly constrained (Calvès et al., 2015). On the basis of nannofossil assemblages and magnetostratigraphy, we demonstrate that sediment lying immediately above and within the mass transport deposit is dated at <10.9 Ma, whereas sediment lying directly underneath the deposit at Site U1456 is dated as 13.5–17.7 Ma (Figure **F10**). The hiatus under the deposit at Site U1457 is too long to provide tight age control on the emplacement. Because the catastrophic emplacement of these deposits may have caused significant erosion of the sediment present in Laxmi Basin before sedimentation, we do not interpret these ages to indicate that mass transport continued for >3.5 million years. Instead, we conclude that the section reflects at least two major phases of mass transport, probably both of them occurring at ~10–11 Ma. A short interval of hemipelagic claystone was found separating two sequences within which there is abundant structural and sedimentary evidence for catastrophic redeposition (e.g., small slump folds, faults, and high dips). In contrast, the claystone shows a normal paleomagnetic signature coupled with a microfossil assemblage that does not indicate significant reworking of older microfossils, such as seen in the rest of the mass transport unit.

Much of the mass transport deposit comprises claystone and silty claystone, with soft-sediment deformation in the form of folds and small brittle reverse faulting structures, consistent with being in the toe region of a large-scale slump (Bovis, 2003). There are examples of larger faults with slickensides indicating brittle deformation at the base of the deposit, which is ~330 m thick at Site U1456 and ~190 m thick at Site U1457. Steeply dipping beds and contorted, folded geometries mark the upper part of the main deposit, which is draped by a subhorizontal muddy blanket likely deposited in the immediate aftermath of the event. There is no sharp lithologic change to distinguish mass transport sediments from the hemipelagic sediment, which are both composed of claystone. However, the mass transport deposit itself, largely comprising lithologic Unit IV at both sites, contains sediment with a strongly reworked microfossil assemblage eroded from Paleogene to lower Neogene sources, whereas the drape has a coherent microfossil assemblage with little reworking.

The mass transport deposit comprises two types of sediment. The first type is composed of well-bedded materials that have undergone soft-sediment plastic deformation. These were presumably originally deposited on the outer shelf or continental slope of western India and were then largely redeposited en masse into the deeper parts of Laxmi Basin. This sediment tends to occur in the upper part of the mass transport unit. The second type of sediment in the mass transport deposit is composed of breccia dominated by angular clasts of limestone whose composition and microfossil content indicates original sedimentation in a carbonate-dominated setting and that must have been broken into the clasts that constitute the breccia during the emplacement of the mass transport deposit. Massive calcarenite is also associated with the breccia toward the base of the deposit. Suitable source rocks for these deposits are present along the western Indian Shelf (Rao and Wagle, 1997). At Site U1456, the breccias are separated by a claystone-dominated sequence (Figure **F9**). This internal structure supports the suggestion that the emplacement of the mass transport deposit took place in two major phases. The breccia is associated with thick-bedded calcarenite that also represents high-energy resedimentation of carbonate material. Although the calcarenite could have been deposited on the Indian continental shelf adjacent to a carbonate platform and then transported into the present position, its association with the breccia units suggests that it represents high-energy deposits linked to the mass transport process itself. Brittle deformation is associated with the base of the two breccia intervals, whereas soft-sediment deformation dominated in the overlying muddier sequences.

Each phase of mass transport could theoretically have been made up of smaller depositional episodes, but we do not anticipate these being separated in time by long periods because there are no other hemipelagic drapes identified within the cores. We think it unlikely that Unit IV at Site U1456 represents a collection of small debris flows. The source of the mass transport deposit must be the Indian continental margin because it preserves a suitable sequence of Cenozoic shallow-water and slope deposits (Biswas, 1987; Whiting et al., 1994). Even the Deccan volcanic rock clasts can be derived from mass transport offshore because the province is known to extend out under the continental shelf (Karisiddaiah and Iyer, 1991; Pandey et al., 2011). In any case, suitable sources are not present on any other topographic high adjacent to Laxmi Basin (i.e., Laxmi Ridge or Panikkar Ridge). Laxmi Ridge has local development of shallow-water carbonates that must have accumulated soon after its initial formation when the ridge crest was still located close to sea level and not in the ~3 km of water as observed today. Laxmi Ridge does have a modest hemipelagic drape (on the order of a couple of hundred meters thick, as observed along seismic Profile W06; Figure **F3**) but may not be a suitable source of shallow-water material spanning such a long period or for the voluminous amounts of clay and siltstone observed.

Moreover, given the long transport (~400 km) from the potential source region (Calvès et al., 2015), it seems unlikely that this deposit could represent the product of numerous small events, which would lack the gravitational potential to travel such great distances. Even if the precise origin of the deposit was disputed, the seismic images indicate a single pulse that stretches almost 400 km along Laxmi Basin, mostly north of Site U1456, without major similar events before or after. The deposit we cored is therefore likely caused by one or two large collapses of the outer shelf and upper slope. Such a collapse would be required to explain such long runout, large volumes, and the homogeneous character in seismic images. In contrast to the Storegga Slide, whose emplacement is associated with gas hydrate dissociation during a time of climatic change (Bünz et al., 2003), we do not yet understand what might have triggered the large-scale collapse of the Indian continental margin at 10–11 Ma.

## Preliminary scientific assessment

Expedition 355 was designed to obtain sediment and igneous basement samples from the eastern Arabian Sea to address two broad categories of objectives as outlined in the *Scientific Prospectus* (Pandey et al., 2014). Through coring into the sediment and basement of Laxmi Basin during this expedition, we addressed many of our primary objectives and also made some additional findings that have significant geodynamic implications. The principal objectives outlined for this expedition are

1. *To reconstruct long-term changes in erosion and weathering rates at submillennial to millennial timescales in order to compare with existing records of high-frequency climatic variability.*

All planned sites of Expedition 355 were designed to drill through the fan sediment in the eastern Arabian Sea to examine the erosional and weathering response of the western Himalaya, Karakoram, and Hindu Kush to the changing intensity of the southwest Asian monsoon at millennial to submillennial scales. Successful coring with the APC and HLAPC, which provided very good recovery through the upper parts of the sections at both Sites U1456 and U1457, provides an opportunity to reconstruct and model orbital-scale variations in erosion, weathering, environment, and climate. The well-constrained spliced sections generated through coring multiple holes at both sites, in conjunction with a robust age model, provide a mostly continuous high-resolution record of weathering and erosion during much of the Pleistocene (since ~2.0 Ma). The recovered intervals may allow us to determine whether the intensity of Himalaya chemical weathering had a role in controlling glacial cycles in the Northern Hemisphere. Significant hiatuses and/or condensed sections at ~1.8–2.2 and ~3.6–5.6 Ma mean that we cannot follow the entire Pliocene–Pleistocene climate variation in terms of its erosional and weathering impact, but because a large number of glacial cycles are spanned by a relatively well recovered and expanded section, the general pattern and response to monsoon change by these processes should be amenable to study. The expanded section represented by Unit II at both sites provides an especially good chance to look at the erosional response to monsoon changes at the millennial scale. The sandy character of Unit II at Site U1456 may represent an even shorter amount of time and be deposited in a small number of major turbidite events.

2. *To reconstruct changes in erosion and weathering intensity over tectonic timescales and assess whether any changes occurred at ~23, 15, and 10–8 Ma to test earlier hypotheses that invoke changes in monsoon intensity at those times.*

Cenozoic sedimentary sections from the Indus Fan are expected to record the erosional and weathering responses of the Indus drainage basin to large-scale climatic changes. Deep penetration through the entire fan was intended to retrieve long-term continuous records. Site U1456 penetrated ~1110 m of sediment cover, whereas sediment penetration of ~1100 m was achieved at Site U1457. Both sites cover the ~10 Ma (late Miocene) and younger section, which will enable us to examine proposed hypotheses on tectonic scales. These include answers to questions such as whether monsoon intensification causes less or more erosion, and whether this erosion occurs in the monsoon-influenced Himalayas or other mountainous regions, such as the westerly influenced Karakoram, within the Indus catchment. Reasonably good age control and decent core recovery may allow us to ascertain if increased grassland (C4) and reduced woodland (C3) flora at ~8 Ma is related to strengthening or weakening of monsoon rainfall and what other environmental changes occurred through that time. For example, are phases of increased productivity in the Arabian Sea linked to changes in continental environments onshore, and are both driven by change in monsoon wind intensity? A moderate hiatus close to 8 Ma itself means that the record will not be continuous but the transition should still be resolvable. Shore-based analyses of core samples collected during Expedition 355 will further improve our understanding of sedimentation in Laxmi Basin and the provenance of this sediment during key intervals of climate change from the late Miocene to present.

Unfortunately, with effective recovery limited to the past ~10 million years, we will be unable to address whether monsoon intensification occurred at 15 Ma and in particular test whether Greater Himalaya exhumation is linked to heavier rainfall and faster erosion after ~23 Ma, as implied by tectonic models such as channel flow (Beaumont et al., 2001). Recent suggestions that the monsoon might have been active during the Eocene (Licht et al., 2014) are also beyond analysis by Expedition 355 cores. Inability to penetrate deep into the fan stratigraphy at either site further makes it impossible to date the start of fan sedimentation, which would have provided a minimum age to the controversial timing of initial India/Eurasia collision. The presence of a short section (~20 m) of Paleocene (62–63 Ma) sediment at Site U1457 should allow us to test whether India/Eurasia collision was before or after this time, and thus at least eliminate some of the more extreme early collision models.

3. *To decipher the nature of basement rocks in Laxmi Basin and constrain the timing of early seafloor spreading and its relationship to the emplacement of Deccan Flood Basalts. Does mantle plume initiation predate or postdate rifting and early spreading?*

Penetration to ~100 m into igneous basement after ~1470 m of sediment cover was planned at Site U1456. This site was designed to core through the base of the Indus Fan, in order to determine the nature of basement in Laxmi Basin and to constrain rifting history and its relationship to Deccan volcanism. We planned a reentry and casing system for this site because of the deep penetration and potential for unconsolidated coarse-grained sediment. Unfortunately, the complex lithologies encountered in the mass transport deposit ultimately resulted in us having to abandon two attempts to reach basement at Site U1456. In both cases, we were unable to work the drill string back to the bottom of the hole after a bit change, likely because of swelling claystone within the mass transport deposit (see **Operations** in the Site U1456 chapter [Pandey et al., 2016]). This unexpected development prevented us from coring the base of the fan, as well as the basement at Site U1456. A third attempt to core into the basement during Expedition 355 was successful at Site U1457 and resulted in recovery of ~8.72 m of massive basalt and associated volcaniclastic sediment. Geochemical analysis indicates that these are low-K, high-Mg subalkalic tholeiitic basalts that are not typical MORB, but instead have a mantle signature.

Our objectives linked to the origin of the basin were further advanced by being able to core through most of the postrift strata in Laxmi Basin at these locations. Because surface processes (e.g., erosion) significantly control the dynamics of rift basins by redefining the surface load distribution through infilling accommodation space, information collected at both sites will be significant for examining the postrift development of this basin and thus its origins. Physical and lithologic knowledge gathered from these sites is equally important in determining the geometry and volume of the sedimentary load. Wireline log data collected in Hole U1456C should allow better regional stratigraphic correlation and precise determination of postrift sediment budget.

As well as the planned objectives, Expedition 355 also confirmed the presence of a huge mass transport deposit along the western continental margin of India that had previously only been recognized seismically (Calvès et al., 2015). Prior to our expedition very little was known about the presence of this mass transport deposit, which is significantly larger than the well-known Storegga Slide of Norway (Bugge et al., 1988; Bryn et al., 2003). Coring during Expedition 355 now allows us to constrain the extent, timing, and volume generated by this large-scale catastrophic event with significant implications for geohazards on this and other margins.

# References

Aitchison, J.C., Ali, J.R., and Davis, A.M., 2007. When and where did India and Asia collide? *Journal of Geophysical Research: Solid Earth,* 112(B5):B05423. **http://dx.doi.org/10.1029/2006JB004706**

Ali, K.F., and de Boer, D.H., 2008. Factors controlling specific sediment yield in the upper Indus River basin, northern Pakistan. *Hydrological Processes,* 22(16):3102–3114. **http://dx.doi.org/10.1002/hyp.6896**

Alizai, A., Carter, A., Clift, P.D., VanLaningham, S., Williams, J.C., and Kumar, R., 2011. Sediment provenance, reworking and transport processes in the Indus River by U-Pb dating of detrital zircon grains. *Global and Planetary Change,* 76(1–2):33–55. **http://dx.doi.org/10.1016/j.gloplacha.2010.11.008**

An, Z., Kutzbach, J.E., Prell, W.L., and Porter, S.C., 2001. Evolution of Asian monsoons and phased uplift of the Himalaya–Tibetan Plateau since late Miocene times. *Nature,* 411(6833):62–66. **http://dx.doi.org/10.1038/35075035**

Anczkiewicz, R., Burg, J.P., Villa, I.M., and Meier, M., 2000. Late Cretaceous blueschist metamorphism in the Indus Suture Zone, Shangla region, Pakistan Himalaya. *Tectonophysics,* 324(1–2):111–134. **http://dx.doi.org/10.1016/S0040-1951(00)00110-4**

Baksi, A.K., 1994. Geochronological studies on whole-rock basalts, Deccan Traps, India: evaluation of the timing of volcanism relative to the K-T boundary. *Earth and Planetary Science Letters,* 121(1–2):43–56. **http://dx.doi.org/10.1016/0012-821X(94)90030-2**

Beaumont, C., Jamieson, R.A., Nguyen, M.H., and Lee, B., 2001. Himalayan tectonics explained by extrusion of a low-viscosity crustal channel coupled to focused surface denudation. *Nature,* 414(6865):738–742. **http://dx.doi.org/10.1038/414738a**

Beck, R.A., Burbank, D.W., Sercombe, W.J., Riley, G.W., Barndt, J.K., Berry, J.R., Afzal, J., Khan, A.M., Jurgen, H., Metje, J., Cheema, A., Shafique, N.A., Lawrence, R.D., and Khan, M.A., 1995. Stratigraphic evidence for an early collision between northwest India and Asia. *Nature,* 373(6509):55–58. **http://dx.doi.org/10.1038/373055a0**

Bernard, A., and Munschy, M., 2000. Were the Mascarene and Laxmi Basins (western Indian Ocean) formed at the same spreading centre? *Comptes Rendus de l'Academie des Sciences, Serie IIa: Sciences de la Terre et des Planetes,* 330(11):777–783. [French with English abstract] **http://dx.doi.org/10.1016/S1251-8050(00)00221-4**

Berner, R.A., Lasaga, A.C., and Garrels, R.M., 1983. The carbonate-silicate geochemical cycle and its effect on atmospheric carbon dioxide over the past 100 million years. *American Journal of Science,* 283(7):641–683. **http://dx.doi.org/10.2475/ajs.283.7.641**

Berner, R.A., and Raiswell, R., 1983. Burial of organic carbon and pyrite sulfur in sediments over Phanerozoic time: a new theory. *Geochimica et Cosmochimica Acta,* 47(5):855–862. **http://dx.doi.org/10.1016/0016-7037(83)90151-5**

Bernet, M., van der Beek, P., Pik, R., Huyghe, P., Mugnier, J.-L., Labrin, E., and Szulc, A., 2006. Miocene to recent exhumation of the central Himalaya determined from combined detrital zircon fission-track and U/Pb analysis of Siwalik sediments, western Nepal. *Basin Research,* 18(4):393–412. **http://dx.doi.org/10.1111/j.1365-2117.2006.00303.x**

Besse, J., and Courtillot, V., 2002. Apparent and true polar wander and the geometry of the geomagnetic field over the last 200 Myr. *Journal of Geophysical Research: Solid Earth,* 107(B11):2300. **http://dx.doi.org/10.1029/2000JB000050**

Bhattacharya, G.C., Chaubey, A.K., Murty, G.P.S., Srinivas, K., Sarma, K.V.L.N.S., Subrahmanyam, V., and Krishna, K.S., 1994. Evidence for seafloor spreading in the Laxmi Basin, northeastern Arabian Sea. *Earth and Planetary Science Letters,* 125(1–4):211–220. **http://dx.doi.org/10.1016/0012-821X(94)90216-X**

Bhattacharyya, R., Verma, P.K., and Majumdar, T.J., 2009. High resolution satellite geoids/gravity over the western Indian offshore for tectonics and hydrocarbon exploration. *Indian Journal of Geo-Marine Sciences,* 38(1):116–125. **http://nopr.niscair.res.in/bitstream/123456789/4252/4/IJMS 38(1)116-125.pdf**

Bhushan, R., Dutta, K., and Somayajulu, B.L.K., 2001. Concentrations and burial fluxes of organic and inorganic carbon on the eastern margins of the Arabian Sea. *Marine Geology,* 178(1–4):95–113. **http://dx.doi.org/10.1016/S0025-3227(01)00179-7**

Biswas, S.K., 1987. Regional tectonic framework, structure and evolution of the western marginal basins of India. *Tectonophysics,* 135(4):307–327. **http://dx.doi.org/10.1016/0040-1951(87)90115-6**

Biswas, S.K., and Singh, N.K., 1988. Western continental margin of India and hydrocarbon potential of deep-sea basins. *Proceedings of the 7th Offshore Southeast Asia (SEAPEX) Conference:* Singapore (Southeast Asia Petroleum Exploration Society), 170–181.

Blöthe, J.H., Munack, H., Korup, O., Fülling, A., Garzanti, E., Resentini, A., and Kubik, P.W., 2014. Late Quaternary valley infill and dissection in the Indus River, western Tibetan Plateau margin. *Quaternary Science Reviews,* 94:102–119. **http://dx.doi.org/10.1016/j.quascirev.2014.04.011**

Boillot, G., Beslier, M.O., Krawczyk, C.M., Rappin, D., and Reston, T.J., 1995. The formation of passive margins: constraints from the crustal structure and segmentation of the deep Galicia margin, Spain. *In* Scrutton, R.A., Stoker, M.S., Shimmield, G.B., and Tudhope, A.W. (Eds.), *The Tectonics, Sedimentation and Palaeoceanography of the North Atlantic Region.* Geological Society Special Publication, 90:71–91. **http://dx.doi.org/10.1144/GSL.SP.1995.090.01.04**

Bollinger, L., Avouac, J.P., Beyssac, O., Catlos, E.J., Harrison, T.M., Grove, M., Goffé, B., and Sapkota, S., 2004. Thermal structure and exhumation history of the Lesser Himalaya in central Nepal. *Tectonics,* 23(5):19. **http://dx.doi.org/10.1029/2003TC001564**

Bookhagen, B., Thiede, R.C., and Strecker, M.R., 2005. Late Quaternary intensified monsoon phases control landscape evolution in the northwest Himalaya. *Geology,* 33(2):149–152. **http://dx.doi.org/10.1130/G20982.1**

Boos, W.R., and Kuang, Z., 2010. Dominant control of the South Asian monsoon by orographic insulation versus plateau heating. *Nature,* 463(7278):218–222. **http://dx.doi.org/10.1038/nature08707**

Bovis, M.J., 2003. Mass movement. *In* Middleton, G.V., Church, M.J., Coniglio, M., Hardie, L.A., and Longstaffe, F.J. (Eds.), *Encyclopedia of Sediments and Sedimentary Rocks* (Encyclopedia of Earth Sciences Series): Amsterdam (Springer), 692–695. **http://dx.doi.org/10.1007/978-1-4020-3609-5_131**

Bryn, P., Solheim, A., Berg, K., Lien, R., Forsberg, C.F., Haflidason, H., Ottesen, D., and Rise, L., 2003. The Storegga slide complex: repeated large scale sliding in response to climatic cyclicity. *In* Locat, J., Mienert, J., and Boisvert, L. (Eds.), *Advances in Natural and Technological Hazards Research* (Volume 19): *Submarine Mass Movements and Their Consequences:* Dordrecht, The Netherlands (Kluwer), 215–222. **http://dx.doi.org/10.1007/978-94-010-0093-2_24**

Budziak, D., Schneider, R.R., Rostek, F., Müller, P.J., Bard, E., and Wefer, G., 2000. Late Quaternary insolation forcing on total organic carbon and $C_{37}$ alkenone variations in the Arabian Sea. *Paleoceanography,* 15(3):307–322. **http://dx.doi.org/10.1029/1999PA000433**

Bugge, T., Belderson, R.H., and Kenyon, N.H., 1988. The Storegga slide. *Philosophical Transactions of the Royal Society, A: Mathematical, Physical & Engineering Sciences,* 325(1586):357–388. **http://dx.doi.org/10.1098/rsta.1988.0055**

Bünz, S., Mienert, J., and Berndt, C., 2003. Geological controls on the Storegga gas-hydrate system of the mid-Norwegian continental margin. *Earth and Planetary Science Letters,* 209(3–4):291–307. **http://dx.doi.org/10.1016/S0012-821X(03)00097-9**

Calvès, G., Clift, P.D., and Inam, A., 2008. Anomalous subsidence on the rifted volcanic margin of Pakistan: no influence from Deccan plume. *Earth and Planetary Science Letters,* 272(1–2):231–239. **http://dx.doi.org/10.1016/j.epsl.2008.04.042**

Calvès, G., Huuse, M., Clift, P.D., and Brusset, S., 2015. Giant fossil mass wasting off the coast of West India: the Nataraja submarine slide. *Earth and Planetary Science Letters,* 432:265–272. **http://dx.doi.org/10.1016/j.epsl.2015.10.022**

Calvès, G., Schwab, A.M., Huuse, M., Clift, P.D., Gaina, C., Jolley, D., Tabrez, A.R., and Inam, A., 2011. Seismic volcanostratigraphy of the western Indian rifted margin: the pre-Deccan igneous province. *Journal of Geophysical Research: Solid Earth,* 116(B1):B01101. **http://dx.doi.org/10.1029/2010JB000862**

Cane, M.A., and Molnar, P., 2001. Closing of the Indonesian Seaway as a precursor to East African aridification around 3–4 million years ago. *Nature,* 411(6834):157–162. **http://dx.doi.org/10.1038/35075500**

Catlos, E.J., Harrison, T.M., Kohn, M.J., Grove, M., Ryerson, F.J., Manning, C.E., and Upreti, B.N., 2001. Geochronologic and thermobarometric constraints on the evolution of the Main Central Thrust, central Nepal Himalaya. *Journal of Geophysical Research: Solid Earth,* 106(B8):16177–16204. **http://dx.doi.org/10.1029/2000JB900375**

Channell, J.E.T., Mazaud, A., Sullivan, P., Turner, S., and Raymo, M.E., 2002. Geomagnetic excursions and paleointensities in the Matuyama Chron at Ocean Drilling Program Sites 983 and 984 (Iceland Basin). *Journal of Geophysical Research: Solid Earth,* 107(B6):2114–2127. **http://dx.doi.org/10.1029/2001JB000491**

Chatterjee, N., and Ghose, N.C., 2010. Metamorphic evolution of the Naga Hills eclogite and blueschist, northeast India: implications for early subduction of the Indian plate under the Burma microplate. *Journal of Metamorphic Geology,* 28(2):209–225. **http://dx.doi.org/10.1111/j.1525-1314.2009.00861.x**

Chatterjee, S., Goswami, A., and Scotese, C.R., 2013. The longest voyage: tectonic, magmatic, and paleoclimatic evolution of the Indian plate during its northward flight from Gondwana to Asia. *Gondwana Research,* 23(1):238–267. **http://dx.doi.org/10.1016/j.gr.2012.07.001**

Chaubey, A.K., Bhattacharya, G.C., Murty, G.P.S., Srinivas, K., Ramprasad, T., and Gopala Rao, D., 1998. Early Tertiary seafloor spreading magnetic anomalies and paleo-propagators in the northern Arabian Sea. *Earth and Planetary Science Letters,* 154(1–4):41–52. **http://dx.doi.org/10.1016/S0012-821X(97)00178-7**

Chaubey, A.K., Dyment, J., Bhattacharya, G.C., Royer, J.-Y., Srinivas, K., and Yatheesh, V., 2002. Paleogene magnetic isochrons and palaeo-propagators in the Arabian and Eastern Somali basins, NW Indian Ocean. *In* Clift, P.D., Kroon, D., Gaedicke, C., and Craig, J. (Eds.), *The Tectonic and Climatic Evolution of the Arabian Sea Region.* Geological Society Special Publication, 195(1):71–85. **http://dx.doi.org/10.1144/GSL.SP.2002.195.01.05**

Chenet, A.-L., Fluteau, F., Courtillot, V., Gérard, M., and Subbarao, K.V., 2008. Determination of rapid Deccan eruptions across the Cretaceous-Tertiary boundary using paleomagnetic secular variation: results from a 1200-m-thick section in the Mahabaleshwar escarpment. *Journal of Geophysical Research: Solid Earth,* 113(B4):B04101. **http://dx.doi.org/10.1029/2006JB004635**

Clemens, S.C., and Prell, W.L., 2003. A 350,000 year summer-monsoon multi-proxy stack from the Owen Ridge, northern Arabian Sea. *Marine Geology,* 201(1–3):35–51. **http://dx.doi.org/10.1016/S0025-3227(03)00207-X**

Clift, P., Gaedicke, C., Edwards, R., Lee, J.I., Hildebrand, P., Amjad, S., White, R.S., and Schlüter, H.-U., 2002. The stratigraphic evolution of the Indus Fan and the history of sedimentation in the Arabian Sea. *Marine Geophysical Research,* 23(3):223–245. **http://dx.doi.org/10.1023/A:1023627123093**

Clift, P.D., 2006. Controls on the erosion of Cenozoic Asia and the flux of clastic sediment to the ocean. *Earth and Planetary Science Letters,* 241(3–4):571–580. **http://dx.doi.org/10.1016/j.epsl.2005.11.028**

Clift, P.D., and Blusztajn, J., 2005. Reorganization of the western Himalayan river system after five million years ago. *Nature,* 438(7070):1001–1003. **http://dx.doi.org/10.1038/nature04379**

Clift, P.D., Campbell, I.H., Pringle, M.S., Carter, A., Zhang, X., Hodges, K.V., Khan, A.A., and Allen, C.M., 2004. Thermochronology of the modern Indus River bedload; new insight into the controls on the marine stratigraphic record. *Tectonics,* 23(5):TC5013. **http://dx.doi.org/10.1029/2003TC001559**

Clift, P.D., Giosan, L., Carter, A., Garzanti, E., Galy, V., Tabrez, A.R., Pringle, M., Campbell, I.H., France-Lanord, C., Blusztajn, J., Allen, C., Alizai, A., Lückge, A., Danish, M., and Rabbani, M.M., 2010. Monsoon control over erosion patterns in the western Himalaya: possible feed-back into the tectonic evolution. *In* Clift, P.D., Tada, R., and Zheng, H. (Eds.), *Monsoon Evolution and Tectonics–Climate Linkage in Asia.* Geological Society Special Publication, 342:185–218. **http://dx.doi.org/10.1144/SP342.12**

Clift, P.D., Giosan, L., Henstock, T.J., and Tabrez, A.R., 2014. Sediment storage and reworking on the shelf and in the canyon of the Indus River-Fan system since the Last Glacial Maximum. *Basin Research,* 26(1):183–202. **http://dx.doi.org/10.1111/bre.12041**

Clift, P.D., Hodges, K.V., Heslop, D., Hannigan, R., Long, H.V., and Calves, G., 2008. Correlation of Himalayan exhumation rates and Asian monsoon intensity. *Nature Geoscience,* 1(12):875–880. **http://dx.doi.org/10.1038/ngeo351**

Clift, P.D., Shimizu, N., Layne, G.D., Blusztajn, J.S., Gaedicke, C., Schlüter, H.-U., Clark, M.K., and Amjad, S., 2001. Development of the Indus Fan and its significance for the erosional history of the western Himalaya and Karakoram. *Geological Society of America Bulletin,* 113(8):1039–1051. **http://dx.doi.org/10.1130/0016-7606(2001)113<1039:DOTIFA>2.0.CO;2**

Clift, P.D., and VanLaningham, S., 2010. A climatic trigger for a major Oligo-Miocene unconformity in the Himalayan foreland basin. *Tectonics,* 29(5):TC5014. **http://dx.doi.org/10.1029/2010TC002711**

Collier, J.S., Sansom, V., Ishizuka, O., Taylor, R.N., Minshull, T.A., and Whitmarsh, R.B., 2008. Age of Seychelles–India break-up. *Earth and Planetary Science Letters,* 272(1–2):264–277. **http://dx.doi.org/10.1016/j.epsl.2008.04.045**

Courtillot, V., Féraud, G., Maluski, H., Vandamme, D., Moreau, M.G., and Besse, J., 1988. Deccan flood basalts and the Cretaceous/Tertiary boundary. *Nature,* 333(6176):843–846. **http://dx.doi.org/10.1038/333843a0**

Courtillot, V., Gallet, Y., Rocchia, R., Féraud, G., Robin, E., Hofmann, C., Bhandari, N., and Ghevariya, Z.G., 2000. Cosmic markers, $^{40}$Ar/$^{39}$Ar dating and paleomagnetism of the KT sections in the Anjar area of the Deccan large igneous province. *Earth and Planetary Science Letters,* 182(2):137–156. **http://dx.doi.org/10.1016/S0012-821X(00)00238-7**

Courtillot, V., Jaupart, C., Manighetti, I., Tapponnier, P., and Besse, J., 1999. On causal links between flood basalts and continental breakup. *Earth and Planetary Science Letters,* 166(3–4):177–195. **http://dx.doi.org/10.1016/S0012-821X(98)00282-9**

DeCelles, P.G., Kapp, P., Gehrels, G.E., and Ding, L., 2014. Paleocene–Eocene foreland basin evolution in the Himalaya of southern Tibet and Nepal: implications for the age of initial India-Asia collision. *Tectonics,* 33(5):824–849. **http://dx.doi.org/10.1002/2014TC003522**

deMenocal, P., Bloemendal, J., and King, J., 1991. A rock-magnetic record of monsoonal dust deposition to the Arabian Sea: evidence for a shift in the mode of deposition at 2.4 Ma. *In* Prell, W.L., Niitsuma, N., et al., *Proceedings of the Ocean Drilling Program, Scientific Results,* 117: College Station, TX (Ocean Drilling Program), 389–407. **http://dx.doi.org/10.2973/odp.proc.sr.117.178.1991**

Dewey, J.F., Cande, S., and Pitman, W.C., III, 1989. Tectonic evolution of the India/Eurasia collision zone. *Eclogae Geologicae Helvetiae,* 82(3):717–734. **http://retro.seals.ch/digbib/view?pid=egh-001:1989:82::733**

Donaldson, D.G., Webb, A.A.G., Menold, C.A., Kylander-Clark, A.R.C., and Hacker, B.R., 2013. Petrochronology of Himalayan ultrahigh-pressure eclogite. *Geology,* 41(8):835–838. **http://dx.doi.org/10.1130/G33699.1**

Dortch, J.M., Owen, L.A., Haneberg, W.C., Caffee, M.W., Dietsch, C., and Kamp, U., 2009. Nature and timing of large landslides in the Himalaya and Transhimalaya of northern India. *Quaternary Science Reviews,* 28(11–12):1037–1054. **http://dx.doi.org/10.1016/j.quascirev.2008.05.002**

Droz, L., and Bellaiche, G., 1991. Seismic facies and geologic evolution of the central portion of the Indus Fan. *In* Weimer, P., and Link, M.H. (Eds.), *Frontiers in Sedimentary Geology* (Volume 4): *Seismic Facies and Sedimentary Processes of Submarine Fans and Turbidite Systems.* Bouma, A.H. (Series Ed.): New York (Springer-Verlag), 383–402. **http://dx.doi.org/10.1007/978-1-4684-8276-8_21**

England, P., and Houseman, G., 1986. Finite strain calculations of continental deformation: 2. Comparison with the India-Asia collision zone. *Journal of Geophysical Research: Solid Earth,* 91(B3):3664–3676. **http://dx.doi.org/10.1029/JB091iB03p03664**

Fleitmann, D., Burns, S.J., Mudelsee, M., Neff, U., Kramers, J., Mangini, A., and Matter, A., 2003. Holocene forcing of the Indian monsoon recorded in a stalagmite from southern Oman. *Science,* 300(5626):1737–1739. **http://dx.doi.org/10.1126/science.1083130**

Garzanti, E., Baud, A., and Mascle, G., 1987. Sedimentary record of the northward flight of India and its collision with Eurasia (Ladakh Himalaya, India). *Geodinamica Acta,* 1(4–5):297–312. **http://dx.doi.org/10.1080/09853111.1987.11105147**

Garzanti, E., Vezzoli, G., Andò, S., Paparella, P., and Clift, P.D., 2005. Petrology of Indus River sands: a key to interpret erosion history of the Western Himalayan syntaxis. *Earth and Planetary Science Letters,* 229(3–4):287–302. **http://dx.doi.org/10.1016/j.epsl.2004.11.008**

Giosan, L., Clift, P.D., Macklin, M.G., Fuller, D.Q., Constantinescu, S., Durcan, J.A., Stevens, T., Duller, G.A.T., Tabrez, A.R., Gangal, K., Adhikari, R., Alizai, A., Filip, F., VanLaningham, S., and Syvitski, J.P.M., 2012. Fluvial landscapes of the Harappan civilization. *Proceedings of the National Academy of Sciences of the United States of America,* 109(26):E1688–E1694. **http://dx.doi.org/10.1073/pnas.1112743109**

Godin, L., Grujic, D., Law, R.D., and Searle, M.P., 2006. Channel flow, ductile extrusion and exhumation in continental collision zones: an introduction. *In* Law, R.D, Searle, M.P., and Godin, L. (Eds.), *Channel Flow, Ductile Extrusion and Exhumation in Continental Collision Zones.* Geological Society Special Publication, 268(1):1–23. **http://dx.doi.org/10.1144/GSL.SP.2006.268.01.01**

Gombos, A.M., Jr., Powell, W.G., and Norton, I.O., 1995. The tectonic evolution of western India and its impact on hydrocarbon occurrences: an overview. *Sedimentary Geology,* 96(1–2):119–129. **http://dx.doi.org/10.1016/0037-0738(94)00129-I**

Goswami, V., Singh, S.K., Bhushan, R., and Rai, V.K., 2012. Temporal variations in $^{87}$Sr/$^{86}$Sr and $\varepsilon_{\mathrm{Nd}}$ in sediments of the southeastern Arabian Sea: impact of monsoon and surface water circulation. *Geochemistry, Geophysics, Geosystems,* 13(1):Q01001. **http://dx.doi.org/10.1029/2011GC003802**

Gupta, A.K., Mohan, K., Sarkar, S., Clemens, S.C., Ravindra, R., and Uttam, R.K., 2011. East–west similarities and differences in the surface and deep northern Arabian Sea records during the past 21 Kyr. *Palaeogeography, Palaeoclimatology, Palaeoecology,* 301(1–4):75–85. **http://dx.doi.org/10.1016/j.palaeo.2010.12.027**

Harris, N., 2007. Channel flow and the Himalayan-Tibetan orogen: a critical review. *Journal of the Geological Society,* 164(3):511–523. **http://dx.doi.org/10.1144/0016-76492006-133**

Hartog Jager, D.D., Giles, M.R., and Griffiths, G.R., 1993. Evolution of Paleogene submarine fans of the North Sea in space and time. *In* Parker, J.R. (Ed.), *Petroleum Geology of Northwest Europe: Proceedings of the 4th Conference,* Geological Society, London, 4:59–71. **http://dx.doi.org/10.1144/0040059**

Haug, G.H., and Tiedemann, R., 1998. Effect of the formation of the Isthmus of Panama on Atlantic Ocean thermohaline circulation. *Nature,* 393(6686):673–676. **http://dx.doi.org/10.1038/31447**

Heine, C., Müller, R.D., and Gaina, C., 2004. Reconstructing the lost eastern Tethys ocean basin: convergence history of the SE Asian margin and marine gateways. *In* Clift, P., Kuhnt, W., Wang, P., and Hayes, D. (Eds.), *Continent-Ocean Interactions within East Asian Marginal Seas.* Geophysical Monograph, 149:37–54. **http://dx.doi.org/10.1029/149GM03**

Hodges, K.V., 2006. A synthesis of the channel flow-extrusion hypothesis as developed for the Himalayan-Tibetan orogenic system. *In* Law, R.D, Searle, M.P., and Godin, L. (Eds.), *Channel Flow, Ductile Extrusion and Exhumation in Continental Collision Zones.* Geological Society Special Publication, 268:71–90. **http://dx.doi.org/10.1144/GSL.SP.2006.268.01.04**

Hopper, J.R., Dahl-Jensen, T., Holbrook, W.S., Larsen, H.C., Lizarralde, D., Korenaga, J., Kent, G.M., and Kelemen, P.B., 2003. Structure of the SE Greenland margin from seismic reflection and refraction data: implications for nascent spreading center subsidence and asymmetric crustal accretion during North Atlantic opening. *Journal of Geophysical Research: Solid Earth,* 108(B5):2269. **http://dx.doi.org/10.1029/2002JB001996**

Huber, M., and Goldner, A., 2012. Eocene monsoons. *Journal of Asian Earth Sciences,* 44:3–23. **http://dx.doi.org/10.1016/j.jseaes.2011.09.014**

Huyghe, P., Galy, A., Mugnier, J.-L., and France-Lanord, C., 2001. Propagation of the thrust system and erosion in the Lesser Himalaya: geochemical and sedimentological evidence. *Geology,* 29(11):1007–1010. **http://dx.doi.org/10.1130/0091-7613(2001)029<1007:POTTSA>2.0.CO;2**

Jaeger, J.-J., Courtillot, V., and Tapponnier, P., 1989. Paleontological view of the ages of the Deccan Traps, the Cretaceous/Tertiary boundary, and the India-Asia collision. *Geology,* 17(4):316–319. **http://dx.doi.org/10.1130/0091-7613(1989)017<0316:PVOTAO>2.3.CO;2**

Karisiddaiah, S.M., and Iyer, S.D., 1991. Petrology of rift-releated basalts at Bombay High waters, Arabian Sea. *Indian Journal of Marine Sciences* 20:208–211.

Karlapati, S., 2004. Seismic reflection and bathymetric study over deep offshore regions off the central west coast of India. [Ph.D. thesis], University of Goa, India.

Kenyon, N.H., Amir, A., and Cramp, A., 1995. Geometry of the younger sediment bodies of the Indus Fan. *In* Pickering, K.T., Hiscott, R.N., Kenyon, N.H., Ricci Lucchi, F., and Smith, R.D.A. (Eds.), *Atlas of Deep Water Environments: Architectural Style in Turbidite Systems*: London (Chapman & Hall), 89–93. **http://dx.doi.org/10.1007/978-94-011-1234-5_16**

Kolla, V., and Coumes, F., 1984. Morpho-acoustic and sedimentologic characteristics of the Indus Fan. *Geo-Marine Letters,* 3(2–4):133–139. **http://dx.doi.org/10.1007/BF02462458**

Kolla, V., and Coumes, F., 1987. Morphology, internal structure, seismic stratigraphy, and sedimentation of Indus Fan. *AAPG Bulletin,* 71(6):650–677. **http://archives.datapages.com/data/bulletns/1986-87/images/pg/00710006/0650/06500.pdf**

Kolla, V., and Coumes, F., 1990. Extension of structural and tectonic trends from the Indian subcontinent into the eastern Arabian Sea. *Marine and Petroleum Geology,* 7(2):188–196. **http://dx.doi.org/10.1016/0264-8172(90)90041-E**

Krishna, K.S., Gopala Rao, D., and Sar, D., 2006. Nature of the crust in the Laxmi Basin (14°–20°N), western continental margin of India. *Tectonics,* 25(1):TC1006. **http://dx.doi.org/10.1029/2004TC001747**

Kroon, D., Steens, T., and Troelstra, S.R., 1991. Onset of monsoonal related upwelling in the western Arabian Sea as revealed by planktonic foraminifers. *In* Prell, W.L., Niitsuma, N., et al., *Proceedings of the Ocean Drilling Program, Scientific Results,* 117: College Station, TX (Ocean Drilling Program), 257–263. **http://dx.doi.org/10.2973/odp.proc.sr.117.126.1991**

Licht, A., van Cappelle, M., Abels, H.A., Ladant, J.-B., Trabucho-Alexandre, J., France-Lanord, C., Donnadieu, Y., Vandenberghe, J., Rigaudier, T., Lécuyer, C., Terry, D., Jr., Adriaens, R., Boura, A., Guo, Z., Soe, A.N., Quade, J., Dupont-Nivet, G., and Jaeger, J.-J., 2014. Asian monsoons in a late Eocene greenhouse world. *Nature*, 513(7519):501–506. **http://dx.doi.org/10.1038/nature13704**

Malod, J.A., Droz, L., Mustafa Kemal, B., and Patriat, B., 1997. Early spreading and continental to oceanic basement transition beneath the Indus deep-sea fan: northeastern Arabian Sea. *Marine Geology,* 141(1–4):221–235. **http://dx.doi.org/10.1016/S0025-3227(97)00074-1**

McCaffrey, W.D., Gupta, S., and Brunt, R., 2002. Repeated cycles of submarine channel incision, infill and transition to sheet sandstone development in the Alpine Foreland Basin, SE France. *Sedimentology*, 49(3):623–635. **http://dx.doi.org/10.1046/j.1365-3091.2002.00477.x**

McKenzie, D., 1978. Some remarks on the development of sedimentary basins. *Earth and Planetary Science Letters,* 40(1):25–32. **http://dx.doi.org/10.1016/0012-821X(78)90071-7**

McKenzie, D., and Bickle, M.J., 1988. The volume and composition of melt generated by extension of the lithosphere. *Journal of Petrology,* 29(3):625–679. **http://dx.doi.org/10.1093/petrology/29.3.625**

Meigs, A.J., Burbank, D.W., and Beck, R.A., 1995. Middle–late Miocene (>10 Ma) formation of the Main Boundary thrust in the Western Himalaya. *Geology,* 23(5):423–426. **http://dx.doi.org/10.1130/0091-7613(1995)023<0423:MLMMFO>2.3.CO;2**

Métivier, F., Gaudemer, Y., Tapponnier, P., and Klein, M., 1999. Mass accumulation rates in Asia during the Cenozoic. *Geophysical Journal International,* 137(2):280–318. **http://dx.doi.org/10.1046/j.1365-246X.1999.00802.x**

Meyers, P.A., 1990. Impacts of late Quaternary fluctuations in water level on the accumulation of sedimentary organic matter in Walker Lake, Nevada. *Palaeogeography, Palaeoclimatology, Palaeoecology,* 78(3–4):229–240. **http://dx.doi.org/10.1016/0031-0182(90)90216-T**

Meyers, P.A., 1997. Organic geochemical proxies of paleoceanographic, paleolimnologic, and paleoclimatic processes. *Organic Geochemistry,* 27(5–6):213–250. **http://dx.doi.org/10.1016/S0146-6380(97)00049-1**

Miles, P.R., Munschy, M., and Ségoufin, J., 1998. Structure and early evolution of the Arabian Sea and East Somali Basin. *Geophysical Journal International,* 134(3):876–888. **http://dx.doi.org/10.1046/j.1365-246x.1998.00625.x**

Miles, P.R., and Roest, W.R., 1993. Earliest sea-floor spreading magnetic anomalies in the north Arabian Sea and the ocean–continent transition. *Geophysical Journal International,* 115(3):1025–1031. **http://dx.doi.org/10.1111/j.1365-246X.1993.tb01507.x**

Milliman, J.D., and Syvitski, J.P.M., 1992. Geomorphic/tectonic control of sediment discharge to the ocean: the importance of small mountainous rivers. *The Journal of Geology,* 100(5):525–544. **http://dx.doi.org/10.1086/629606**

Minshull, T.A., Lane, C.I., Collier, J.S., and Whitmarsh, R.B., 2008. The relationship between rifting and magmatism in the northeastern Arabian Sea. *Nature Geoscience,* 1(7):463–467. **http://dx.doi.org/10.1038/ngeo228**

Mishra, R., Pandey, D.K., Ramesh, P., and Shipboard Scientific Party SK-306, 2015. Active channel system in the middle Indus fan: results from high-resolution bathymetry surveys. *Current Science,* 108(3):409–412. **http://www.currentscience.ac.in/Volumes/108/03/0409.pdf**

Mishra, V., Smoliak, B.V., Lettenmaier, D.P., and Wallace, J.M., 2012. A prominent pattern of year-to-year variability in Indian summer monsoon rainfall. *Proceedings of the National Academy of Sciences of the United States of America,* 109(19):7213–7217. **http://dx.doi.org/10.1073/pnas.1119150109**

Misra, A.A., Sinha, N., and Mukherjee, S., 2015. Repeat ridge jumps and microcontinent separation: insights from NE Arabian Sea. *Marine and Petroleum Geology,* 59:406–428. **http://dx.doi.org/10.1016/j.marpetgeo.2014.08.019**

Miyashiro, A., 1994. *Metamorphic Petrology:* New York (Oxford University Press).

Molnar, P., Boos, W.R., and Battisti, D.S., 2010. Orographic controls on climate and paleoclimate of Asia: thermal and mechanical roles for the Tibetan Plateau. *Annual Review of Earth and Planetary Sciences,* 38(1):77–102. **http://dx.doi.org/10.1146/annurev-earth-040809-152456**

Molnar, P., England, P., and Martinod, J., 1993. Mantle dynamics, uplift of the Tibetan Plateau, and the Indian monsoon. *Reviews of Geophysics,* 31(4):357–396. **http://dx.doi.org/10.1029/93RG02030**

Molnar, P., and Tapponnier, P., 1975. Cenozoic tectonics of Asia: effects of a continental collision: features of recent continental tectonics in Asia can be interpreted as results of the India-Eurasia collision. *Science,* 189(4201):419–426. **http://dx.doi.org/10.1126/science.189.4201.419**

Moore, J.G., 1970. Water content of basalt erupted on the ocean floor. *Contributions to Mineralogy and Petrology,* 28(4):272–279. **http://dx.doi.org/10.1007/BF00388949**

Müller, A., and Mathesius, U., 1999. The palaeoenvironments of coastal lagoons in the southern Baltic Sea, I. The application of sedimentary $C_{org}$/N ratios as source indicators of organic matter. *Palaeogeography, Palaeoclimatology, Palaeoecology,* 145(1–3):1–16. **http://dx.doi.org/10.1016/S0031-0182(98)00094-7**

Mutti, E., 1977. Distinctive thin-bedded turbidite facies and related depositional environments in the Eocene Hecho Group (south-central Pyrenees, Spain). *Sedimentology,* 24(1):107–132. **http://dx.doi.org/10.1111/j.1365-3091.1977.tb00122.x**

Mutti, E., 1992. *Turbidite Sandstones:* Milan (Agip S.p.A., S. Donato Milanese).

Naini, B.R., 1980. Geological and geophysical study of the continental margin of western India, and the adjoining Arabian Sea including the Indus cone [Ph.D. Thesis]. Columbia University.

Naini, B.R., and Talwani, M., 1982. Structural framework and the evolutionary history of the continental margin of Western India. *In* Watkins, J.S., and Drake, C.L. (Eds.), *Studies in Continental Margin Geology.* AAPG Memoir, 167–191.

Najman, Y., 2006. The detrital record of orogenesis: a review of approaches and techniques used in the Himalayan sedimentary basins. *Earth-Science Reviews,* 74(1–2):1–72. **http://dx.doi.org/10.1016/j.earscirev.2005.04.004**

Najman, Y., Appel, E., Boudagher-Fadel, M., Bown, P., Carter, A., Garzanti, E., Godin, L., Han, J., Liebke, U., Oliver, G., Parrish, R., and Vezzoli, G., 2010. Timing of India-Asia collision: geological, biostratigraphic, and palaeomagnetic constraints. *Journal of Geophysical Research: Solid Earth,* 115(B12):B12416. **http://dx.doi.org/10.1029/2010JB007673**

Normark, W.R., Piper, D.J.W., and Hess, G.R., 1979. Distributary channels, sand lobes, and mesotopography of Navy submarine fan, California Borderland, with applications to ancient fan sediments. *Sedimentology,* 26(6):749–774. **http://dx.doi.org/10.1111/j.1365-3091.1979.tb00971.x**

Norton, I.O., and Sclater, J.G., 1979. A model for the evolution of the Indian Ocean and the breakup of Gondwanaland. *Journal of Geophysical Research: Solid Earth,* 84(B12):6803–6830. **http://dx.doi.org/10.1029/JB084iB12p06803**

Pandey, D.K., Clift, P.D., Kulhanek, D.K., Andò, S., Bendle, J.A.P., Bratenkov, S., Griffith, E.M., Gurumurthy, G.P., Hahn, A., Iwai, M., Khim, B.-K., Kumar, A., Kumar, A.G., Liddy, H.M., Lu, H., Lyle, M.W., Mishra, R., Radhakrishna, T., Routledge, C.M., Saraswat, R., Saxena, R., Scardia, G., Sharma, G.K., Singh, A.D., Steinke, S., Suzuki, K., Tauxe, L., Tiwari, M., Xu, Z., and Yu, Z., 2016. Site U1456. *In* Pandey, D.K., Clift, P.D., Kulhanek, D.K., and the Expedition 355 Scientists, *Arabian Sea Monsoon.* Proceedings of the International Ocean Discovery Program, 355: College Station, TX (International Ocean Discovery Program). **http://dx.doi.org/10.14379/iodp.proc.355.103.2016**

Pandey, D.K., Clift, P.D., and Kulhanek, D.K., 2014. *Expedition 355 Scientific Prospectus: Arabian Sea Monsoon.* International Ocean Discovery Program. **http://dx.doi.org/10.14379/iodp.sp.355.2014**

Pandey, D.K., Pandey, A., and Rajan, S., 2011. Offshore extension of Deccan Traps in Kachchh, central western India: implications for geological sequestration studies. *Natural Resources Research,* 20(1):33–43. **http://dx.doi.org/10.1007/s11053-010-9133-x**

Pandey, D.K., Rajan, S., and Pandey, A., 2010. Seismic imaging of Paleogene sediments of Kachchh Shelf, (western Indian margin) and their correlation with sea-level fluctuations. *Marine and Petroleum Research,* 27(6):1166–1174. **http://dx.doi.org/10.1016/j.marpetgeo.2010.02.002**

Pandey, O.P., Agrawal, P.K., and Negi, J.G., 1995. Lithospheric structure beneath Laxmi Ridge and Late Cretaceous geodynamic events. *Geo-Marine Letters,* 15(2):85–91. **http://dx.doi.org/10.1007/BF01275411**

Ponton, C., Giosan, L., Eglinton, T.I., Fuller, D.Q., Johnson, J.E., Kumar, P., and Collett, T.S., 2012. Holocene aridification of India. *Geophysical Research Letters,* 39(3):L3407. **http://dx.doi.org/10.1029/2011GL050722**

Prell, W.L., and Kutzbach, J.E., 1992. Sensitivity of the Indian monsoon to forcing parameters and implications for its evolution. *Nature,* 360(6405):647–652. **http://dx.doi.org/10.1038/360647a0**

Prell, W.L., Murray, D.W., Clemens, S.C., and Anderson, D.M., 1992. Evolution and variability of the Indian Ocean summer monsoon: evidence from the western Arabian Sea drilling program. *In* Duncan, R.A., Rea, D.K., Kidd, R.B., von Rad, U., and Weissel, J.K. (Eds.), *Synthesis of Results from Scientific Drilling in the Indian Ocean.* Geophysical Monograph, 70:447–469. **http://dx.doi.org/10.1029/GM070p0447**

Prins, M.A., Postma, G., Cleveringa, J., Cramp, A., and Kenyon, N.H., 2000. Controls on terrigenous sediment supply to the Arabian Sea during the late Quaternary: the Indus Fan. *Marine Geology,* 169(3–4):327–349. **http://dx.doi.org/10.1016/S0025-3227(00)00086-4**

Radha Krishna, M., Verma, R.K., and Purushotham, A.K., 2002. Lithospheric structure below the eastern Arabian Sea and adjoining west coast of India based on integrated analysis of gravity and seismic data. *Marine Geophysical Research,* 23(1):25–42. **http://dx.doi.org/10.1023/A:1021288003781**

Ramstein, G., Fluteau, F., Besse, J., and Joussaume, S., 1997. Effect of orogeny, plate motion and land–sea distribution on Eurasian climate change over the past 30 million years. *Nature,* 386(6627):788–795. **http://dx.doi.org/10.1038/386788a0**

Rao, V.P., and Wagle, B.G., 1997. Geomorphology and surficial geology of the western continental shelf and slope of India: a review. *Current Science,* 73(4):330–340. **http://www.currentscience.ac.in/Downloads/article_id_073_04_0330_0350_0.pdf**

Rea, D.K., 1992. Delivery of Himalayan sediment to the northern Indian Ocean and its relation to global climate, sea level, uplift, and seawater strontium. *In* Duncan, R.A., Rea, D.K., Kidd, R.B., von Rad, U., and Weissel, J.K. (Eds.), *Synthesis of Results from Scientific Drilling in the Indian Ocean.* Geophysical Monograph, 70:387–402. **http://dx.doi.org/10.1029/GM070p0387**

Reading, H.G., and Richards, M., 1994. Turbidite systems in deep-water basin margins classified by grain size and feeder system. *AAPG Bulletin,* 78(5):792–822. **http://aapgbull.geoscienceworld.org/cgi/content/abstract/78/5/792**

Replumaz, A., and Tapponnier, P., 2003. Reconstruction of the deformed collision zone between India and Asia by backward motion of lithospheric blocks. *Journal of Geophysical Research: Solid Earth,* 108(B6):2285. **http://dx.doi.org/10.1029/2001JB000661**

Robinson, D.M., DeCelles, P.G., and Copeland, P., 2006. Tectonic evolution of the Himalayan thrust belt in western Nepal: implications for channel flow models. *Geological Society of America Bulletin,* 118(7–8):865–885. **http://dx.doi.org/10.1130/B25911.1**

Rowley, D.B., 1996. Age of initiation of collision between India and Asia: a review of stratigraphic data. *Earth and Planetary Science Letters,* 145(1–4):1–13. **http://dx.doi.org/10.1016/S0012-821X(96)00201-4**

Royer, J.-Y., Chaubey, A.K., Dyment, J., Bhattacharya, G.C., Srinivas, K., Yatheesh, V., and Ramprasad, T., 2002. Paleogene plate tectonic evolution of the Arabian and eastern Somali basins. *In* Clift, P.D., Kroon, D., Gaedicke, C., and Craig, J. (Eds.), *The Tectonic and Climatic Evolution of the Arabian Sea Region.* Geological Society Special Publication, 195(1):7–23. **http://dx.doi.org/10.1144/GSL.SP.2002.195.01.02**

Ryan, W.B.F., Carbotte, S.M., Coplan, J.O., O'Hara, S., Melkonian, A., Arko, R., Weissel, R.A., Ferrini, V., Goodwillie, A., Nitsche, F., Bonczkowski, J., and Zemsky, R., 2009. Global multi-resolution topography synthesis. *Geochemistry, Geophysics, Geosystems,* 10(3):Q03014. **http://dx.doi.org/10.1029/2008GC002332**

Self, S., Blake, S., Sharma, K., Widdowson, M., and Sephton, S., 2008. Sulfur and chlorine in Late Cretaceous Deccan magmas and eruptive gas release. *Science,* 319(5870):1654–1657. **http://dx.doi.org/10.1126/science.1152830**

Shipboard Scientific Party, 1974. Site 221. With contribution by R.E. Coleman and N. Hamilton. *In* Whitmarsh, R.B., Weser, O.E., Ross, D.A., et al., *Initial Reports of the Deep Sea Drilling Project,* 23: Washington (U.S. Government Printing Office), 167–210. **http://dx.doi.org/10.2973/dsdp.proc.23.105.1974**

Singh, A., Singh, C., and Kennett, B.L.N., 2015. A review of crust and upper mantle structure beneath the Indian subcontinent. *Tectonophysics,* 644–645:1–21. **http://dx.doi.org/10.1016/j.tecto.2015.01.007**

Singh, A.D., Jung, S.J.A., Darling, K., Ganeshram, R., Ivanochko, T., and Kroon, D., 2011. Productivity collapses in the Arabian Sea during glacial cold phases. *Paleoceanography,* 26(3):PA3210. **http://dx.doi.org/10.1029/2009PA001923**

Singh, A.P., 1999. The deep crustal accretion beneath the Laxmi Ridge in the northeastern Arabian Sea: the plume model again. *Journal of Geodynamics,* 27(4–5):609–622. **http://dx.doi.org/10.1016/S0264-3707(98)00019-2**

Sinha-Roy, S., and Mohanty, M., 1988. Blueschist facies metamorphism in the ophiolitic mélange of the late Proterozoic Delhi fold belt, Rajasthan, India. *Precambrian Research,* 42(1–2):97–105. **http://dx.doi.org/10.1016/0301-9268(88)90012-5**

Skogseid, J., Planke, S., Faleide, J.I., Pedersen, T., Eldholm, O., and Neverdal, F., 2000. NE Atlantic continental rifting and volcanic margin formation. *In* Nøttvedt, A. (Ed.), *Dynamics of the Norwegian Margin.* Geological Society Special Publication, 167(1):295–326. **http://dx.doi.org/10.1144/GSL.SP.2000.167.01.12**

Sleep, N.H., 1990. Hotspots and mantle plumes: some phenomenology. *Journal of Geophysical Research: Solid Earth,* 95(B5):6715–6736. **http://dx.doi.org/10.1029/JB095iB05p06715**

Stein, C.A., and Stein, S., 1992. A model for the global variation in oceanic depth and heat flow with lithospheric age. *Nature,* 359(6391):123–129. **http://dx.doi.org/10.1038/359123a0**

Stein, R., Boucsein, B., and Meyer, H., 2006. Anoxia and high primary production in the Paleogene Central Arctic Ocean: first detailed records from Lomonosov Ridge. *Geophysical Research Letters,* 33(18):L18606. **http://dx.doi.org/10.1029/2006GL026776**

Stein, R. and Macdonald, R.W., 2004. Geochemical proxies used for organic carbon source identification in Arctic Ocean sediments. *In* Stein, R., and MacDonald, R.W. (Eds.), *The Organic Carbon Cycle in the Arctic Ocean: Chapter 1. The Arctic Ocean: boundary conditions and background information:* Berlin (Springer), 24–32. **http://dx.doi.org/10.1007/978-3-642-18912-8_1**

Storey, M., Mahoney, J.J., Saunders, A.D., Duncan, R.A., Kelley, S.P., and Coffin, M.F., 1995. Timing of hot spot—related volcanism and the breakup of Madagascar and India. *Science,* 267(5199):852–855. **http://dx.doi.org/10.1126/science.267.5199.852**

Szulc, A.G., Najman, Y., Sinclair, H.D., Pringle, M., Bickle, M., Chapman, H., Garzanti, E., Andò, S., Huyghe, P., Mugnier, J.-L., Ojha, T., and DeCelles, P., 2006. Tectonic evolution of the Himalaya constrained by detrital $^{40}$Ar-$^{39}$Ar, Sm-Nd and petrographic data from the Siwalik foreland basin succession, SW Nepal. *Basin Research,* 18(4):375–391. **http://dx.doi.org/10.1111/j.1365-2117.2006.00307.x**

Talwani, M., and Reif, C., 1998. Laxmi Ridge—a continental sliver in the Arabian Sea. *Marine Geophysical Research,* 20(4):259–271. **http://dx.doi.org/10.1023/A:1004674909280**

Tobgay, T., McQuarrie, N., Long, S., Kohn, M.J., and Corrie, S.L., 2012. The age and rate of displacement along the Main Central Thrust in the western Bhutan Himalaya. *Earth and Planetary Science Letters,* 319–320:146–158. **http://dx.doi.org/10.1016/j.epsl.2011.12.005**

Todal, A., and Edholm, O., 1998. Continental margin off western India and Deccan large igneous province. *Marine and Geophysical Research,* 20(4):273–291. **http://dx.doi.org/10.1023/A:1004640508371**

Tonarini, S., Villa, I.M., Oberli, F., Meier, M., Spencer, D.A., Pognante, U., and Ramsay, J.G., 1993. Eocene age of eclogite metamorphism in Pakistan Himalaya: implications for India-Eurasia collision. *Terra Nova,* 5(1):13–20. **http://dx.doi.org/10.1111/j.1365-3121.1993.tb00221.x**

Twichell, S.C., Meyers, P.A., and Diester-Haass, L., 2002. Significance of high C/N ratios in organic-carbon-rich Neogene sediments under the Benguela Current upwelling system. *Organic Geochemistry,* 33(7):715–722. **http://dx.doi.org/10.1016/S0146-6380(02)00042-6**

Villinger, H., Grevemeyer, I., Kaul, N., Hauschild, J., and Pfender, M., 2002. Hydrothermal heat flux through aged oceanic crust: where does the heat escape? *Earth and Planetary Science Letters,* 202(1):159–170. **http://dx.doi.org/10.1016/S0012-821X(02)00759-8**

von der Heydt, A., and Dijkstra, H.A., 2006. Effect of ocean gateways on the global ocean circulation in the late Oligocene and early Miocene. *Paleoceanography,* 21(1):PA1011. **http://dx.doi.org/10.1029/2005PA001149**

Walker, R.G., 1978. Deep-water sandstone facies and ancient submarine fans: models for exploration of stratigraphic traps. *AAPG Bulletin,* 62:932–966.

Whipple, K.X., 2009. The influence of climate on the tectonic evolution of mountain belts. *Nature Geoscience,* 2:97–104. **http://dx.doi.org/10.1038/ngeo413**

White, N.M., Pringle, M., Garzanti, E., Bickle, M., Najman, Y., Chapman, H., and Friend, P., 2002. Constraints on the exhumation and erosion of the High Himalayan Slab, NW India, from foreland basin deposits. *Earth and Planetary Science Letters,* 195(1–2):29–44. **http://dx.doi.org/10.1016/S0012-821X(01)00565-9**

Whiting, B.M., Karner, G.D., and Driscoll, N.W., 1994. Flexural and stratigraphic development of the west Indian continental margin. *Journal of Geophysical Research: Solid Earth,* 99(B7):13791–13812. **http://dx.doi.org/10.1029/94JB00502**

Whitmarsh, R.B., Manatschal, G., and Minshull, T.A., 2001. Evolution of magma-poor continental margins from rifting to seafloor spreading. *Nature,* 413(6852):150–154. **http://dx.doi.org/10.1038/35093085**

Willett, S.D., 1999. Orogeny and orography: the effects of erosion on the structure of mountain belts. *Journal of Geophysical Research: Solid Earth,* 104(B12):28957–28981. **http://dx.doi.org/10.1029/1999JB900248**

Wu, F.-Y., Ji, W.-Q., Wang, J.-G., Liu, C.-Z., Chung, S.-L., and Clift, P.D., 2014. Zircon U–Pb and Hf isotopic constraints on the onset time of India-Asia collision. *American Journal of Science,* 314(2):548–579. **http://dx.doi.org/10.2475/02.2014.04**

Yatheesh, V., Bhattacharya, G.C., and Dyment, J., 2009. Early oceanic opening off western India–Pakistan margin: the Gop Basin revisited. *Earth and Planetary Science Letters,* 284(3–4):399–408. **http://dx.doi.org/10.1016/j.epsl.2009.04.044**

Zhang, P., Molnar, P., and Downs, W.R., 2001. Increased sedimentation rates and grain sizes 2–4 Myr ago due to the influence of climate change on erosion rates. *Nature,* 410(6831):891–897. **http://dx.doi.org/10.1038/35073504**